FINAL
CONTRACT REPORT
VTRC 08-CR5

PARAMETERS GOVERNING THE CORROSION PROTECTION EFFICIENCY OF FUSION-BONDED EPOXY COATINGS ON REINFORCING STEEL

ANDREI RAMNICEANU
Graduate Research Assistant
Via Department of Civil and Environmental Engineering
Virginia Polytechnic Institute & State University

RICHARD E. WEYERS, Ph.D., P.E.
Charles E. Via Jr. Professor
Via Department of Civil and Environmental Engineering
Virginia Polytechnic Institute & State University

MICHAEL C. BROWN, Ph.D., P.E.
Research Scientist
Virginia Transportation Research Council

MICHAEL M. SPRINKEL
Associate Director
Virginia Transportation Research Council

http://www.virginiadot.org/vtrc/main/online_reports/pdf/08-cr5.pdf

Standard Title Page - Report on State Project

Report No.	Report Date	No. Pages	Type Report: Final Contract Report	Project No. 73186
VTRC 08-CR5	January 2008	70	Period Covered: 7-1-2002 through 12-10-2007	Contract No.

Title:
Parameters Governing the Corrosion Protection Efficiency of Fusion-Bonded Epoxy Coatings on Reinforcing Steel

Key Words:
Reinforcement, Deck, Life, Corrosion, Concrete, Bridge

Authors:
Andrei Ramniceanu, Richard E. Weyers, Michael C. Brown, and Michael M. Sprinkel

Performing Organization Name and Address:

Virginia Polytechnic Institute & State University
Blacksburg, VA

Sponsoring Agencies' Name and Address

Virginia Department of Transportation
1401 E. Broad Street
Richmond, VA 23219

Virginia Transportation Research Council
530 Edgemont Road
Charlottesville, VA 22903

Supplementary Notes

Abstract

The purpose of this study was to investigate various epoxy coating and exposure parameters to determine their effects on the corrosion of reinforcing steel. The parameters investigated were: chloride content at the bar depth, coated bar corroded area, corrosion product color under the coating, epoxy coating adhesion, coating color, coating damage (holidays and holes), coating thickness, TGA, DSC and EDS analysis and SEM coating cracking investigation.

This study demonstrated that the ECR coating samples extracted from concrete exhibited extensive cracking compared to the new ECR samples in which the coating cracking was limited to only one sample. The coating cracking correlated with the amount of chloride at bar level, residual adhesion of the epoxy to the steel surface, and the percent moisture in the coating. The coating cracking is also related to the change in color of the epoxy and indicates that the epoxy coating degradation in concrete influences the surface condition of the coating.

The DSC results showed that both the extracted epoxy coating samples as well as new samples are not fully cured during the manufacturing process. Additionally, the extracted epoxy coated samples investigated presented significant permanent adhesion loss with little or no epoxy coating residue present on the bar surface, while the EDS analysis showed that once adhesion is lost, corrosion will proceed unimpeded under the coating even in the absence of chlorides.

The parameters that presented a direct correlation with the observed corrosion activity were the number of holidays and the number of damaged areas per unit length of bar. The results also show a distinct loss of quality control in the handling and possibly storage of new coated bars. The new ECR samples had significantly higher damage density than the samples extracted from concrete, while there was no change in the number of holidays and cure condition.

FINAL CONTRACT REPORT

PARAMETERS GOVERNING THE CORROSION PROTECTION EFFICIENCY OF FUSION-BONDED EPOXY COATINGS ON REINFORCING STEEL

Andrei Ramniceanu
Graduate Research Assistant
Via Department of Civil and Environmental Engineering
Virginia Polytechnic Institute & State University

Richard E. Weyers, Ph.D., P.E.
Charles E. Via Jr. Professor
Via Department of Civil and Environmental Engineering
Virginia Polytechnic Institute & State University

Michael C. Brown, Ph.D., P.E.
Research Scientist
Virginia Transportation Research Council

Michael M. Sprinkel
Associate Director
Virginia Transportation Research Council

Project Manager
Michael M. Sprinkel, Virginia Transportation Research Council

Contract Research Sponsored by the
Virginia Transportation Research Council

Virginia Transportation Research Council
(A partnership of the Virginia Department of
Transportation and the University of Virginia since 1948)

Charlottesville, Virginia

January 2008
VTRC 08-CR5

NOTICE

The project that is the subject of this report was done under contract for the Virginia Department of Transportation, Virginia Transportation Research Council. The contents of this report reflect the views of the authors, who are responsible for the facts and the accuracy of the data presented herein. The contents do not necessarily reflect the official views or policies of the Virginia Department of Transportation, the Commonwealth Transportation Board, or the Federal Highway Administration. This report does not constitute a standard, specification, or regulation.

Each contract report is peer reviewed and accepted for publication by Research Council staff with expertise in related technical areas. Final editing and proofreading of the report are performed by the contractor.

ABSTRACT

The purpose of this study was to investigate various epoxy coating and exposure parameters to determine their effects on the corrosion of reinforcing steel. The parameters investigated were: chloride content at the bar depth, coated bar corroded area, corrosion product color under the coating, epoxy coating adhesion, coating color, coating damage (holidays and holes), coating thickness, TGA, DSC and EDS analysis and SEM coating cracking investigation.

This study demonstrated that the ECR coating samples extracted from concrete exhibited extensive cracking compared to the new ECR samples in which the coating cracking was limited to only one sample. The coating cracking correlated with the amount of chloride at bar level, residual adhesion of the epoxy to the steel surface, and the percent moisture in the coating. The coating cracking is also related to the change in color of the epoxy and indicates that the epoxy coating degradation in concrete influences the surface condition of the coating.

The DSC results showed that both the extracted epoxy coating samples as well as new samples are not fully cured during the manufacturing process. Additionally, the extracted epoxy coated samples investigated presented significant permanent adhesion loss with little or no epoxy coating residue present on the bar surface, while the EDS analysis showed that once adhesion is lost, corrosion will proceed unimpeded under the coating even in the absence of chlorides.

The parameters that presented a direct correlation with the observed corrosion activity were the number of holidays and the number of damaged areas per unit length of bar. The results also show a distinct loss of quality control in the handling and possibly storage of new coated bars. The new ECR samples had significantly higher damage density than the samples extracted from concrete, while there was no change in the number of holidays and cure condition.

INTRODUCTION

By the early 1970s it became clear that the increase in deicing salt application lead to premature deterioration of transportation structures, primarily reinforced concrete bridge decks. The premature deterioration exhibited through delaminations and spalling of the riding surface was caused by the corrosion of the reinforcing steel. To combat the problem, one of the corrosion prevention methods investigated was the barrier protection method implemented through the application of an organic coating, specifically fusion-bonded epoxy. By 1981, barely five years after the first research, application of epoxy coated reinforcing steel (ECR); fusion-bonded epoxy coatings became the prevalent corrosion protection method in the United States (Manning, 1995 and Weyers, 1995).

Since then, studies have shown that epoxy coating will debond from the steel reinforcement in as little as 4 years (Pyc, 2000) allowing instead a much more insidious form of corrosion to proceed unimpeded under the coating. More recently, studies conducted at Virginia Tech on samples collected from eight Virginia bridge decks have shown that the epoxy coating develops microscopic cracks (Wheeler, 2003). These cracks may allow the chloride-laden water to pass through leading to the initiation of the corrosion process. Furthermore, ECR exposure to a simulated concrete pore solution as well as chlorides deteriorated in only 100 to 150 days of a wet/dry exposure period before the onset of corrosion (Singth and Ghosh, 2005).

Although some studies have shown that fusion-bonded epoxy coatings are an effective corrosion protection method (Poon and Tasker, 1998), the performance of ECR remains highly controversial. Adding to the controversy is the fact that even after almost 30 years of field use, questions are constantly raised regarding its corrosion protection efficacy. Although some state transportation agencies have started to implement other corrosion protection methods such as using corrosion inhibitors, stainless steel, galvanized steel and micro-composite multi-structural formable steel (MMFX-2), the fact remains that at the time of this study, fusion-bonded epoxy coatings remain the prevalent corrosion protection method.

Thus, it is important that the influence coating parameters that may be manipulated during production such as thickness and the degree of curing have on coating performance and therefore corrosion activity are thoroughly understood. In addition, the non-destructive testing methods currently used to assess the corrosion activity in bare steel reinforced concrete should be further studied with respect to ECR reinforced concrete. Being able to collect concrete parameters and corrosion activity information quickly and accurately will be invaluable to bridge engineers searching for means of assessing and increasing the service life of ECR reinforced concrete bridges.

PURPOSE AND SCOPE

The purpose of this study was to investigate the relationship between the epoxy coating parameters of thickness, curing level, holidays and adhesion, and the corrosion parameters of corrosion current density, corrosion potential, percent corroded area and corrosion product color.

In addition, the relationships between the field corrosion related measurements for bare steel as applied to ECR were also assessed. The ability of measured parameters to determine the condition of the bar underneath the coating was investigated. The study encompassed extending the use of these testing methods to parameters currently only available through destructive testing, as well as investigating the effect the epoxy coating has on the corrosion test results. Furthermore, having verified in a previous study the fact that the non-destructive corrosion activity measurements obtained from bridge decks reinforced with ECR bars are indeed valid (Ramniceanu et al., 2006), the objective of this investigation was to determine the degree to which the epoxy coating influences those non-destructive measurements.

The scope of this study included a representative sample of Virginia's bridge decks consisting of 27 ECR reinforced structures located in the state's six environmental zones. This sample was further divided into two groups: one group consisting of 16 structures cast using concrete with a specified water/cement ratio (w/c) of 0.45, and another group consisting of 11 structures cast using concrete with a specified water/cementatious materials ratio (w/cm) of 0.45. Furthermore, for the purpose of laboratory testing approximately 12 core samples, containing a section of a top mat reinforcing bar, were obtained from each bridge deck.

In addition to the field samples discussed above, new epoxy coated reinforcing steel samples were collected from five, currently ongoing, bridge projects when sampled and one rebar supplier in the Commonwealth of Virginia. Also, three epoxy coating powder samples were provided for analysis by 3M, DuPont and Valspar.

METHODS AND MATERIALS

Bridges

A total of 27 bridges in Virginia were selected for study. The bridges were built between 1984 and 1991 with a specified maximum water/cement of 0.45. The indicated maximum water/cement ratio is the applicable specification at the time of construction. However, it is most likely not the actual w/c used in the construction of each of the selected bridge decks. Also, the information regarding the inclusion of fly ash or ground granulated blast furnace slag (GGBFS) was indicated by the appropriate Engineering District personnel and later verified by petrographic analysis. The sample was then divided into two groups: one with fly ash or slag as a supplemental cementing material and one with only Portland cement. Furthermore, the bridge decks selected for the project were distributed throughout the six Virginia climate regions, see Figure 1. The sampled bridge details are presented in Table 1.

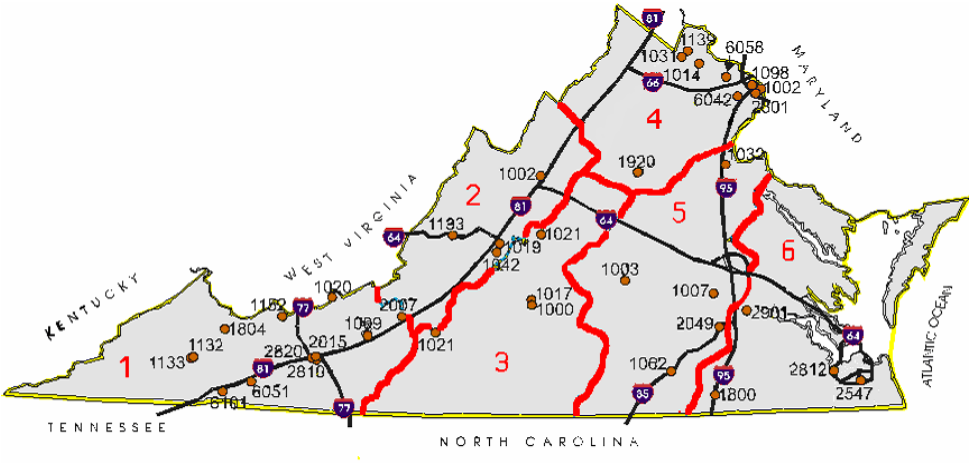

Figure 1. Bridge Locations

Table 1. Bridges Selected for Study

District	County	Structure Number	Year Built	Age at Survey (Years)	Climate Region	Specified Concrete
4	Prince George	2901	1991	12	6	0.45 w/c
7	Orange	1920	1991	12	4	
9	Loudoun	1031	1990	13	4	
1	Russell	1132	1988	15	1	
2	Franklin	1021	1988	15	1	
3	Cumberland	1003	1988	15	5	
1	Tazewell	1152	1987	16	1	
8	Alleghany	1133	1987	16	1	
9	Loudoun	1139	1987	16	2	
1	Wytheville	2815	1986	17	1	
1	Wytheville	2820	1986	17	1	
2	Giles	1020	1986	17	1	
5	Chesapeake	2547	1984	19	5	
8	Rockbridge	1019	1984	19	2	
3	Campbell	1000	1991	12	3	0.45 w/cm
5	Suffolk	2812	1991	12	6	
9	Fairfax	6058	1991	12	4	
1	Smyth	6051	1990	13	1	
3	Campbell	1017	1990	13	3	
4	Chesterfield	1007	1990	13	5	
8	Rockbridge	1042	1990	13	2	
1	Russell	1133	1988	15	1	
8	Augusta	1002	1988	15	2	
9	Arlington	1098	1988	15	4	
9	Arlington	1002	1987	16	4	
9	Loudoun	1014	1987	16	4	
1	Wytheville	2819	1986	17	1	

The chloride exposure data per climatic region are presented in Table 2. The average chloride exposure per climatic region was measured over a three year winter period, 2000-2002, in terms of average annual tons Cl^-/lane-km.

Table 2. Chloride Exposure by Environmental Zone

Zone #	Climatic Zone	Tons Cl^-/lane-km
1	Southwestern Mountain (SM)	0.76
2	Central Mountain (CM)	0.74
3	Western Piedmont (WP)	0.24
4	Northern (N)	0.58
5	Eastern Piedmont (EP)	0.24
6	Tidewater (TW)	4.82

Sampling of Epoxy Powder and New ECR

Epoxy Powder

Three epoxy powder manufacturers were represented in the powder analysis. The manufacturers/powders were 3M Scotchkote 413, Valspar Greenbar 720A009 and DuPont FBE Rebar. One sample of approximately 5 lbs from the three manufacturers was provided by VTRC, while one sample of Valspar Greenbar 720A009 was obtained from a site visit at a coating facility located in North Carolina.

New ECR

ECR samples from three currently ongoing projects in Virginia were collected for this study. The projects were the north bound span of I-81 over Buffalo Creek, Woodrow Wilson Bridge over the Potomac River and Route 123 Bridge over the Occoquan River in Northern Virginia. The sample from the Buffalo Creek project (BFC) and one sample from the Woodrow Wilson project (WWBVT) were collected by Virginia Tech (VT). The second sample from the Woodrow Wilson project (WWBVDOT) and the sample from the Occoquan River project (OBP) were supplied by VDOT project representatives. During the site visits, it was observed that the ECR bars were generally stored off the ground and were covered with a commercially available tarp. No other damage mitigation measures were noted. Interviewed site personnel indicated that the turn-over rate for ECR bars was approximately 2 weeks for BFC and a few days for WWB. We were unable to determine the age of the bar as delivered to the construction sites.

Additionally, an ECR sample was collected from Bay Shore precast plant located in Cape Charles, on the Eastern Shore of Virginia. The sample available for collection had been exposed to the elements approximately 12 month. Finally, ECR samples from four coating manufacturers were tested. One sample was provided for testing by the Hall Hodges plant located in Chesapeake, Virginia. Samples from three construction sites representing coaters Free State Coaters, Florida Steel and Lane Enterprises were stored at the VT testing facilities and remained from a previous study (Pyc, 1998 and Zemajtis, 1998). The ECR bars had been stored indoors, supported off the floor and individually separated using wooden spacers and covered with a black plastic tarp.

Deck Survey

The field survey was limited to one traffic lane, generally selected on the basis of traffic and surface drainage conditions for each individual deck. Under field conditions, however, the right traffic lane was selected for safety and practicality, as this is normally the lane with the most traffic and subsequently the one deteriorating first. The field survey data used in this study included half-cell corrosion potentials, corrosion current densities and concrete resistivity. Core samples from the decks measuring 101.6 mm in diameter and containing an ECR bar section were also collected.

Half-cell Potentials

Half-cell potential measurements were collected at 1.22 m intervals in both wheel paths of the right lane. A copper-copper sulfate half-cell was used, and the test was performed in accordance with ASTM 876 (ASTM, 1991) even though the standard test method states that the test is applicable to only uncoated reinforcing bar.

Linear Polarization

Based on the half-cell potential values and the bridge deck length, 4 to 6 corrosion current density measurements were performed. The test was carried out using an unguarded three electrode linear polarization (3LP) instrument (Clear, 1989), and the data was usually collected from the right wheel path of the right lane for safety reasons. Generally, the tests were performed at two locations determined to have the most negative potential values, two locations with the least negative potential values and if deck length permitted, at two locations with potential values midway between the most and least negative values.

Concrete Resistivity

The test was performed at nine locations using a four-probe Wenner apparatus. Four to 6 of the 9 locations selected were at the same locations as the corrosion current density measurements, while three locations selected were the same locations from which cores were obtained for petrographic analysis and contained no reinforcing steel. Five measurements were obtained at each test location using due diligence not to conduct the measurements directly over the reinforcing steel bar. For the purpose of calculating the resistivity of the concrete, the spacing between the four probes was maintained at 50.8 mm.

Core Samples

Generally, 12 core samples were collected from each bridge deck. Core drilling was performed with a water cooled diamond set drill bit. Six cores were drilled at the same locations where the corrosion current density measurements were performed, and contained an ECR section. Three core samples obtained included the reinforcing steel, but were located over a crack. Also, three un-cracked “companion” cores were drilled adjacent to the cracked cores. The “companion” cores contained the next parallel reinforcing steel bar that was not cracked. Each specimen measured 101.6 mm in diameter by approximately 152.4 mm. After extraction, each

specimen was allowed to air dry only long enough for surface moisture to evaporate. The samples were then wrapped in multiple layers, consisting of a layer of 101.6 μm polyethylene sheet, followed by a layer of aluminum foil, and another layer of polyethylene sheet. Finally, the specimen and protective layers were wrapped tightly with duct tape. The purpose of the immediate wrapping of the cores was to maintain as closely as practical the in-place moisture condition of the concrete during transport and storage (Brown, 2002).

Laboratory Testing

Concrete Tests

The Virginia Transportation Research Council at their facility located in Charlottesville, Virginia have conducted chloride content test at the ECR bar depth.

Reinforcing Steel Tests

The condition of the ECR sections extracted from the concrete cores was assessed as follows. The visible ECR corroded surface area was measured. The colors of both the epoxy coating and the corrosion products present under the coating were recorded. Additionally, for a limited number of samples, the steel substrate was also examined using the scanning electron microscope (SEM).

The color of the steel surface under the coating at the residual adhesion (RA) test locations was noted, and based on the interpretation criteria presented in Table 3, a value from 1 to 5 was assigned to each specimen (adapted from Pyc et al., 2000).

Table 3. Corrosion Product Interpretation

Number	Steel Surface Color
1	Shining
2	Gray, shining
3	Dark gray, shining
4	Black, Shining
5	Black

Because of the time lag between the RA tests and the Energy Dispersive X-ray Microanalysis (EDAX) analysis, EDAX tests on the freshly exposed steel surfaces were not possible. Therefore, the surface chemical composition of freshly exposed steel surface corresponding to each steel surface color in Table 4 was obtained from a previous study and is presented in Table 4 (Pyc et al., 2000).

Table 4. Rebar Surface Chemical Composition

Element	Weight %				
	Shining (1)	Gray shining (2)	Dark gray shining (3)	Black shining (4)	Black (5)
Fe	97.7	93.9	92.1	93.6	83.7
Mn	1.7	2.1	1.1	2.3	n/a
Cr	0.7	1.2	0.5	n/a	< 0.2
Ti	n/a	0.7	n/a	0.6	n/a
Ni	n/a	n/a	n/a	0.2	n/a
Al	n/a	n/a	< 0.2	n/a	0.4
Si	n/a	0.3	0.6	n/a	6.7
Cu	n/a	0.4	2.7	0.8	2.5
Ca	n/a	0.3	n/a	n/a	n/a
K	n/a	n/a	n/a	0.4	1.3
O	n/a	1.0	3.2	2.3	5.4

Epoxy Coating Tests

Testing of the epoxy coating was conducted on bars extracted from the concrete cores and are identified as EECR samples. New ECR and epoxy powder samples were also tested. The samples on which tests were performed are indicated in each of the following individual epoxy tests.

Coating Thickness

The coating thickness was measured in accordance with ASTM G-12 (ASTM, 1998). The test was carried out using the same Elektro-Phisik Minitest 500 coating thickness gauge on the EECR as well as the new ECR samples

Coating Adhesion

The coating adhesion test was performed on the EECR field samples at the VTRC facilities. The peel or knife test is performed as follows: an x-cut is made in the coating between the bar lugs and the steel substrate is exposed by inserting the blade of an X-acto knife underneath the coating. A number between 1 and 5 is assigned to each test based on the size of the exposed area and represents a degree of RA of the epoxy to an oxidized steel surface layer. A total of 6 RA tests were performed on each ECR specimen and the average adhesion was calculated for each specimen. The interpretation guidelines are presented in Table 5 (Pyc, 1998).

Table 5. Adhesion Rating

RA Number RA	Exposed Area
1	Unable to insert blade tip under coating
2	Total exposed area < 2 mm^2
3	2 mm^2 < Total exposed area < 4 mm^2
4	Total exposed area > 4 mm^2
5	Blade tip slides easily under the coating. Levering action removes the entire section of coating

The RA test was attempted on the new ECR samples. The adhesion of the epoxy to the iron oxide layer, for ECR that has not been exposed to the moist/wet concrete environment, is greater than the cohesive strength of the epoxy coating and thus, the RA cannot be measured.

Coating Damage Assessment

The coating damage was assessed using three different techniques: 1) by counting the number of defects visible to the unaided eye. 2) By assigning a coating cracking number from 1 through 4 based on the SEM micrograph guidelines illustrated in Figure 2.

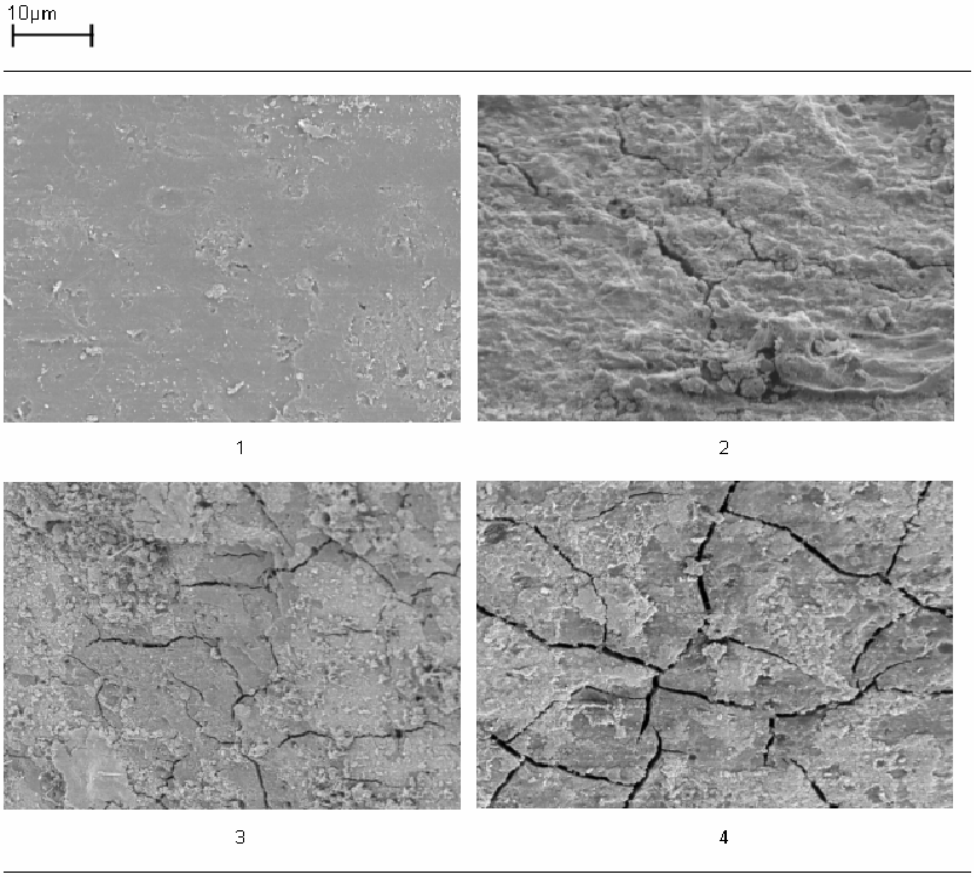

Figure 2. SEM Micrographs at 2k Magnification

3) Finally, by using the image analysis program ImageJ on images collected during the SEM investigation. ImageJ is a shareware image analysis program developed by the National Institutes of Health (NIH). A 5k magnification SEM micrograph is converted to a binary image, which is then used to quantify the surface coating damage. The damage is recorded as a percentage of the surface area. Unlike technique 2, which takes into account only cracks, all damage types (cracks, pores, gouges) are included, using this method. Figure 3 illustrates a typical SEM 5k micrograph and its accompanying binary image.

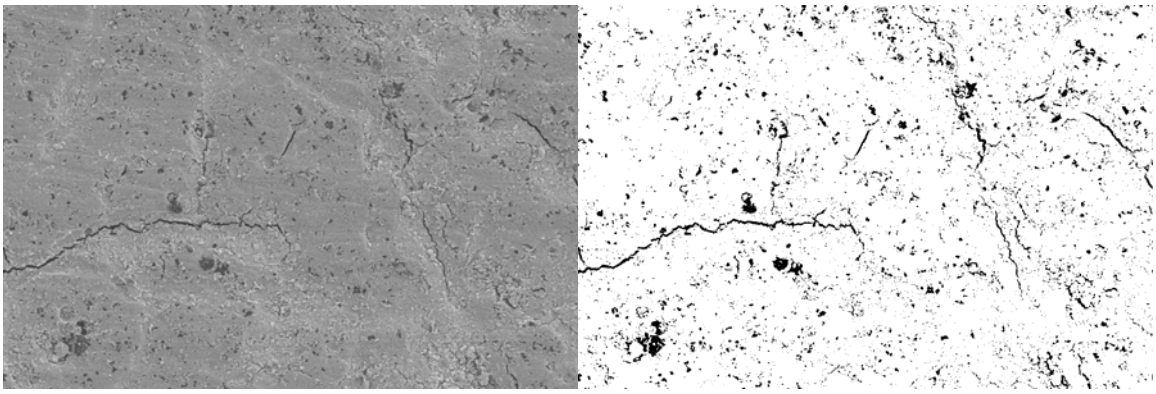

Figure 3. Structure 1019-8 C-4 5Kx SEM Micrograph and Binary

Epoxy Coating Color

In addition to the color of the steel surface under the coating at the time of investigation, the color of the epoxy coating itself was also recorded. This was carried out based on the observation that the epoxy coating degradation (increase in brittleness) under certain exposure conditions is accompanied by color change. Five typical coating colors were observed. The colors are presented in Table 6 along with the values assigned and an interpretation visual guide is presented in the Appendix.

Table 6. Coating Color

Value	Coating color
1	Glossy Green
2	Dull Green
3	Glossy Light Green
4	Dull Dark Green
5	Pale Green

Holidays

Holidays are flaws in the coating indiscernible to the naked eye. These discontinuities are detected by testing the continuity of the coating. The test was performed on the EECR and new ECR samples. The tests were performed using a Tinker & Rasor Model M-1 holiday detector according to ASTM G 62 (ASTM, 1998).

Glass Transition

A TA DSC Q1000 v5.1 instrument was used to determine the initial and final glass transition temperature (T_g) of the samples and thereby assess the level of curing of the epoxy coating. Eighty three EECR samples and 18 new ECR coating samples, weighing approximately 12 mg were tested. 10 powder samples weighing approximately 12 mg were also tested to determine the curing temperature and T_g value of the three unadulterated powder coatings. The testing regimen imposed is presented in Table 7.

Table 7. DSC Process

Process
Equilibrate to 25°C
Ramp 10°C/min to 250°C
Isothermal 30 seconds
Equilibrate to 25°C
Ramp 10°C/min to 250°C
Terminate process

Moisture Content

A TA TGA Q100 instrument was used to determine the moisture content of the same number of coating samples as the ones for which the T_g values were obtained. Coating samples weighting approximately 15 mg were heated to 160 °C. The temperature was then held constant for 30 minutes to ensure all moisture was removed. The pan was flame-dried over a Bunsen burner prior to each test, and each test was performed in an air atmosphere. The weight loss was recorded both as a function of time as well as temperature.

Testing Methods

Field-emission scanning electron microscopy (FE-SEM)

Micrographs of the coating samples were obtained using a LEO 1550 FE-SEM at an accelerating voltage of 5Kv. Micrographs were taken at magnifications of 100x, 500x, 2Kx, 5Kx and 10Kx. The condition of the epoxy surface was examined for evidence of cracking, porosity and other damage. The chemical composition for all specimens imaged was determined using the EDS and was performed by an Iridium Microanalysis (I/RF) System. EDS sample preparation included cleaning the specimens with acetone and ethanol to remove any oils from the sample preparation process, and sputter-coating with a palladium/gold alloy 10 μm thick.

Energy dispersive spectrometry (EDS)

EDS was also performed to determine the chemical composition of the samples, specifically the presence of Cl^-, which is a critical element in the corrosion process of reinforcing steel. The chemical analysis composition was performed concurrently with the SEM image analysis, which insured that the image was indeed that of the epoxy and not artifacts such as cement paste or steel oxidation products present on the coating sample.

Fourier Transform Infrared Spectrometry (FT-IR)

Spectra from four powder samples were collected. The spectra were obtained directly from the powder samples, with no additional preparation, using the attenuated total reflection technique (ATR).

Data Analysis

Since the effects of the different coating parameters on corrosion activity are not entirely understood, the aim of this study is to identify the probability of parameter inter-relationship and possibly create a regression model that will correlate the coating parameters with the observed corrosion activity. Minitab® statistical software was used in the analysis of results.

RESULTS

Epoxy Powder

Infrared spectra were obtained from the four powder samples indicates that there are no discernible differences in the general structures of the different products. The T_g was also determined. The values are presented in Table 8. The DuPont sample had the lowest T_g with a three test average value of 84.7°C, while the 3M Scotchkote sample collected from the coating plant was the highest with a three test average value of 120.9°C.

Table 8. Epoxy Powder T_g Values

Powder Sample	T_g1 (°C)	T_g2 (°C)	T_g3 (°C)	Average T_g (°C)
3M Scotchkote - VTRC	114.9	125.9	121.9	120.9
Valspar - VTRC	98.2	100.7	96.7	98.5
DuPont - VTRC	86.8	84.2	83.2	84.7
Valspar	103.1	97.4	102.3	100.9

New ECR Samples Test Results

The new ECR samples collected consisted of one No. 5 coated bar 6.1 m or 7.62 m cut into four or five 1.52 m length samples labeled S1 through S4 or S5, respectively. Samples WWBVDOT that were provided for analysis by VDOT representatives at the construction site were already cut to the 1.52 m length and wrapped when picked up, as were the OBP samples. The OBP samples were No. 3 bars, all other ECR project samples were No. 5 bars. Measurements performed on the epoxy coating taken from the new ECR samples were moisture content, determination of the T_g before and after additional curing and coating thickness.

The T_g values and moisture content are presented in Table 9. The initial T_g values ranged from a low of 84.56°C (BSCC – S3) to a high of 102.22°C (LNE – S4) while fully cured values ranged from a low of 96.84°C (OBP – S4) to a high of 102.22°C (LNE – S4). LNE – S4 was the only sample that was fully cured, exhibiting no change in T_g following a curing treatment designed to fully cure the film. The remaining samples exhibited changes in T_g ranging from 9.69°C (FSC – S2) to 15.86°C (WWBVDOT – S3). The moisture content ranged from a low of 0.34% (FSC – S4) to a high of 1.59% (BSCC – S1).

Table 9. New ECR Coating T_g and Moisture Content

Specimen	Sample	T_g (°C)	Full T_g (°C)	ΔT_g (°C)	ΔT_g (°C) Due to Moisture	Differerence in ΔT_g	Moisture %
Woodrow Wilson Bridge (WWBVT)	S2	89.48	102.4	12.92	9.0	3.9	1.39
	S4	87.68	100.21	12.53	7.8	4.7	1.23
Woodrow Wilson Bridge (WWBVDOT)	S1	87.79	101.59	13.8	9.2	4.6	1.44
	S3	87.57	103.43	15.86	9.2	6.7	1.42
Hall Hodges Plant (HHP)	S2	88.37	102.17	13.8	7.3	6.5	1.13
	S4	89.08	102.62	13.54	7.9	5.6	1.22
Buffalo Creek (BFC)	S2	90.06	101.36	11.3	9.2	2.1	1.43
	S4	89.02	101.49	12.47	8.0	4.5	1.25
Bay Shore Cape Charles (BSCC)	S1	87.1	100.9	13.8	10.1	3.7	1.59
	S3	84.56	99.89	15.33	8.5	6.8	1.33
Florida Steel (FS)	S2	87.63	101.34	13.71	8.8	4.9	1.38
	S4	86.14	101.15	15.01	8.0	7.0	1.25
Occoquan Bridge Project (OBP)	S2	86.98	98.75	11.77	7.6	4.2	1.2
	S4	85.38	96.84	11.46	8.3	3.2	1.33
Free State Coaters (FSC)	S2	91.37	101.06	9.69	7.2	2.5	1.12
	S4	85.89	99.58	13.69	2.2	11.5	0.34
Lane Enterprises (LNE)	S2	88.98	99.34	10.36	4.0	6.4	0.63
	S4	102.22	102.22	0	5.3	-5.3	0.81

The column labeled "ΔT_g (°C) due to Moisture" represents the maximum change in T_g attributable to the measured moisture level, assuming all the moisture contributes to a change in T_g. However, only a small portion of the measured moisture may in fact be responsible for a decrease in the coating T_g; the remaining water being bulk water, which is not bound to the polymer chains, and will therefore have no effect on the epoxy T_g. The change in T_g was calculated using the Gordon-Taylor equation, presented below:

$$\frac{1}{T_g} = \frac{W_1}{T_{g1}} + \frac{W_2}{T_{g2}}$$

Where:
T_g = Glass transition temperature of the Coating/Water mix (Kelvin)
W_1 = Weight percent of water in the coating
T_{g1} = Glass transition temperature of water (136 Kelvin)
W_2 = Weight percent of coating
T_{g2} = Glass transition temperature of fully cured dry coating (Kelvin).

Figure 4 illustrates a typical DSC plot showing the difference in T_g due to additional curing. The initial T_g of sample LNE – S2 was 91.37°C as shown by the upper plot in the figure, with maximum additional curing occurring at 130.82°C. The fully cured T_g of this sample was 101.06°C, with the sample showing no additional curing as evidenced by the constant slope of the lower plot at 130.82°C.

ECR coating thickness, the visible damage number, holidays and the approximate age of the sample at collection time are presented in Table 10. The OBP samples had the least damage number at 0.3/m as well as the least number of holidays with 0.0/m. The LNE samples had the greatest damage number with 5.78/m, while the holiday detector beeped continuously. The LNE holiday results were not used in further analysis because of continuous holiday detection. At collection time, the age of the samples, was noted as time in field because we could not determine the manufacture date. Also, the time in field represents information provided by construction personnel. The stated age at the time of collection was 1 week for the Woodrow Wilson Bridge projects and Hall Hodges Plant and 2 weeks for the Occoquan Bridge and Buffalo Creek projects. The Bay Shore Concrete sample was 68 weeks old, being exposed to the environment at the casting plant for that time period. The Free State Coaters, Florida Steel, and Lane Enterprises samples were exposed to a field environment of 4 weeks plus 4 years in the laboratory covered by a black plastic tarp to protect the ECR from UV light.

The thickness measurements were performed at 20 random locations along the bars. Three measurements were taken at each of the 20 locations and the results averaged. As illustrated in Figure 5, the thickness measurements were normally distributed.

The average thickness measurements and the 95% confidence intervals are presented in Figure 6 for the individual samples with the minimum and maximum specified thickness represented by the two horizontal lines at 175 µm and 300 µm. Three sample sets, WWBVDOT, BSCC, and LNE failed to meet the current coating thickness specifications. The average thickness of WWBVDOT is 344 µm with a standard deviation of 46 µm, and the average thickness of BSCC is 321 µm with a standard deviation of 60 µm. The average thickness of both sample sets is above the maximum current specification. Inversely, the average thickness of LNE is below the current specified minimum of 175 µm at 141 µm with a standard deviation of 34 µm.

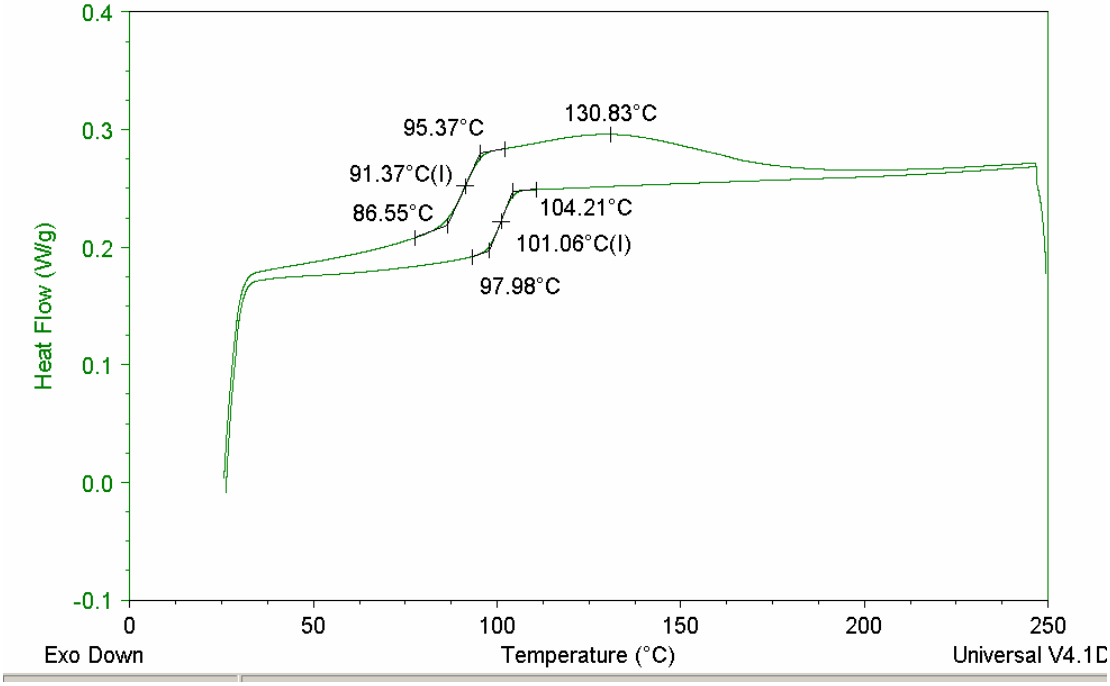

Figure 4. Sample LNE S2 DSC Plot

Table 10. New ECR Sample Measurements

Specimen	Damaged Areas /m	Thickness (µm)	Thickness Stdev (µm)	Holidays /m	Time in Field (weeks)
WWBVT	33.46	263	34	3.28	1
WWBVDOT	5.90	344	46	0.66	1
HHP	68.22	263	39	13.12	1
BFC	32.80	218	50	14.43	2
OBP	3.94	243	37	0.00	2
BSCC	25.58	321	60	2.62	68
FS	29.52	242	76	24.93	4*
FSC	41.33	251	62	9.18	4*
LNE	69.54	141	37	∞	4*

* - Plus additional 4 years laboratory storage

Extracted ECR Samples Test Results

The same tests and measurements performed on the new ECR samples were conducted on select specimens from the EECR samples. The tests were limited to three random specimens from each structure investigated due to time and cost limitations. Since one of the goals of the study was to determine the condition and deterioration level of the coating, the samples obtained from cracked cores were not analyzed. ECR specimens from cracked concrete locations were excluded because the coating may have been damaged by the rapid ingress of chlorides and possible subsequent corrosion.

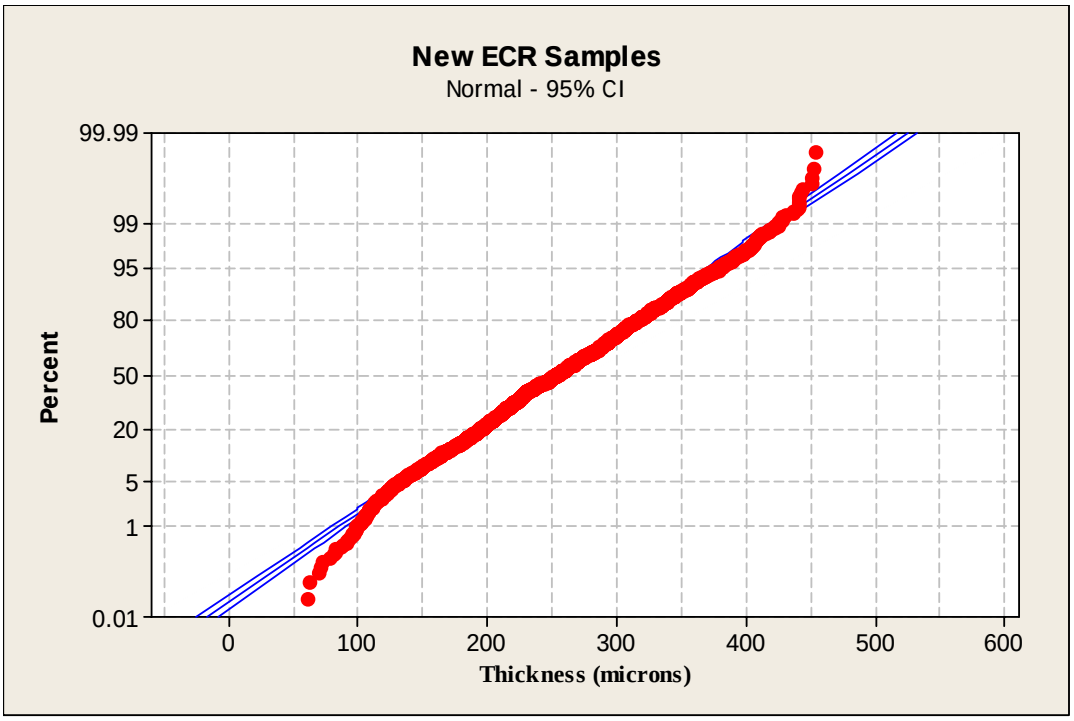

Figure 5. ECR Epoxy Coat Thickness Measurements Distribution

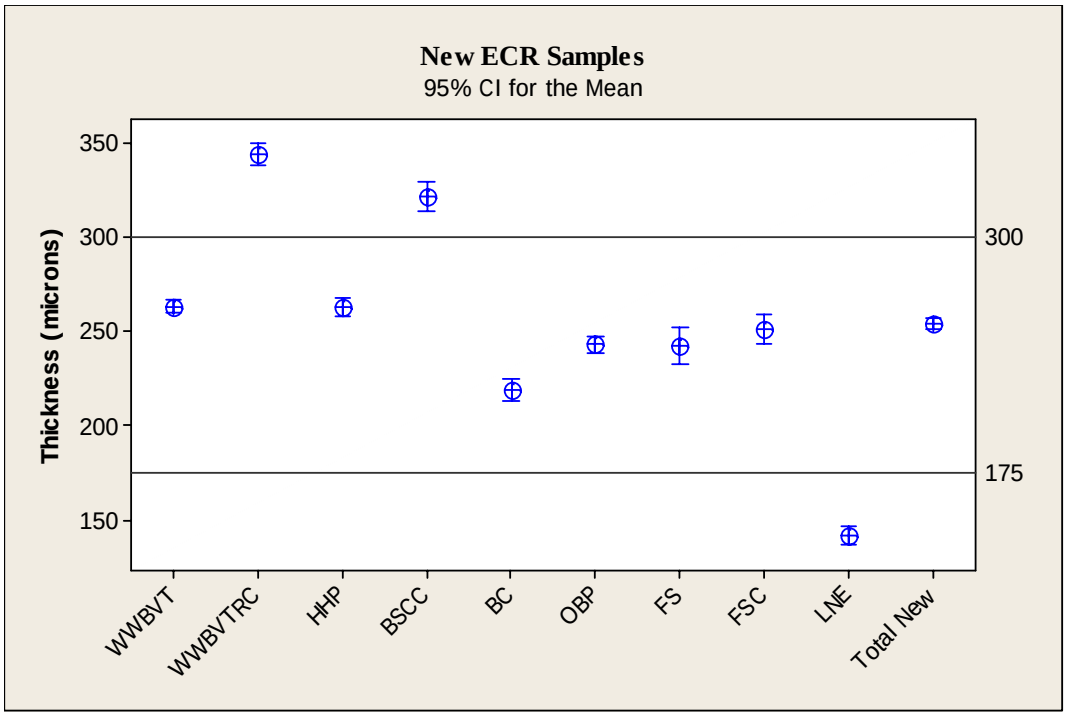

Figure 6. New ECR Coating Thickness

T_g and Moisture Content

The T_g and moisture content of the sampled specimens are presented in Table 11.

Table 11. EECR Coating T_g and Moisture Content

Structure	Core Sample	T_g (°C)	Final T_g (°C)	ΔT_g (°C)	ΔT_g (°C) Due to Moisture	Difference in ΔT_g	Moisture %
1003-3	C2	*	*	*	*	*	1.75
	C7	*	*	*	*	*	*
	C1	99.09	112.83	13.74	10.77	2.97	1.5
1019-8	C1	99.23	111.51	12.28	11.15	1.13	1.57
	C4	99.53	110.95	11.42	11.45	-0.03	1.62
	C5	98.22	110.86	12.64	10.64	2.00	1.5
1020-2	C1	87.01	111.28	24.27	9.12	15.15	1.27
	C3	102.05	113.31	11.26	9.24	2.02	1.27
	C6	102.08	115.13	13.05	10.04	3.01	1.37
1031-9	C1	86.63	112.46	25.83	10.01	15.82	1.39
	C4	94.3	110.5	16.2	10.48	5.72	1.48
	C5	105.48	113.31	7.83	8.90	-1.07	1.22
1132-1	C1	94.93	109.19	14.26	10.27	3.99	1.46

	C4	98.93	108.51	9.58	9.69	-0.11	1.38
	C6	98.21	109.14	10.93	10.39	0.54	1.48
1133-8	C1	90.84	108.88	18.04	11.04	7.00	1.58
	C3	95.11	110.35	15.24	11.21	4.03	1.59
	C5	97.44	112.02	14.58	10.25	4.33	1.43
1139-9	C1	97.59	111.71	14.12	11.64	2.48	1.64
	C3	86.65	113.37	26.72	10.81	15.91	1.5
	C6	81.22	115.1	33.88	5.92	27.96	0.78
1152-1	C1	95.95	112.63	16.68	10.02	6.66	1.39
	C2	104.27	111.62	7.35	7.92	-0.57	1.09
	C3	103.24	112.65	9.41	7.77	1.64	1.06
2547-5	C1	86.92	113.13	26.21	12.68	13.53	1.78
	C2	84.15	110.07	25.92	11.38	14.54	1.62
	C6	87.16	102.34	15.18	7.15	8.03	1.04
2815-1	C1	103.74	114.58	10.84	9.04	1.80	1.23
	C3	98.57	113.34	14.77	11.62	3.15	1.62
	C6	78.9	113.41	34.51	8.83	25.68	1.21
1000-3A	C1	100.95	110.3	9.35	10.40	-1.05	1.47
	C2	99.51	109.73	10.22	9.24	0.98	1.3
	C4	99.9	109.51	9.61	9.42	0.19	1.33
1000-3B	C1	100.53	110.18	9.65	9.46	0.19	1.33
	C2	98.9	109.89	10.99	6.21	4.78	0.85
	C4	83.01	110.05	27.04	9.79	17.25	1.38
1002-8	C1	86.16	109.9	23.74	9.58	14.16	1.35
	C3	83.1	111.69	28.59	12.17	16.42	1.72
	C4	106.98	109.48	2.5	8.49	-5.99	1.19
1002-9	C2	95.95	110.62	14.67	8.34	6.33	1.16
	C4	87.57	110.6	23.03	9.49	13.54	1.33
	C6	98.35	109.79	11.44	10.77	0.67	1.53
1007-4	C1	99.58	110.98	11.4	10.45	0.95	1.47
	C3	83.84	108.72	24.88	12.01	12.87	1.73
	C6	101.56	108.49	6.93	10.68	-3.75	1.53
1014-9	C1	101.65	111.43	9.78	7.37	2.41	1.01
	C3	83.58	104	20.42	10.89	9.53	1.61
	C6	81.72	103.64	21.92	10.67	11.25	1.58
1017-3	C1	99.46	107.57	8.11	7.92	0.19	1.12
	C2	83.38	109.8	26.42	8.84	17.58	1.24
	C4	85.78	109.04	23.26	7.46	15.80	1.04
1042-8	C1	106.4	111.09	4.69	8.17	-3.48	1.13
	C3	103.17	111.1	7.93	8.10	-0.17	1.12
	C4	99.87	109.24	9.37	9.14	0.23	1.29
1098-9	C2	101.92	109.99	8.07	8.71	-0.64	1.22
	C4	100.99	110.9	9.91	8.90	1.01	1.24
	C7	104.18	110.99	6.81	7.89	-1.08	1.09

1133-1	C1	84.11	110.13	26.02	10.53	15.49	1.49
	C3	95.65	108.44	12.79	9.69	3.10	1.38
	C6	82.67	108.4	25.73	11.59	14.14	1.67
2819-1	C1	98.64	109.19	10.55	11.39	-0.84	1.63
	C3	96.15	108.37	12.22	9.42	2.80	1.34
	C5	97.15	107.57	10.42	12.18	-1.76	1.77
6051-1	C1	102.33	112.42	10.09	11.08	-0.99	1.55
	C4	99.48	109.22	9.74	8.87	0.87	1.25
	C6	86.76	109.59	22.83	12.07	10.76	1.73
2820-1	C1	100.24	111.04	10.8	10.39	0.41	1.46
	C4	98.65	108.28	9.63	13.01	-3.38	1.89
	C6	99.94	112.83	12.89	11.45	1.44	1.6
1021-2	C1	99.89	109.13	9.24	7.93	1.31	1.11
	C2	100.62	107.77	7.15	8.86	-1.71	1.26
	C4	104.18	110.31	6.13	7.38	-1.25	1.02
2901-4	C1	*	*	*	*	*	1.83
	C5	87.85	109.57	21.72	11.68	10.04	1.67
	C6	87.75	108.08	20.33	8.35	11.98	1.18
2812-5	C1	100.1	108.78	8.68	11.55	-2.87	1.66
	C4	84.15	111.14	26.99	10.79	16.20	1.52
	C6	83.64	111.27	27.63	12.40	15.23	1.76
1920-7	C2	102.42	112.6	10.18	10.83	-0.65	1.51
	C3	99.99	110.38	10.39	11.21	-0.82	1.59
	C6	98.52	111.68	13.16	10.29	2.87	1.44
6058-9	C1	93.43	97.83	4.4	7.38	-2.98	1.11
	C3	90.48	102.23	11.75	7.78	3.97	1.14
	C6	96.61	99.11	2.5	5.61	-3.11	0.82

Note: * - Unable to collect data from sample

The initial T_g values ranged from a low of 78.90°C (2815-1 C6) to a high of 106.98°C (1002-8 C4) while fully cured values ranged from a low of 97.83°C (6058-9 C1) to a high of 115.10°C (1139-9 C6). The EECR samples showed changes in T_g ranging from 2.50°C (1002-8 C4 and 6058-9 C6) to 27.63°C (2812-5 C6). The moisture content ranged from a low of 0.82% (6058-9 C6) to a high of 1.89% (2820-1 C4).

Figure 7 illustrates a typical DSC plot showing the difference in T_g due to additional curing. The initial T_g of sample 1017-3 C1 was 99.46°C as shown by the upper plot in the figure, with maximum additional curing occurring at 150°C. The fully cured T_g of this sample was 107.57°C, with the sample showing no additional curing as evidenced by the constant slope of the lower plot at 150°C.

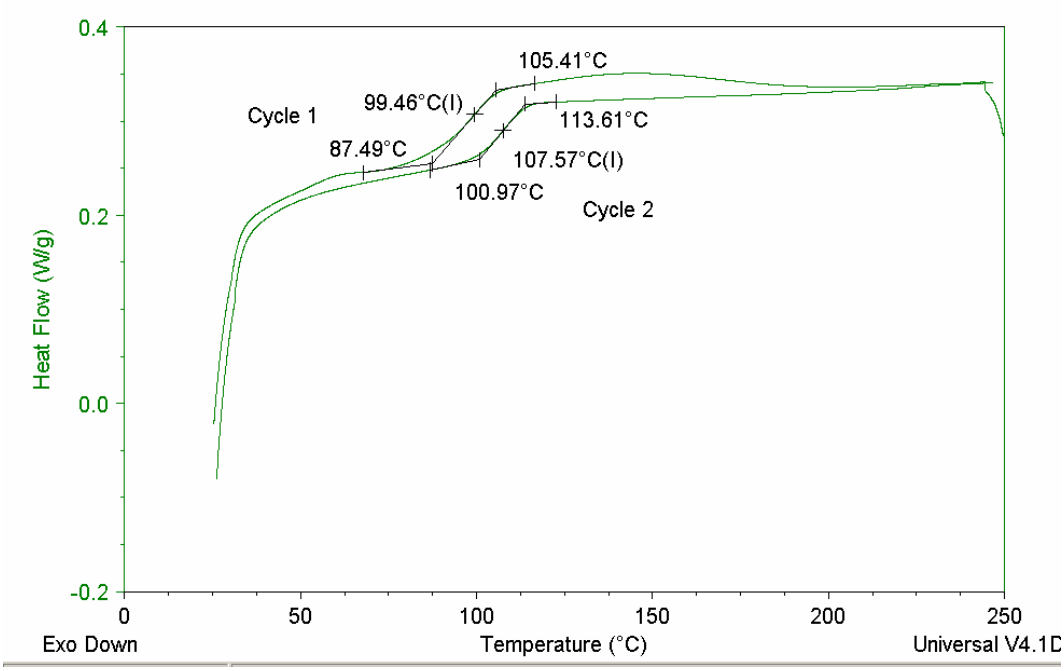

Figure 7. 1017-3 C1 DSC Plot

Coating Thickness

The average coating thickness, coating color, average residual adhesion, holidays, the number of damaged areas, % corroded area, the color of corrosion products under the coating, the coating cracking number, % cracking and porosity and % moisture content are presented in Table 12.

Table 12. EECR Test Data

Structure	Core Sample	Average Thickness (microns)	Coating Color	Average Residual Adhesion	Holidays/m	# Damaged Areas/m	% Corroded Area	Color of Corrosion Products	Cracking	% Cracking and Porosity
1003-3	C2	209	1	5.00	0.00	0.00	0.000	4.00	*	*
	C7	*	1	3.67	*	4.10	0.750	3.00	2	6.441
	C1	233	1	4.33	5.74	0.00	0.000	4.00	1	6.950
1019-8	C1	266	2	4.00	0.82	0.82	0.180	2.00	4	11.652
	C4	191	2	5.00	13.12	1.64	0.250	2.67	3	6.111
	C5	247	1	3.00	0.82	0.82	0.150	3.00	2	5.554
1020-2	C1	169	4	1.33	36.08	46.74	2.070	1.67	2	4.653
	C3	276	4	4.00	10.66	16.40	0.790	2.00	3	8.408
	C6	243	4	5.00	1.64	7.38	0.260	2.33	1	3.633
1031-9	C1	267	2	5.00	0.82	4.10	0.140	5.00	1	1.845
	C4	192	2	5.00	14.76	7.38	0.130	5.00	1	7.162
	C5	251	2	2.67	2.46	2.46	0.130	2.00	1	3.766
1132-1	C1	276	2	5.00	2.46	3.28	0.260	4.00	1	3.855
	C4	261	2	2.00	1.64	1.64	0.056	1.33	2	3.509
	C6	260	2	2.33	1.64	0.00	0.000	1.00	1	5.351
1133-8	C1	199	2	3.67	4.10	7.38	0.180	1.67	3	2.833
	C3	177	2	3.00	9.84	13.94	0.650	2.00	3	3.545
	C5	214	2	2.33	13.12	4.10	0.130	2.00	2	4.184
1139-9	C1	232	4	2.00	0.82	0.00	0.000	1.00	4	7.742
	C3	195	1	2.67	0.00	9.84	0.590	2.33	1	6.626
	C6	256	2	2.00	0.00	0.00	0.000	1.00	2	3.810
1152-1	C1	328	1	3.33	3.28	12.30	0.190	2.00	2	6.909
	C2	250	1	2.00	4.10	14.76	0.380	1.00	1	8.740
	C3	294	1	2.33	4.92	4.92	0.900	1.00	1	4.095
2547-5	C1	194	2	4.00	33.62	17.22	0.800	3.67	2	4.471
	C2	256	2	4.33	26.24	18.86	1.500	3.00	4	4.440
	C6	170	*	1.00	11.48	7.38	0.350	1.00	*	*
2815-1	C1	237	2	5.00	3.28	13.94	0.700	4.00	2	4.725
	C3	172	4	3.00	16.40	8.20	0.330	3.00	*	*
	C6	126	4	5.00	22.96	10.66	0.360	4.00	1	2.045
1000-3A	C1	246	2	5.00	1.64	15.58	0.740	4.00	2	8.755
	C2	294	2	3.67	4.10	3.28	0.190	3.00	1	15.801
	C4	253	2	3.67	0.82	9.02	0.380	3.00	1	8.499
1000-3B	C1	*	2	2.67	*	*	*	3.00	*	*
	C2	*	2	2.00	*	*	*	2.00	*	*

	C4	*	2	5.00	*	*	*	4.00	*	*
1002-8	C1	236	4	5.00	5.74	21.32	0.450	4.00	3	7.053
	C3	190	2	5.00	27.06	18.86	0.620	3.00	3	2.359
	C4	241	2	2.33	1.64	1.64	0.090	1.00	*	*
1002-9	C2	180	2	4.00	1.64	1.64	0.086	3.00	1	5.157
	C4	182	2	2.00	9.84	13.12	1.250	3.00	1	7.177
	C6	169	4	2.00	12.30	2.46	0.000	2.00	2	9.517
1007-4	C1	284	2	3.33	0.82	0.82	0.090	3.67	2	7.010
	C3	231	2	5.00	2.46	4.10	0.240	4.00	1	6.543
	C6	242	2	2.00	0.00	2.46	0.090	2.00	2	11.315
1014-9	C1	271	4	2.00	1.64	10.66	1.400	1.00	2	7.416
	C3	272	3	3.67	0.00	7.38	0.270	3.00	1	2.449
	C6	*	3	5.00	1.64	4.92	0.310	2.00	1	0.709
1017-3	C1	459	2	2.00	0.00	7.38	0.250	1.00	3	7.034
	C2	278	2	5.00	1.64	4.92	0.210	4.00	1	1.609
	C4	329	2	2.67	0.00	0.00	0.000	1.00	2	5.488
1042-8	C1	309	1	2.33	9.02	3.28	0.800	1.33	1	2.973
	C3	265	1	3.00	1.64	2.46	0.500	2.33	1	5.198
	C4	478	1	2.33	0.82	2.46	1.000	2.00	1	2.432
1098-9	C2	271	2	2.67	6.56	4.92	0.350	2.00	2	5.673
	C4	*	2	3.00	*	*	*	1.00	2	4.478
	C7	*	2	2.33	*	*	*	1.00	3	5.769
1133-1	C1	286	4	5.00	5.74	9.02	0.350	4.00	3	17.294
	C3	233	4	5.00	6.56	13.94	0.400	4.00	4	6.770
	C6	271	4	5.00	4.92	13.94	0.340	3.00	3	10.006
2819-1	C1	238	4	4.67	13.12	8.20	0.500	2.00	3	5.512
	C3	188	4	4.00	12.30	3.28	0.000	2.00	3	3.930
	C5	274	2	5.00	19.68	36.90	12.000	5.00	*	*
6051-1	C1	300	2	3.33	1.64	0.82	0.070	4.00	1	6.201
	C4	277	2	4.00	0.82	0.00	0.000	4.00	3	4.767
	C6	271	4	3.67	4.10	7.38	0.550	3.00	4	12.783
2820-1	C1	252	2	3.67	13.12	12.30	0.375	2.67	1	5.193
	C4	223	4	3.33	22.14	41.00	7.350	2.33	1	4.768
	C6	227	2	4.33	0.00	13.94	0.400	3.00	2	3.792
1021-2	C1	305	2	2.00	0.00	0.82	0.100	3.00	*	*
	C2	266	4	2.00	8.20	8.20	0.350	2.00	4	9.451
	C4	246	2	2.00	6.56	0.82	0.050	2.00	2	5.881
2901-4	C1	288	4	5.00	7.38	9.02	0.420	3.00	2	1.677

	C5	259	4	5.00	4.10	9.02	0.780	4.00	2	3.053
	C6	235	4	5.00	4.10	27.06	1.870	4.00	4	8.097
2812-5	C1	229	4	5.00	2.46	6.56	0.510	4.00	*	*
	C4	151	4	5.00	9.84	6.56	0.530	4.00	4	3.006
	C6	225	4	5.00	1.64	7.38	0.420	4.00	4	6.144
1920-7	C2	337	4	4.00	9.84	18.86	0.880	4.00	2	9.530
	C3	*	4	3.33	*	*	*	3.00	3	1.776
	C6	296	4	2.33	0.00	5.74	0.230	1.00	1	3.820
6058-9	C1	316	5	3.00	2.46	17.22	0.830	3.00	*	*
	C3	318	5	3.00	0.00	6.56	0.310	3.00	1	1.759
	C6	248	2	2.67	1.64	2.46	0.520	2.00	1	2.275

Note: * - Unable to collect data from sample

The thickness measurements were performed at 6 random locations along the bar sample. Three measurements were taken at each of the 6 locations and the results averaged. As illustrated in Figure 8, the thickness measurements were normally distributed.

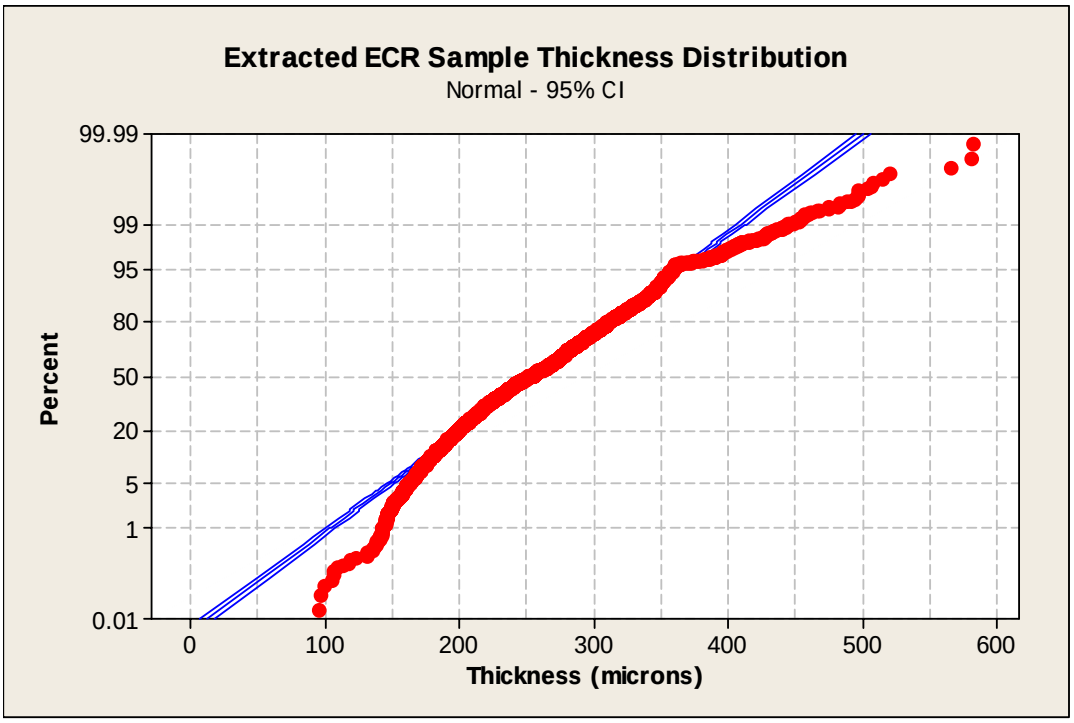

Figure 8. EECR Epoxy Coat Thickness Measurements Distribution

The average thickness measurements and the 95% confidence intervals are presented in Figure 9 with the minimum and maximum specified thickness represented by the two horizontal lines at 175 µm and 300 µm. Three sample sets, 1014-9, 1017-3, and 1042-8 failed to meet the current coating thickness specifications. The average thickness of 1014-9 is 310 µm with a standard deviation of 67.1 µm, the average thickness of 1017-3 is 322 µm with a standard deviation of 78.5 µm, and finally, the average thickness of 1042-8 is 335 µm with a standard deviation of 79.1 µm. The average thickness of the three specimens is above the maximum current specification. There were no samples failing the minimum specified thickness.

Color Change

Since a change in color from the original glossy green can be an indicator of coating degradation, this color change was recorded on a scale from 1 through 5, and the interpretation scale is presented in Methods and Materials. From the sample population, the coating color of two structures showed no apparent change from new. The structures were 1003-3 and 1042-8. The remaining structures all presented some degree of coating color degradation with most experiencing loss of gloss rather than pigmentation. The distribution of color values is presented in Figure 10, while the mean and the standard deviation of each structure are presented in Figure 11.

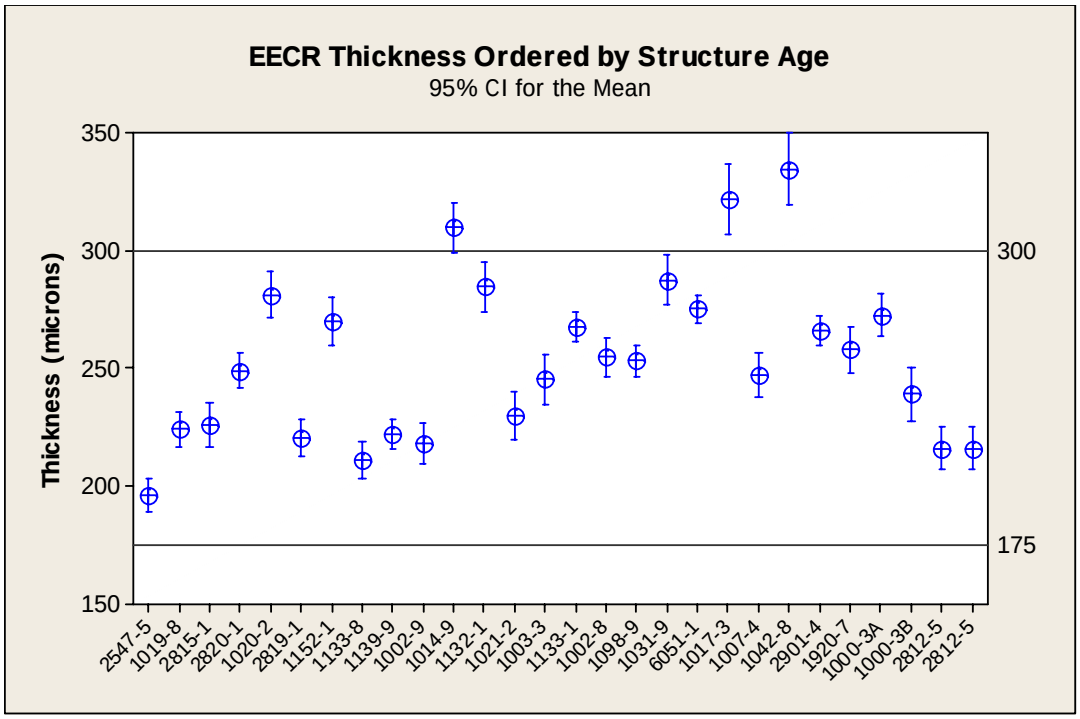

Figure 9. EECR Coating Thickness

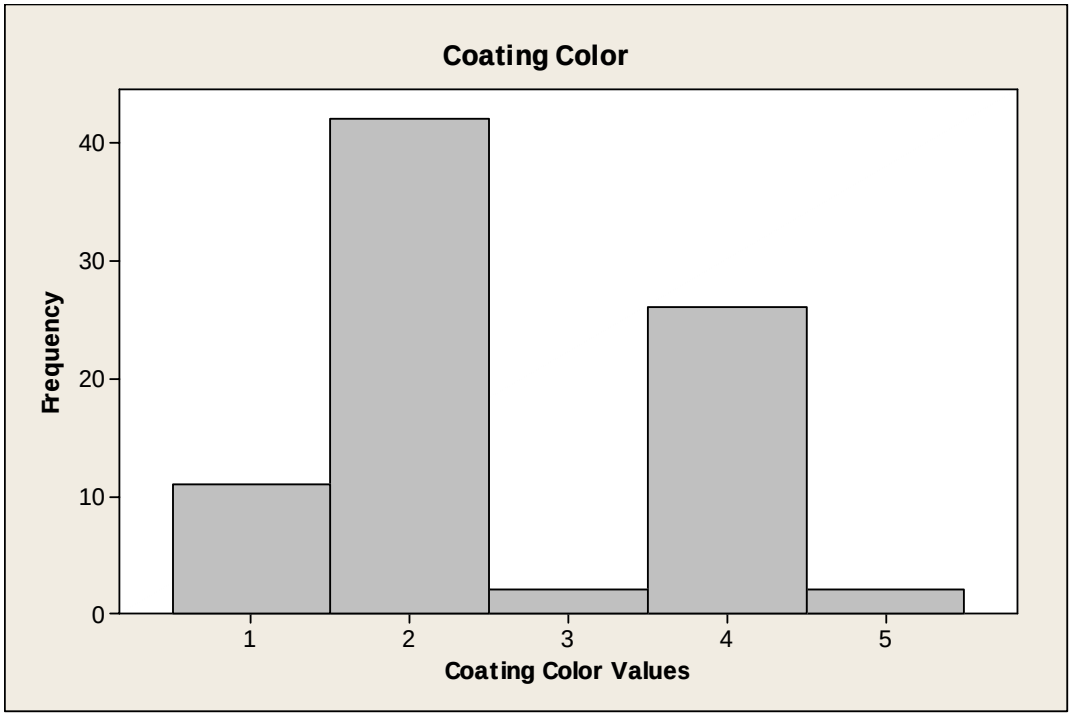

Figure 10. Coating Color Distribution

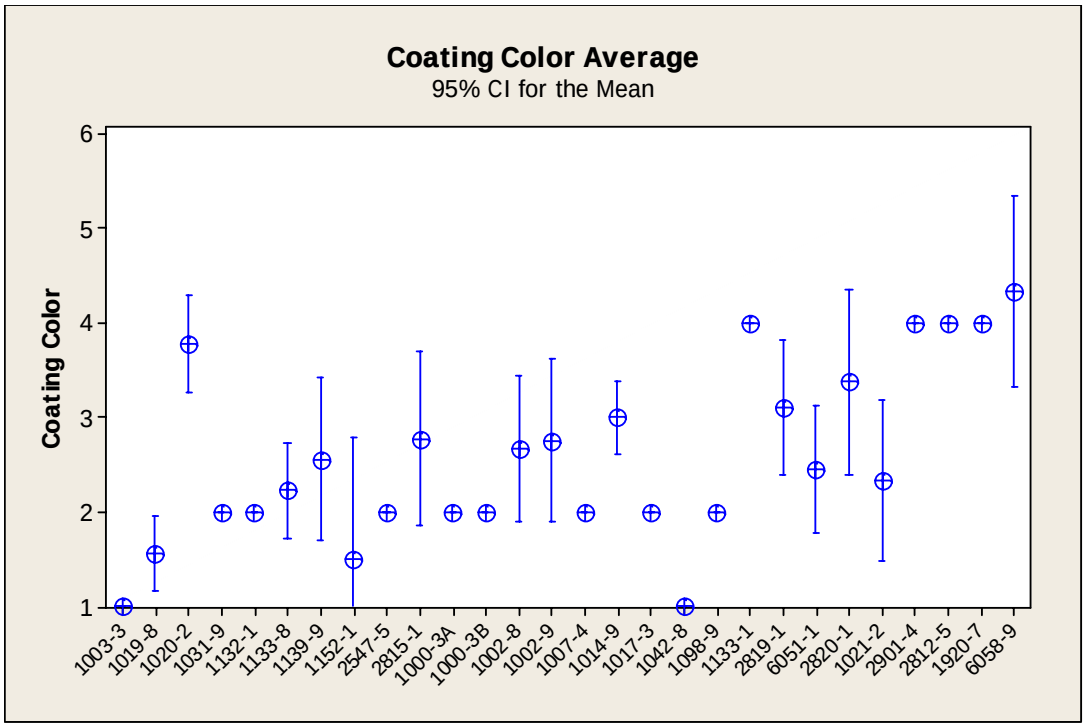

Figure 11. EECR Coating Color

Residual Adhesion

Loss of adhesion between the epoxy coating and the steel surface rebar upon aging was significant. From a total of 666 measurements, only 18 exhibited no adhesion loss. From the remaining 648 measurements, 229 samples showed a complete loss of adhesion. All the remaining samples showed some level of adhesion loss with RA values ranging from 2 to 4. This information is illustrated in Figure 12 while the average and 95% confidence interval are presented in Figure 13. While there were a limited number of individual samples that showed no adhesion loss, every single structure investigated exhibited adhesion loss to some degree. Additionally, one structure, 2812-5, exhibited complete adhesion loss with an average of 5 and a standard deviation of 0, while six additional structures had RA averages greater than 4, indicating an almost complete loss of adhesion.

Holidays

From a total of 244 individual specimens, 37 had no holidays while 74 had 3 holidays or less per meter. The remaining 133 specimens had more than the allowable 3 holidays/m as currently specified. Conversely, out of 28 structures investigated, the average number of holidays/m to EECR bar of 18 structures failed to meet the maximum allowable number of holidays. Structure 1017-3 exhibited the lowest number of holidays with an average of 0.67 holidays/m and a standard deviation of 0.82 holidays/m. Structure 2547-5 exhibited the highest number of holidays with an average of 18.04 holidays/m and a standard deviation of 12.80 holidays/m. The average number of holidays/m and the 95% confidence intervals are presented in Figure 14 with the maximum specified number of holidays/m represented by the horizontal

line at 1 holiday/0.31m. The number of holidays/m is also highly positively skewed as shown in Figure 15.

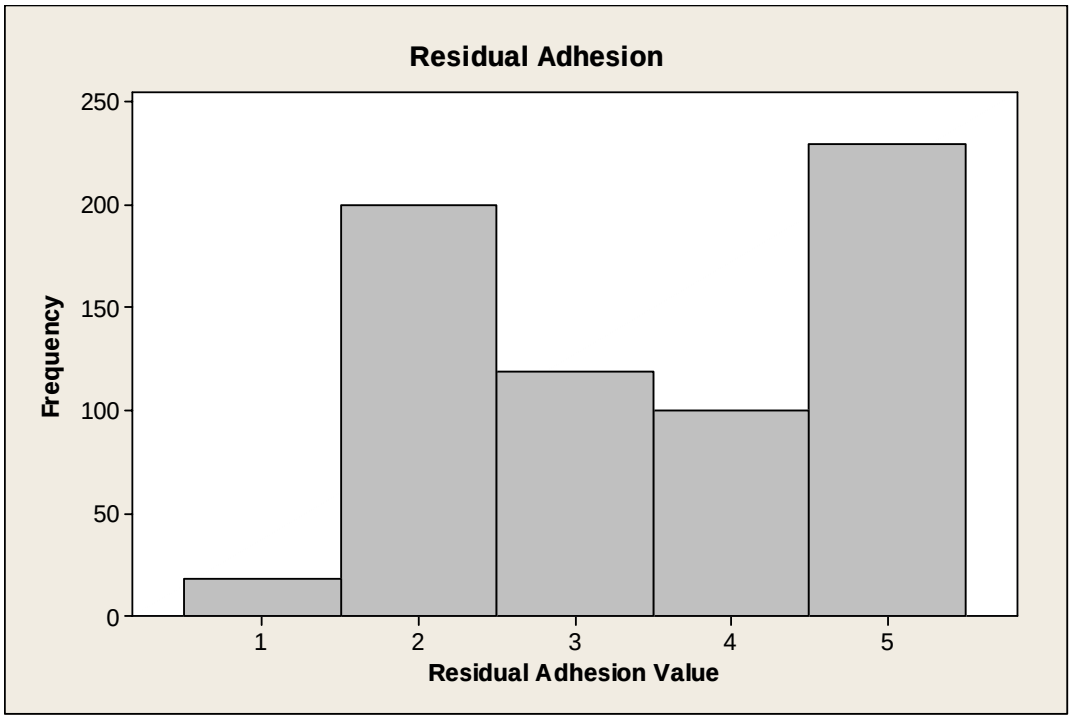

Figure 12. EECR Residual Adhesion Distribution

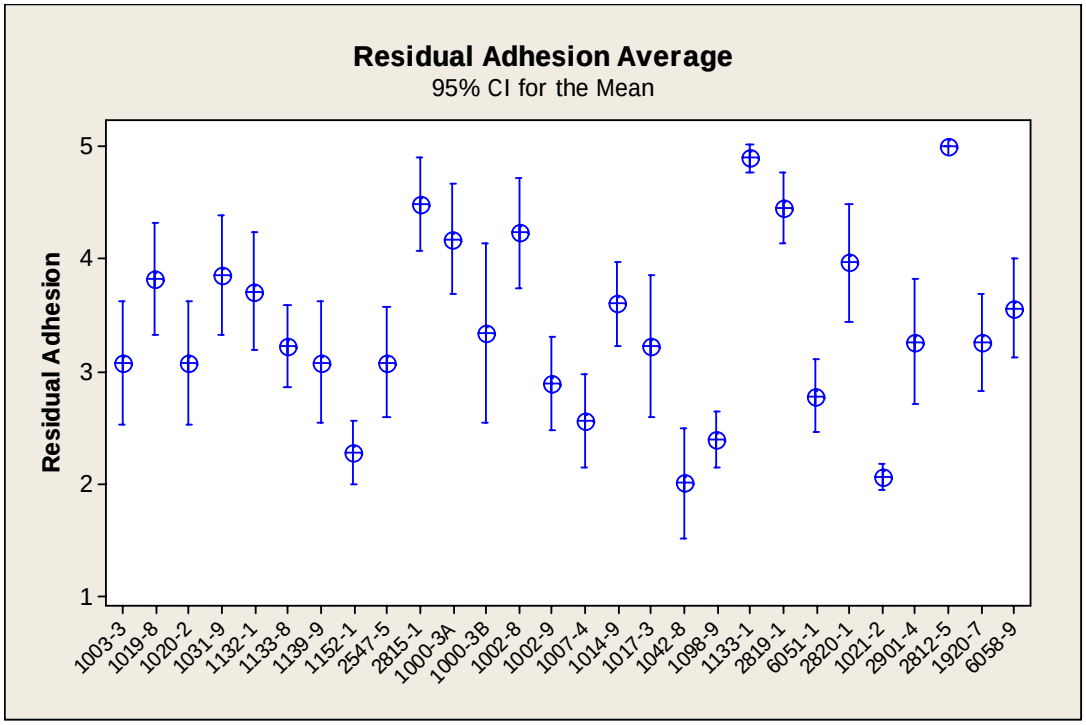

Figure 13. EECR Residual Adhesion

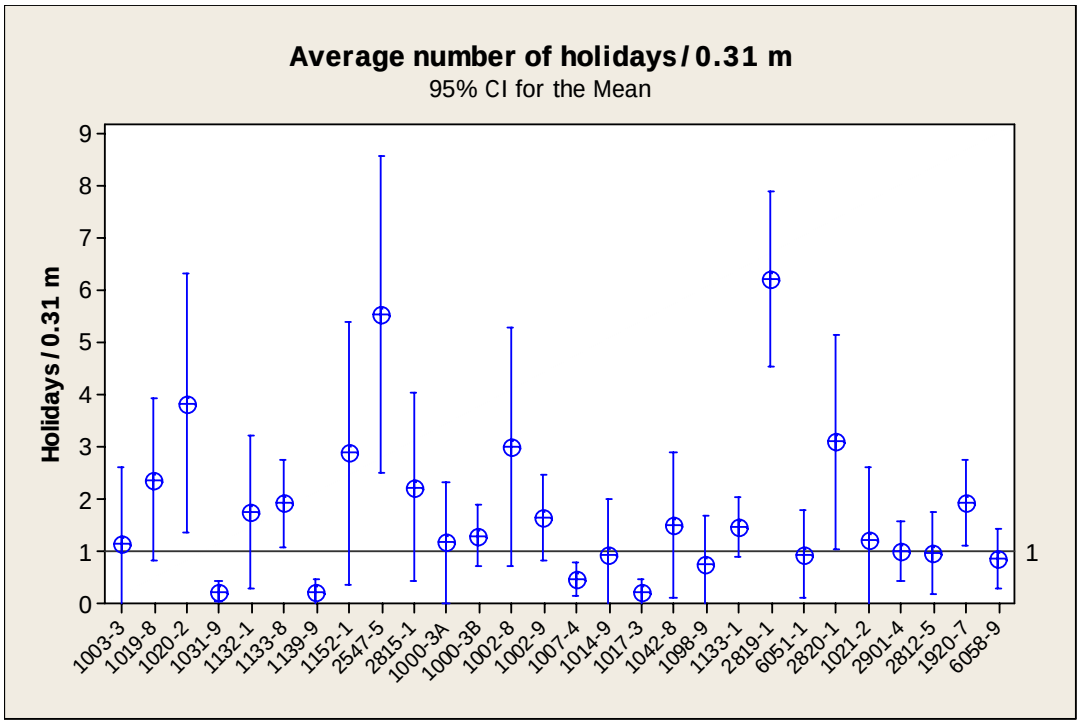

Figure 14. EECR Holidays

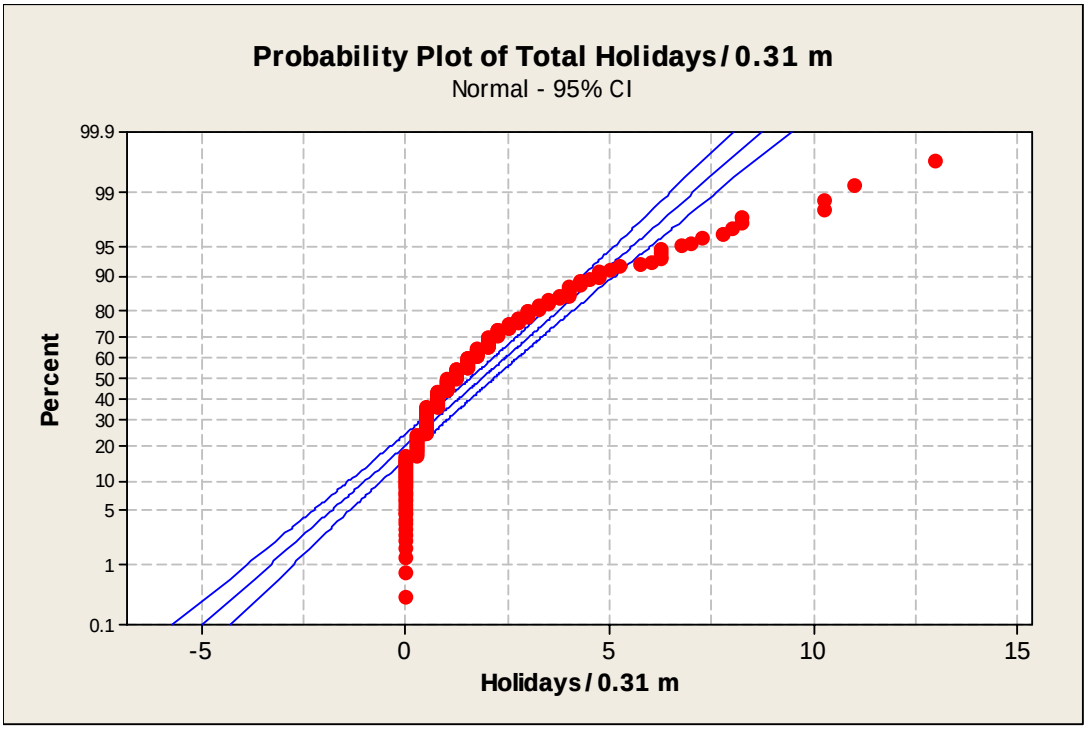

Figure 15. EECR Holiday Probability Plot

Damages

Similarly, the number of visible damages was also assessed. The number of damages follows a similar probability distribution as the holidays, as illustrated in Figure 16. Interestingly,

there were no structures with zero damages per 0.31 m as shown in Figure 17. The lowest number of damages was shown by structure 1021-2 with 1.77 damages/m and a standard deviation of 3.18. Structure 1019-8 had a similarly low number of damages with 1.84 damages/m, but a significantly lower standard deviation at 1.64. The highest number of damages was exhibited by structure 1020-2 with 20.00 damages/m and a standard deviation of 4.5. The average number of damages for the entire sample population is 8.04 damages/m and a standard deviation of 8.13. There were however, individual bars with zero counted damages. Specifically, out of 244 individual specimens, 26 specimens had 0 damages/m, while 46 specimens had 3 damages/m or less. This leaves 172 specimens with more than 3 damages/m and one sample with damages as high as 50.02 damages/m.

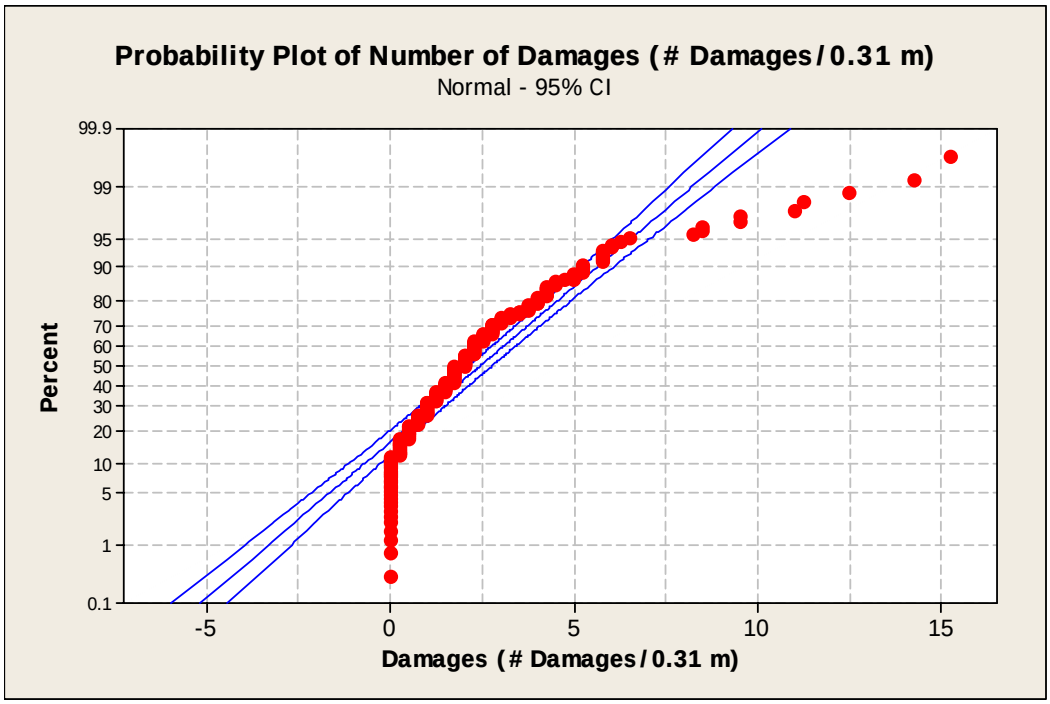

Figure 16. EECR Number of Damaged Areas Probability Plot

Corroded Area

The probability distribution of the measured percent corroded area followed a pattern similar to the holidays and the number of damages as illustrated in Figure 18. As with the number of damages, there were no structures showing absolutely no signs of corrosion although there were individual bars that showed no visible signs of corrosion. The average percent corroded area and the standard deviation of each structure are presented in Figure 19. Out of 244 specimens, 28 showed no visible signs of corrosion leaving 216 specimens with corrosion ranging from a low of 0.05% to a high of 12%. From the investigated structures, 1132-1 showed the least average amount of visible corrosion with 0.15% corroded area and a standard deviation of 0.14. Structure 2820-1 had the greatest corrosion with an average of 3.57% corroded area and a standard deviation of 3.49. The total average for the sample population is 0.59% corroded area with a standard deviation of 1.22.

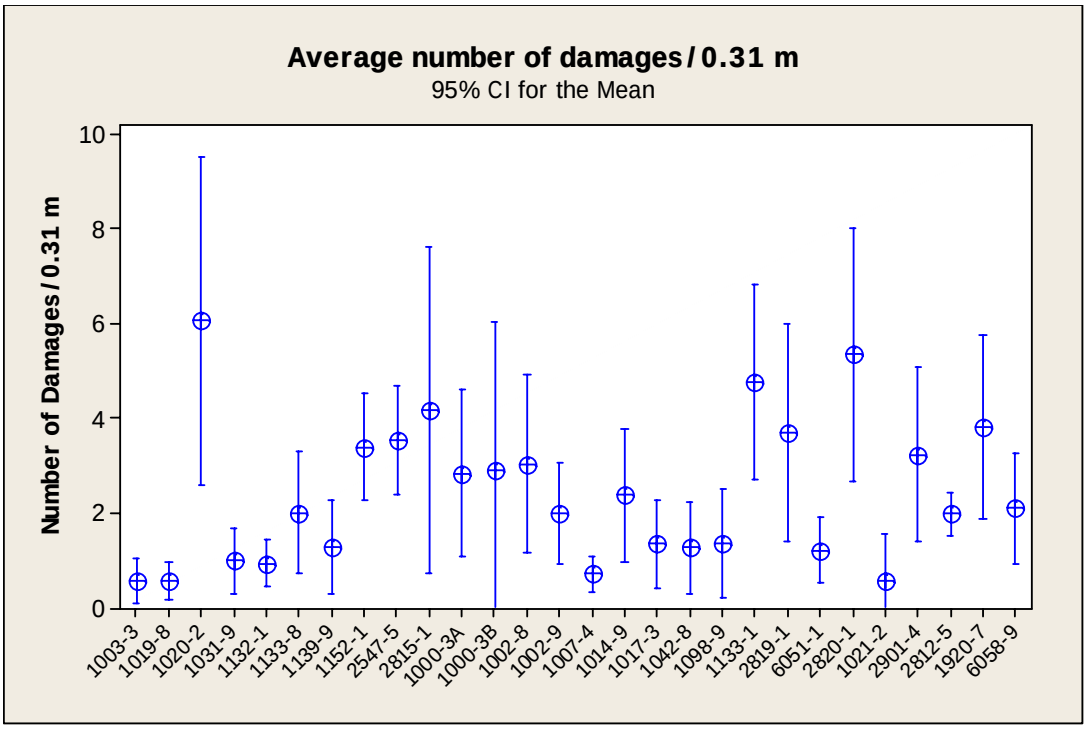

Figure 17. EECR Number of Damaged Areas

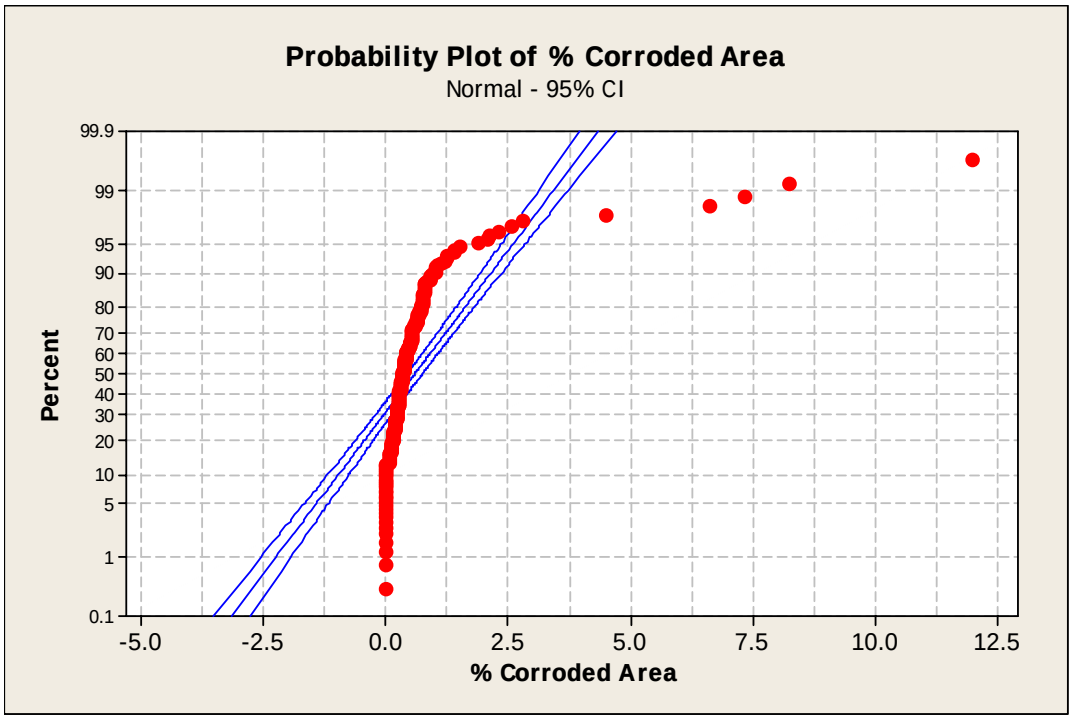

Figure 18. EECR Percent Corroded Area Probability Plot

Coating Cracking and Porosity

A coating cracking value was assigned to each examined specimens using a 2000x magnification scanning electron micrograph. Figure 20 illustrates the average and 95% confidence interval for each structure. The coating samples of only three structures showed no cracking. Those structures were: 1031-9, 1042-8 and 6058-9. The remaining structures presented a mean of 2 with a standard deviation of 1.

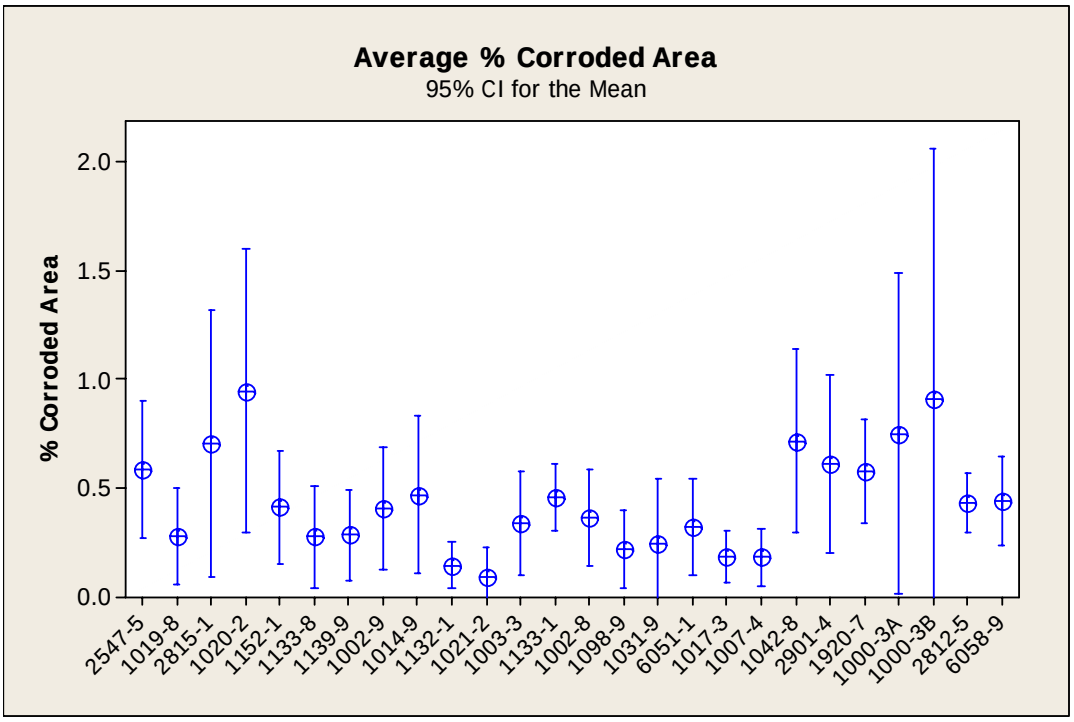

Figure 19. EECR Percent Corroded Area

The average percent cracking and porosity for each structure are presented in Figure 21. Structure 6058-9 had the lowest percent cracking and porosity with an average 2.017 and a standard deviation of 0.37. Structure 1133-1 had the highest percent cracking and porosity with an average of 11.36 and a standard deviation of 5.39. Out of the individual samples examined, sample 1014-9 C6 had the lowest percent cracking and porosity with 0.71, while sample 1133-1 C1 had the highest percent cracking and porosity with 17.29. The total average and standard deviation for the entire sample population were determined to be 5.77 and 3.16, respectively. Unlike holidays and the number of damaged areas, the percent cracking and porosity were normally distributed as illustrated in Figure 22.

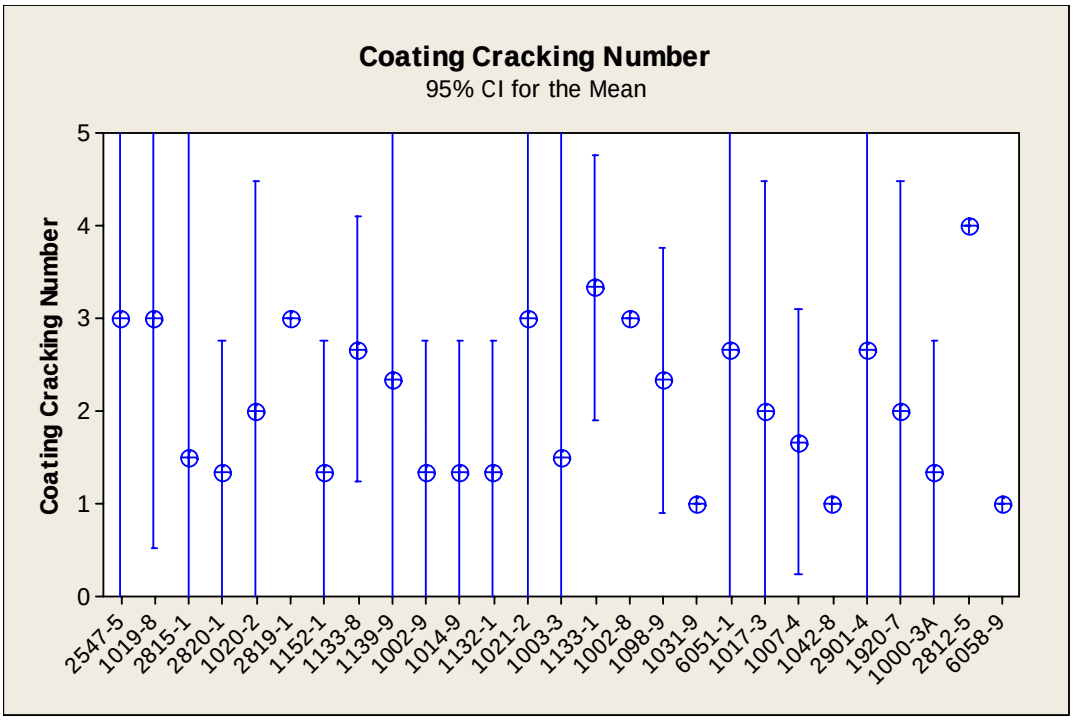

Figure 20. EECR Coating Cracking

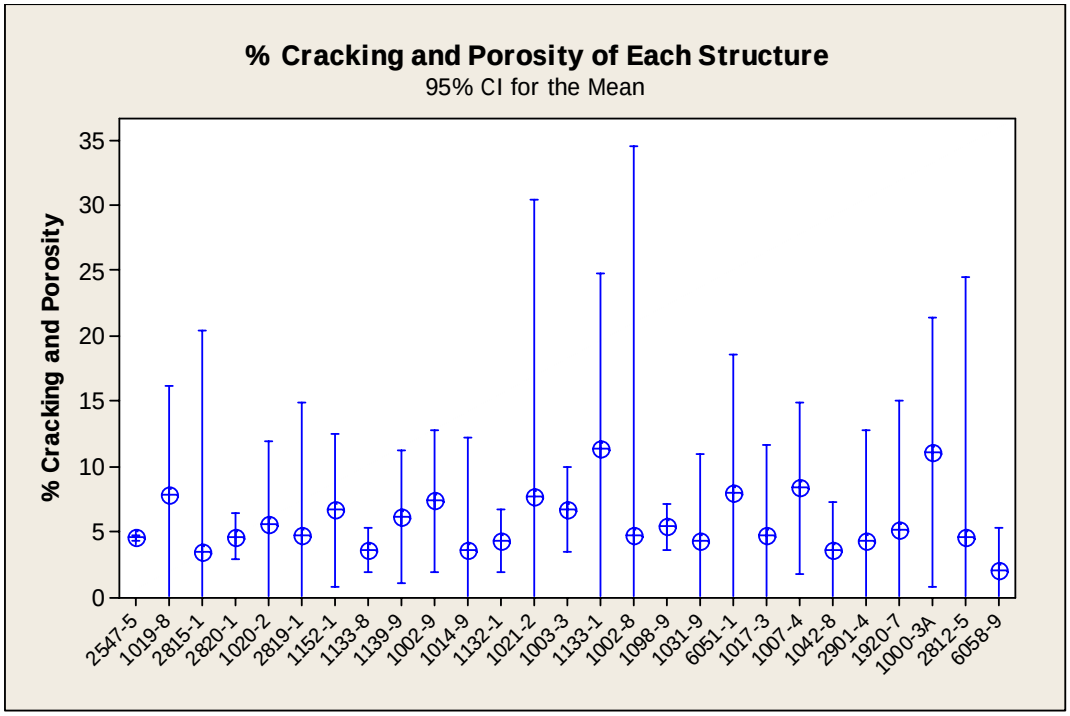

Figure 21. EECR Percent Cracking and Porosity

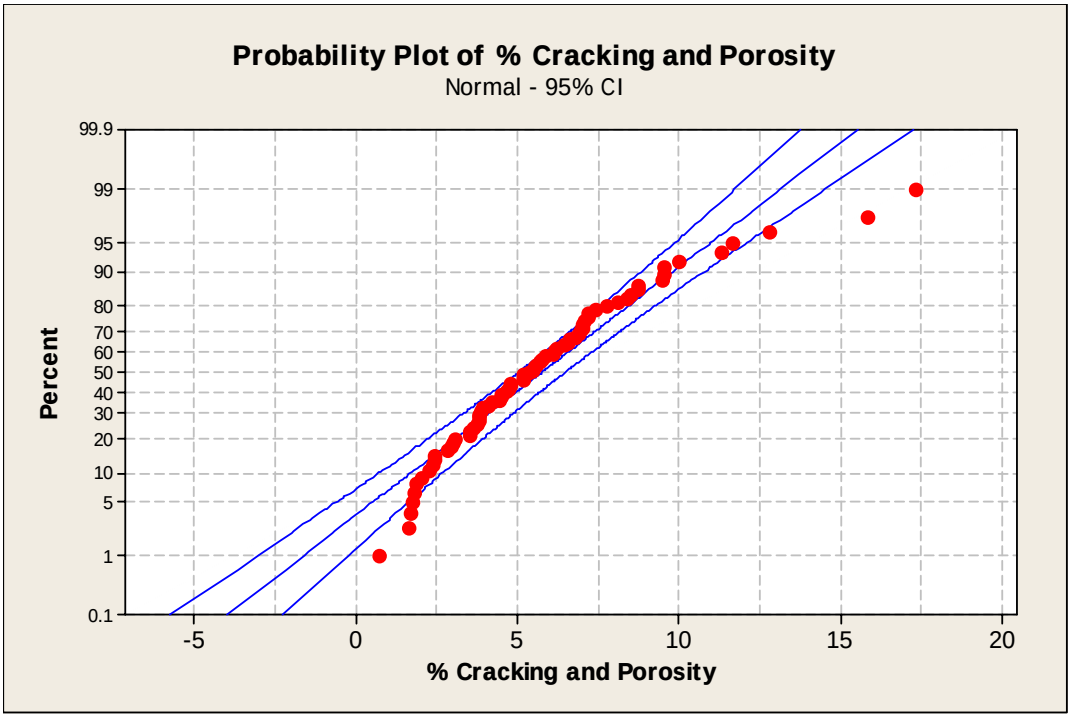

Figure 22. EECR Percent Cracking and Porosity Probability Plot

Deck Survey

The non-destructive corrosion activity data as well as the concrete chloride concentration at the level of the reinforcing bar are presented in Table 13.

Table 13. Corrosion Measurements and Chloride Concentration

Structure	Core Sample	Ecorr (-mV)	R (kΩ-cm)	icorr (μA/cm^2)	Cl at Bar Level (kg/m^3)
1003-3	C2	284	17.678	7.2911	0.860
	C7	295	12.497	15.6906	0.099
	C1	200	13.106	9.5181	0.140
1019-8	C1	331	33.528	2.2270	0.000
	C4	341	29.870	3.1792	0.287
	C5	364	30.175	2.6307	0.176
1020-2	C1	243	76.200	7.2294	0.504
	C3	296	140.208	0.4140	0.001
	C6	387	60.960	13.0188	1.790
1031-9	C1	257	30.480	0.7560	0.454
	C4	260	16.154	0.7663	1.260
	C5	452	28.042	0.7046	0.998
1132-1	C1	251	12.802	16.1261	1.070
	C4	298	16.154	17.6073	0.973
	C6	435	10.668	23.6966	2.340
1133-8	C1	124	30.480	1.6569	0.001
	C3	220	30.480	1.9373	0.001
	C5	172	29.870	2.1232	0.001
1139-9	C1	386	24.689	0.8495	0.001
	C3	527	18.288	1.0354	0.001

	C6	273	30.480	0.7355	0.001
1152-1	C1	245	143.256	0.5177	0.053
	C2	107	161.544	7.9229	0.105
	C3	328	143.256	2.2008	0.086
2547-5	C1	131	51.816	1.6672	0.000
	C2	118	64.008	1.5121	0.000
	C6	*	79.300	*	0.019
2815-1	C1	290	295.656	2.4447	0.001
	C3	318	204.216	8.9172	0.001
	C6	313	304.800	2.8064	0.001
1000-3A	C1	319	161.544	2.3410	0.006
	C2	237	158.496	2.0503	0.024
	C4	283	185.928	2.3307	0.001
1000-3B	C1	*	*	*	*
	C2	*	*	*	*
	C4	*	*	*	*
1002-8	C1	334	70.104	4.9922	0.001
	C3	256	97.536	3.6157	0.013
	C4	320	64.008	4.9090	0.001
1002-9	C2	161	30.480	2.0092	0.058
	C4	308	30.480	4.6090	0.001
	C6	265	60.960	3.6353	0.001
1007-4	C1	380	15.545	0.3832	0.204
	C3	294	25.298	0.8186	0.001
	C6	265	48.768	3.2418	0.055
1014-9	C1	289	82.296	2.5269	0.050
	C3	159	70.104	2.6204	0.001
	C6	262	64.008	1.8130	0.001
1017-3	C1	313	124.968	0.7355	1.350
	C2	277	143.256	0.7046	1.600
	C4	242	124.968	0.9112	0.000
1042-8	C1	697	30.480	2.7793	4.570
	C3	393	36.576	6.0762	0.021
	C4	*	30.180	*	0.015
1098-9	C2	309	112.776	1.2018	0.145
	C4	299	137.160	1.4289	0.147
	C7	270	82.296	1.3672	0.066
1133-1	C1	403	12.802	5.7791	1.353
	C3	208	15.240	3.8633	0.162
	C6	313	12.802	25.0124	2.822
2819-1	C1	168	121.920	8.3275	0.138
	C3	188	167.640	9.0835	0.352
	C5	202	88.392	9.9115	5.020
6051-1	C1	193	14.935	0.5486	0.177
	C4	285	10.058	0.3420	0.867
	C6	305	11.278	2.4550	0.249
2820-1	C1	154	167.640	10.6778	0.001
	C4	141	164.592	9.7358	0.001
	C6	210	158.496	5.9557	0.001
1021-2	C1	285	152.400	0.6420	0.034
	C2	328	131.064	0.5803	0.037
	C4	277	152.400	0.4037	0.066
2901-4	C1	342	36.576	7.5191	0.642

	C5	315	36.576	10.8853	0.001
	C6	277	39.624	11.7142	0.055
2812-5	C1	222	33.528	6.8668	1.275
	C4	262	33.528	6.9809	0.008
	C6	290	51.816	3.1381	0.081
1920-7	C2	287	21.946	26.5039	1.839
	C3	437	30.175	0.6215	0.937
	C6	405	33.528	0.5177	0.709
6058-9	C1	278	64.008	0.8906	0.001
	C3	255	51.816	0.2383	0.001
	C6	264	42.672	0.2467	0.008

Note: * - Data unavailable

Resistivity

For the resistivity range of values, the interpretation guidelines proposed by Feliu et al were chosen (Feliu, et al., 1996) and are presented as the three horizontal lines at 10, 50 and 100 kΩ-cm in Figure 24. From 10 to 50 kΩ-cm the potential corrosion rate is high to moderate; between 50 and 100 kΩ-cm the potential corrosion rate is low; above 100 kΩ-cm the potential corrosion rate is negligible. Based on these interpretation guidelines, almost half of the structures investigated, 13 structures, lie within the high to moderate potential corrosion rate region while 5 structures are located in the low potential corrosion rate region of Figure 23. The remaining 9 structures theoretically would have low potential corrosion rates or the concrete was too dry to support a high or moderate active corrosion when tested.

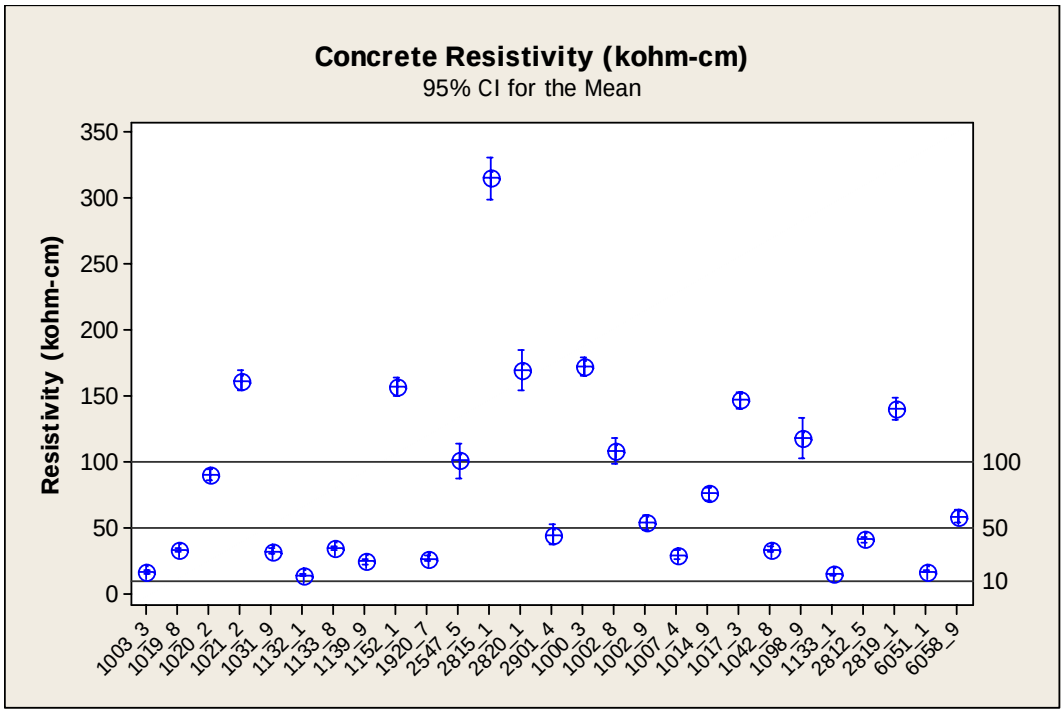

Figure 23. EECR Structures Concrete Resistivity

Half-cell Potentials

The corrosion half-cell potentials are presented in Figure 24 with the horizontal lines at -200 mV and -350 mV representing the current interpretation guidelines for uncoated bar. The corrosion activity in the majority of the bridges investigated, based on half-cell potential measurements is uncertain. Three structures, 1139-9, 1142-8 and 1098-9 showed high probability of corrosion occurring with average half-cell potential measurements of -380 mV, -434 mV and -364 mV, respectively. Four structures, 1133-8, 2547-5, 2820-1 and 2819-1 showed very low probability of corrosion occurring with average half-cell potential measurements of -177 mV, -164 mV, -149 mV and -162 mV, respectively.

Corrosion Rates

The corrosion rates, obtained using an unguarded 3LP instrument, are presented in Figure 25. The horizontal lines at 0.2, 1 and 10 µA/cm^2 represent the instrument provided interpretation guidelines for uncoated bar (Clear, 1989). From the figure, it is clear that the majority of structures investigated are located between 1 and 10 µA/cm^2. In that region, damage to concrete due to corrosion activity is expected to take place between 2 to 10 years. Two structures, 1003-3 and 1031-9 presented significantly higher corrosion rates with values of 16.8 and 21.1 µA/cm^2, respectively. In these cases, concrete damage due to corrosion activity is expected to occur within 2 years or less. Five structures, 1021-2, 1031-9, 1139-9, 1017-3 and 6058-9 presented very low corrosion rates with damage due to corrosion activity expected between 10 to 15 years.

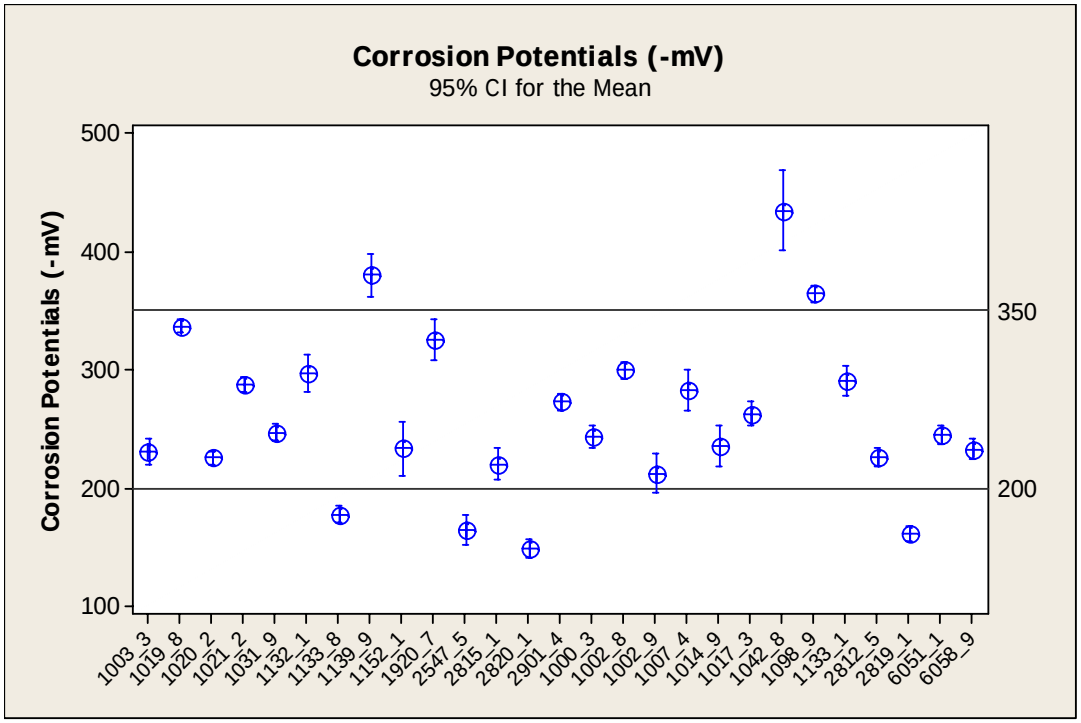

Figure 24. EECR Structures Corrosion Potentials

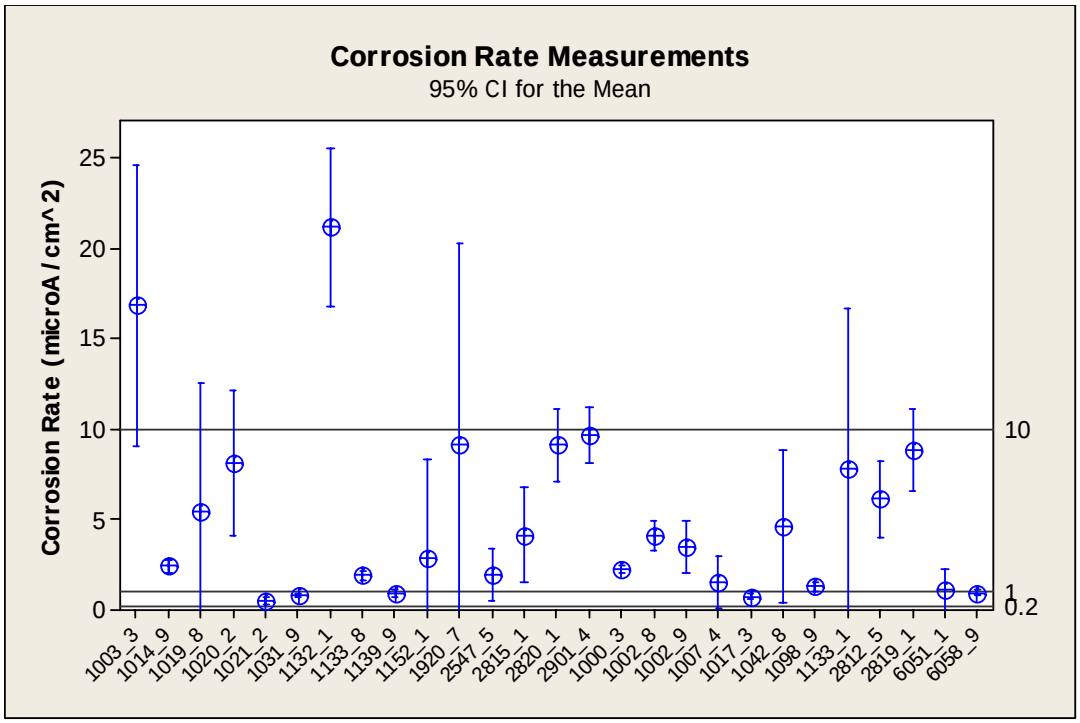

Figure 25. Corrosion Rate Measurements

Chloride

Figure 26 illustrates the average chloride concentration at bar level, while the reference line at 0.71 kg/m^3 of concrete represents a conservatively low corrosion initiation level for uncoated bar. With the exception of five structures, the chloride concentration at bar level was below a commonly used corrosion initiation threshold of 0.71 kg/m^3 of concrete. The five structures that exhibited higher chloride concentrations were: 1132-1, 1133-1, 1920-7, 1042-8 and 1031-9. The average chloride concentration of these structures was 1.78, 0.99, 1.06, 1.54 and 0.71 kg/m^3 of concrete, respectively.

Micro-photographs

Finally, SEM and EDS analyses were performed. Figure 27 illustrates an electron scanning micrograph of structure 1020-2 C6. The EDS spectra were collected at the numbered locations and are presented in Figures 28, 29 and 30.

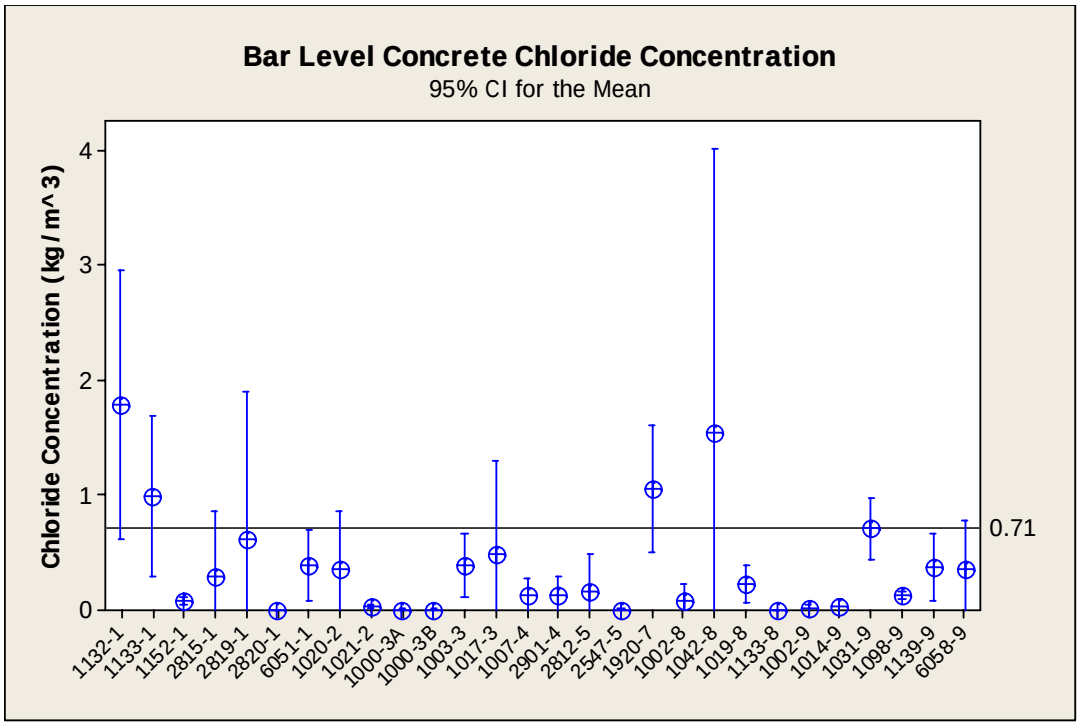

Figure 26. Concrete Chloride Concentration at Bar Level

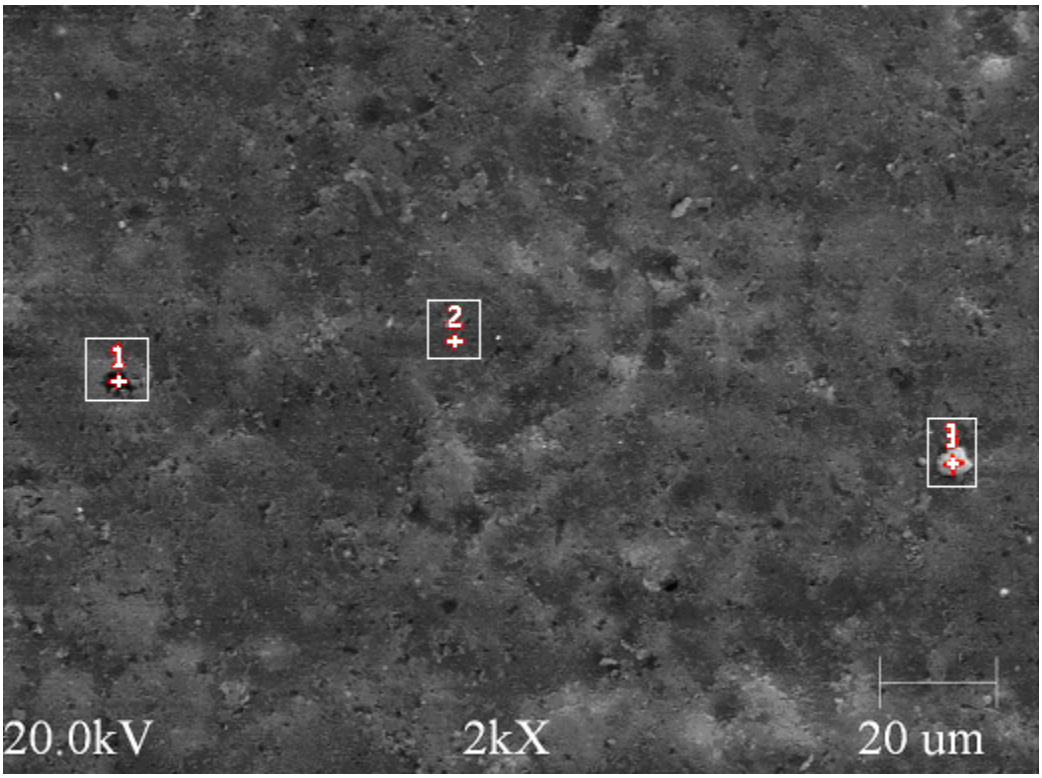

Figure 27. Structure 1020-2 C6 SEM Micrograph

The spectrum at location 1 (Figure 28) would indicate that the pore in the coating is continuous to the steel substrate. Although the signals are weak due to interference from the

pore walls, iron still presents the strongest peak, followed by silica, chloride, potassium and calcium, which may all be found in the concrete pore solution. Location 2 (Figure 29) spectra is dominated by the carbon signature as expected from an organic coating. There are traces of other elements that are commonly found in concrete or the concrete pore solution. This is due to adsorption of the pore solution on the coating surface. Finally, the third spectrum (Figure 30) illustrates the typical signature of cement. There is no carbon present, as expected from an organic coating, but the calcium and the silica signatures dominate.

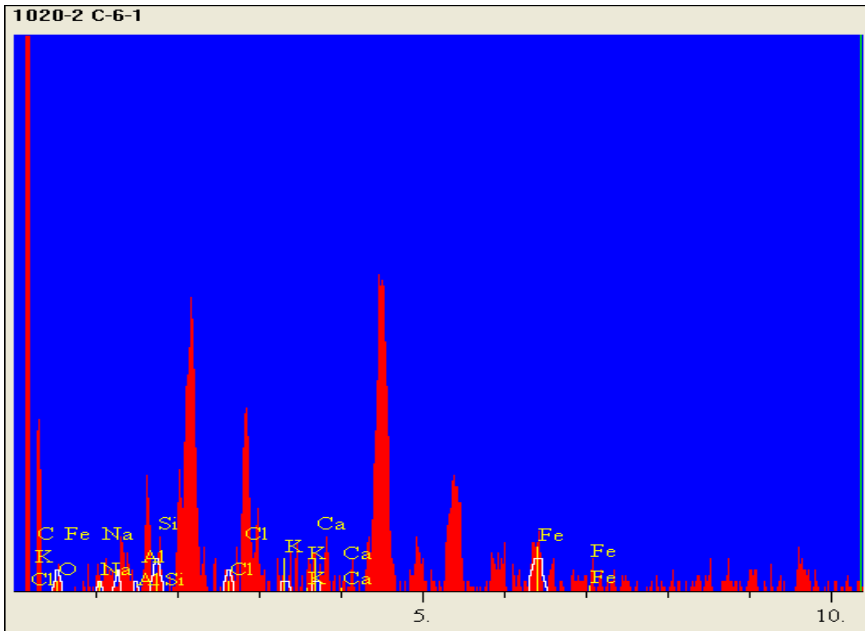

Figure 28. EDS Spectra 1020-2 C-6-1

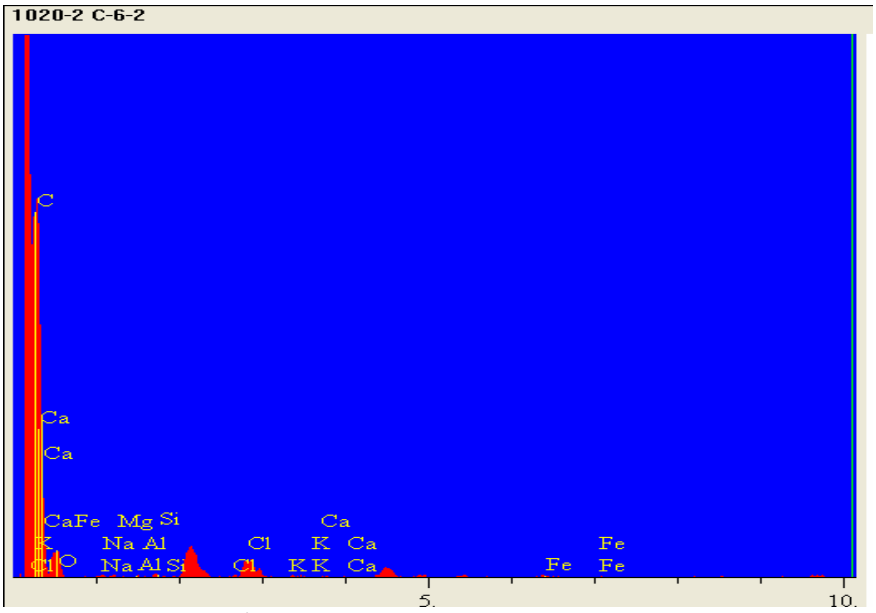

Figure 29. EDS Spectra 1020-2 C-6-2

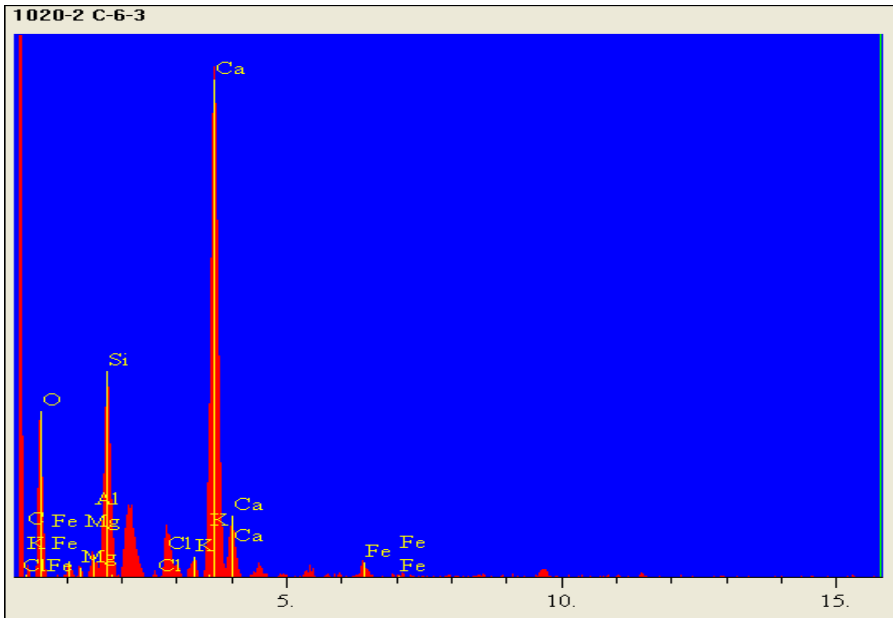

Figure 30. EDS Spectra 1020-2 C-6-3

DISCUSSION

Analysis of the data revealed several coating conditions; specifically, the extent of coating surface cracking, the insufficient degree of coating curing and the generalized loss of adhesion. The ramifications of these conditions as well as other correlations will be discussed in detail in the following subsections.

Coating Cracking

The presence of micro-cracks on the fusion-bonded epoxy coating surface has been established by a previous study (Wheeler, 2003) that also provided a visual assessment guide. Several coating and exposure parameters were investigated during the course of this current study to determine if any correlations exist. The presence of cracking in new ECR samples before embedment into concrete as well as the extent of cracking in extracted ECR samples was confirmed and ranked.

With the exception of only one new specimen (WWBVT-S4), which is presented in Figure 31, no map-like cracking was noted in the remaining new ECR samples. Based on the interpretation guide, WWBVT-S4 was assigned a cracking value of 3. The colors in Figure 31 were inverted for better contrast. Unlike the new ECR samples, the majority of the extracted ECR samples showed surface coating cracking spanning the severity scale with a total average cracking value of 2. This significant difference between the new and the extracted ECR samples indicates that while it is possible that there are factors that may contribute to coating cracking prior to concrete embedment, the majority of the cracking occurs in concrete.

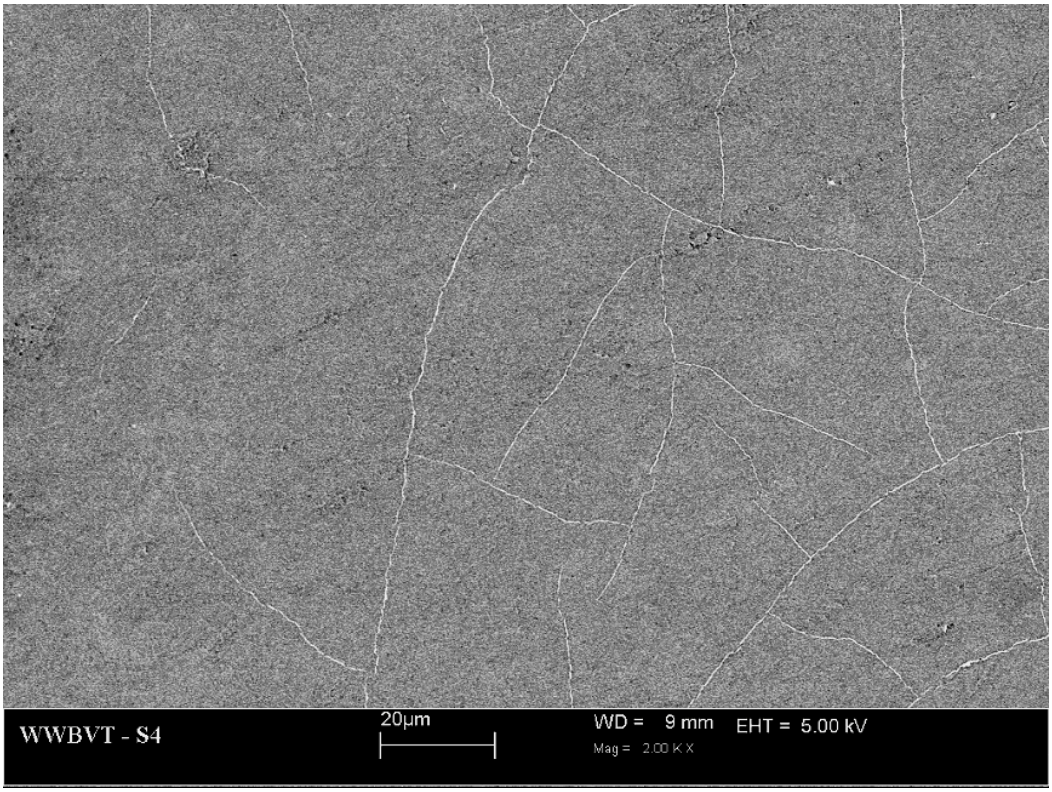

Figure 31. New ECR WWBVT – S4 cracking SEM micrograph

Using a confidence level of 80% allows for the inclusion of chlorides at bar level, residual adhesion, color of corrosion products under the coating and % moisture as cracking prediction parameters. The individual P-values were 0.171, 0.115, 0.118 and 0.186, respectively. Further regression performed using only the parameters with P-values ≤ 0.20 ultimately yielded only the coating color as the strongest predictor of coating cracking. At the 95% confidence level, the coating color P-value was 0.003. Based on individual correlations, excluding combined effects, the cracking value correlated with the % moisture, with a Pearson correlation value of 0.637 and a P-value of 0.001 (Figure 32).

While the change in coating glossiness and/or color, residual adhesion, and the color of the corrosion products under the coating may simply be a result of and not the cause of coating degradation; percent moisture content relationship points to hydrothermal degradation coupled with chloride induced ageing. Furthermore, prior exposure to UV light exacerbates the effect of hydrothermal ageing in the presence of chlorides (Kotnarowska, 1999). Apicella showed that in a DGEBA based epoxy "micro-cavities can be formed by effect of crazing in the plasticized system exposed to high temperatures" in the presence of moisture (Apicella, 2003). Although the ECR steel embedded in concrete may not necessarily be exposed to high temperatures as were the samples tested by Apicella (i.e. 100°C), bridge deck concrete at bar level commonly reaches 40°C in Virginia while the relative humidity of the concrete at bar level can vary between 75 and 100% (Liu, 1996). Additionally, the bars themselves may be exposed to temperatures as high as 50°C prior to embedment in concrete. As such, hydrothermal ageing effects may not become evident for several years.

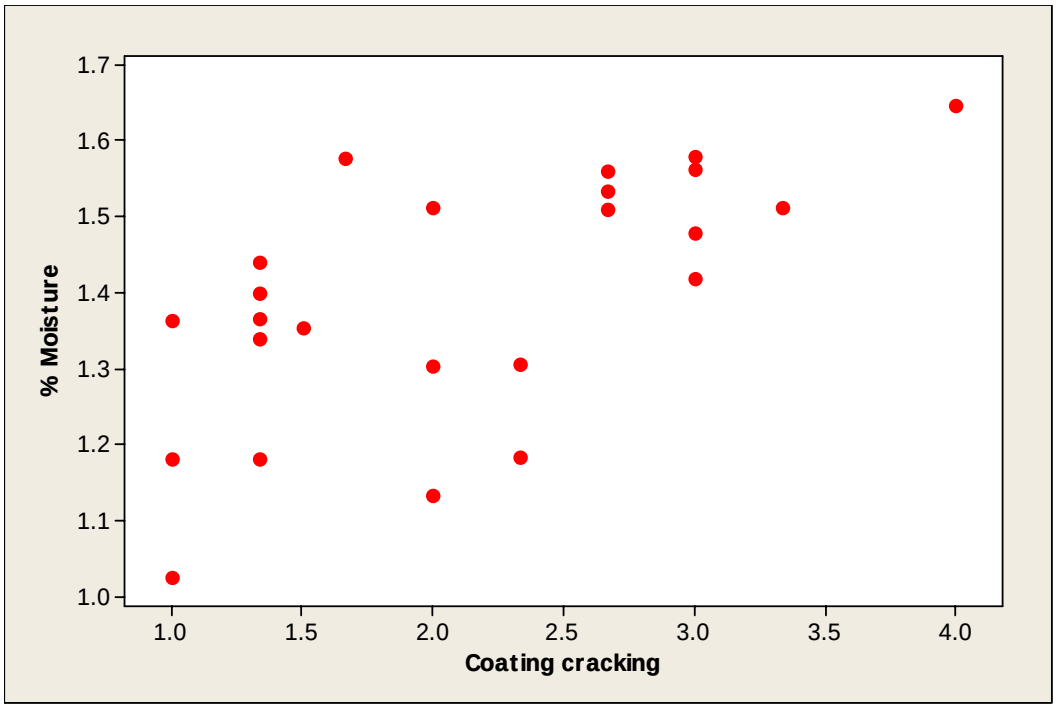

Figure 32. EECR scatter plot of % moisture vs. coating cracking

Degree of Coating Curing

Coating samples from both the new as well as the extracted specimens were not fully cured as demonstrated by the DSC data presented in the previous section. The new ECR samples show a minimal degree of improvement, but statistically there are no differences between the new and the extracted ECR samples as verified by a 2-sample T-test

One of the consequences of the incomplete curing of the coating is its increased absorptivity. The correlation of the moisture content with the ΔT_g in the extracted ECR samples, as illustrated by Figure 33, is an indicator of the porous nature of the coating and not necessarily the plasticizing effects of water.

While the effect of moisture on the T_g of the tested epoxy coating samples is not as trivial as some have suggested (Wheeler, 2003), nor is it so drastic that it explains the entire observed change in T_g. De'Nève and Shanahan were able to show that 1% moisture content leads to an approximately 8°C reduction in T_g when the moisture lies within the epoxy structure (De′Néve, and Shanahan, 1993); however, even based on this temperature reduction rate, there are still structures that exhibit differences in glass transition temperatures as high as 27°C indicating that the coating is indeed not fully cured.

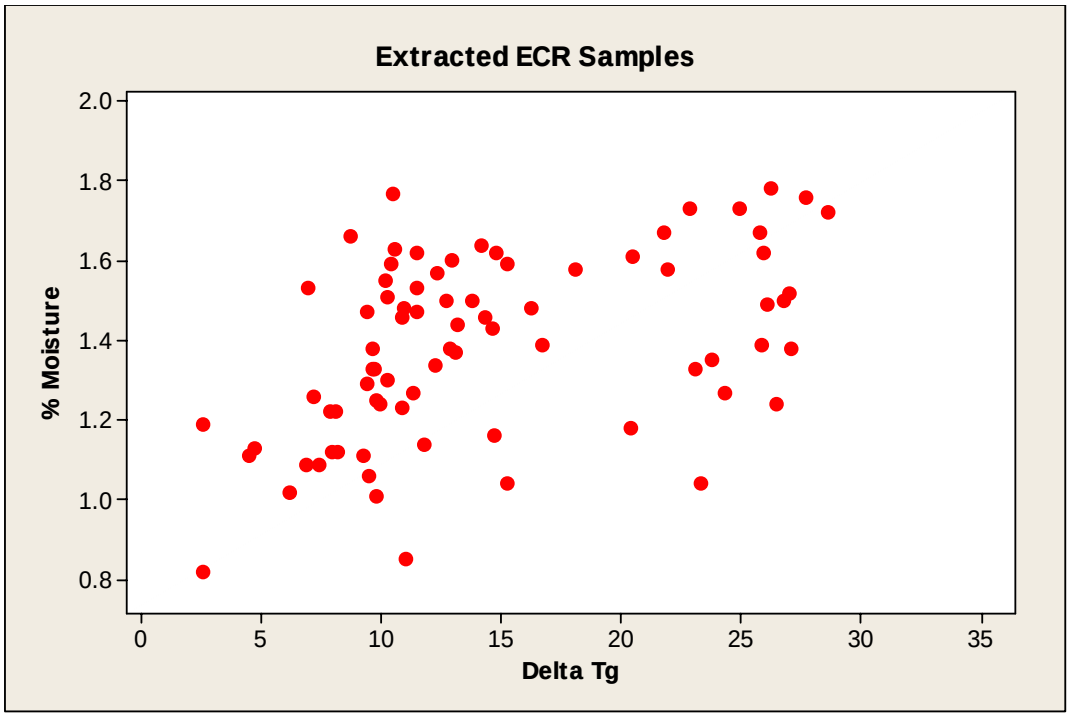

Figure 33. Scatter Plot of % Moisture vs. ΔT_g

The porous structure of coating samples collected from structures 1017-3 C-2 and 2820-1 C-4 is illustrated in Figures 34 and 35. The ΔT_g of sample 1017-3 C-2 is 26.42 °C while the ΔT_g of sample 2820-1 C-4 is 9.63 °C. Both coating samples have capillary-sized pores throughout the bulk of the coating. The size of the pores was 10.4 and 10.2 µm for the 1017-3 C-2 sample and 18.9 and 37.6 µm for the 2820-1 C-4 sample in addition to the multitude of pores 1 µm or less occupying the bulk of the coating. Since the examples of the porous structure presented were obtained from three structures only, we cannot conclusively state that this is a common condition. However, based on the random nature of the investigated samples, this may in fact be the prevailing coating condition. Using the 1% moisture to 8°C conversion leads to ΔT_g due to insufficient curing of 16.50°C and -5.49°C, respectively. The -5.49°C in this case may be explained by the fact that some of the moisture is in fact free or bulk water residing in the large pores, which has no plasticizing effect as does the moisture within the epoxy structure.

The presence of the pore network throughout the bulk of the coating also addresses the question of whether the cracks go to the steel surface as being irrelevant. The large capillaries providing not only open conduits for moisture, oxygen, and later chloride transfer between the concrete environment and the steel substrate, but also crevices which allow moisture to collect creating an ionic conductive path.

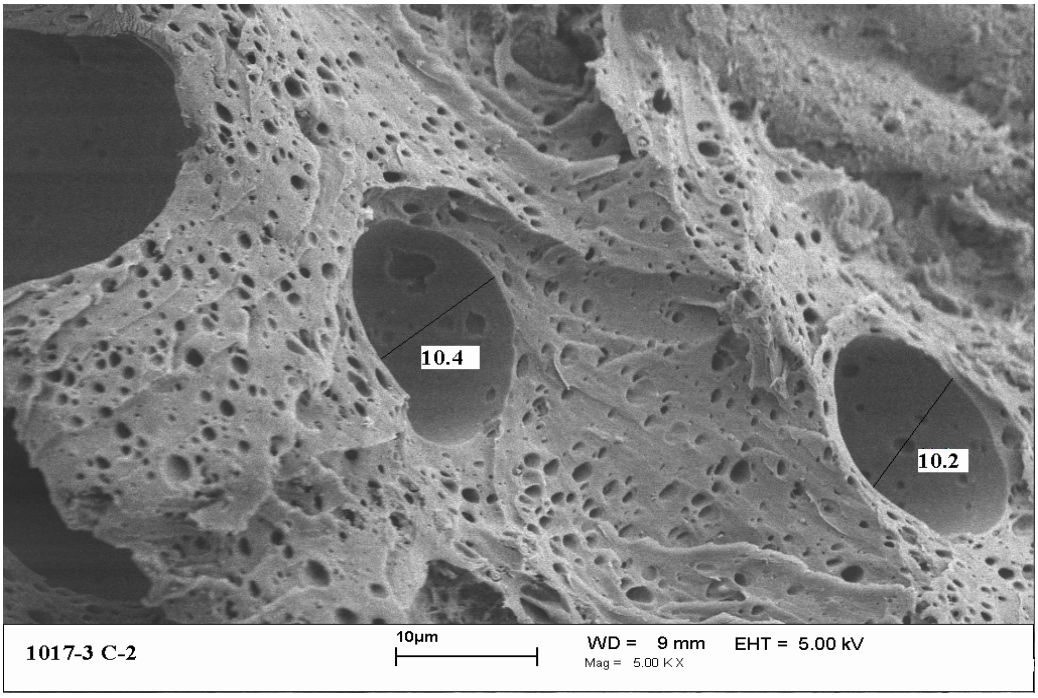

Figure 34. EECR 1017–3 C–2 5x SEM Coating Micrograph

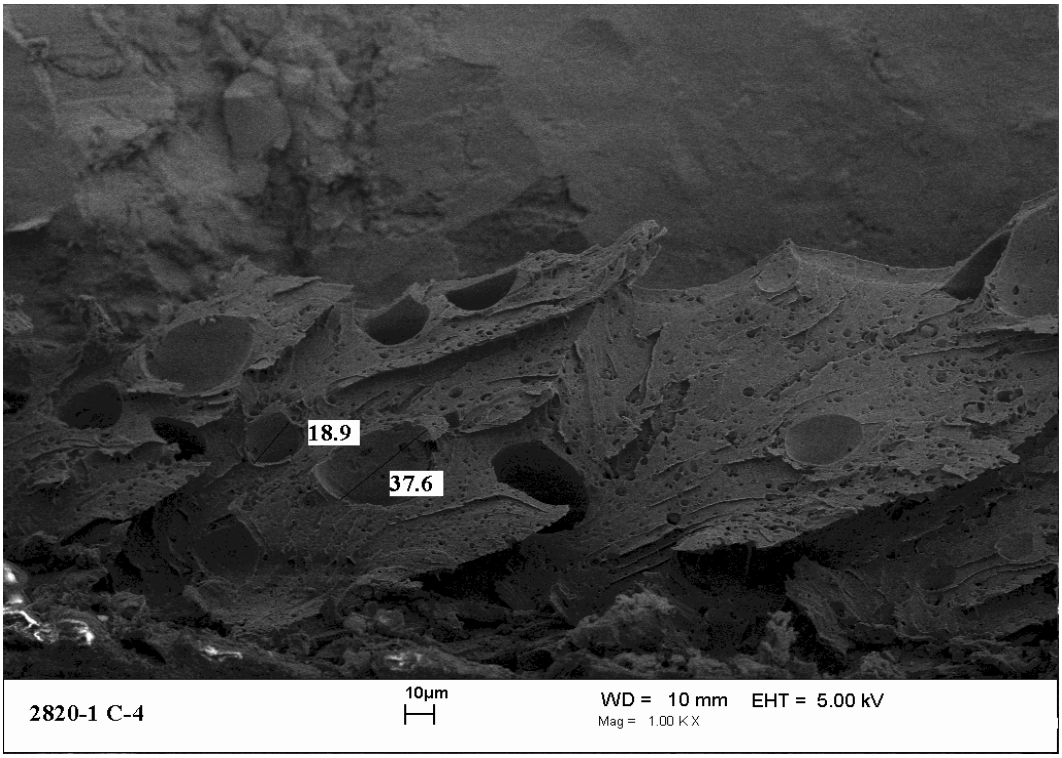

Figure 35. EER 2820–1 C–4 1x SEM Coating Micrograph

In addition to % moisture, ΔT_g also correlated well with the coating thickness with a Pearson correlation value of -0.340 and P-value of 0.003. The data presented in Figure 36 leads to an influence that has not yet been fully discussed in literature: the coating speed at the ECR manufacturing facility. The negative Pearson correlation value and the scatter diagram indicate

that thicker coatings are more fully cured than thinner ones. Since the degree of curing is independent of the material thickness, the relationship can be explained as follows: greater manufacturing speeds produce low and uneven heating of the bar element. Following the heating of the bar element, the greater speed not only impedes the adhesion of sufficient epoxy powder to the bar, but it also limits the time available for the fusion-bonded epoxy to cure leading to a more porous and therefore more permeable coating structure. The LNE data deviates from this conclusion with a ΔT_g of zero indicating a fully cured coating, yet exhibiting the thinnest coating and continuous holiday detection. In this case, the bar may have in fact been overheated, flash-curing the powder coating without allowing sufficient time for the epoxy to flow and fully coat the bar and thus accounting for the continuous holiday detection results.

In support of the above, insufficient curing should result in as increase in the number of holidays per unit length of bar. The Pearson correlation value is 0.282 and the P-value of this relationship is 0.014, however the highly variable nature of the data makes this conclusion tenuous at best.

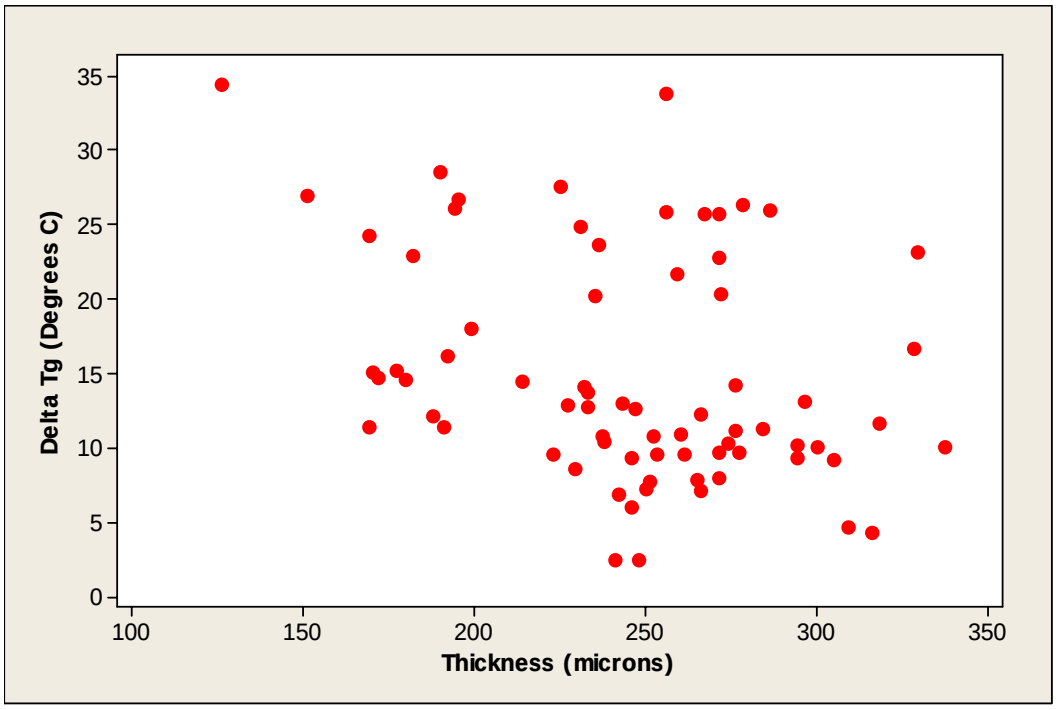

Figure 36. EECR ΔT_g vs. Thickness

Finally, the color of the corrosion products under the coating also correlated reasonably well with the coating degree of curing with a Pearson correlation value of 0.341 and a P-value of 0.002 (Figure 37). The same relationship can also be seen between % moisture and the average steel surface color with a Pearson correlation value of 0.422 and a P-value of 0.000 (Figure 38), which would indicate that the moisture present in the coating plays an active role in the corrosion activity under the coating. The gross classification of the steel surface color possibly being an indicator of the hydration level of the oxide layer present on the steel surface.

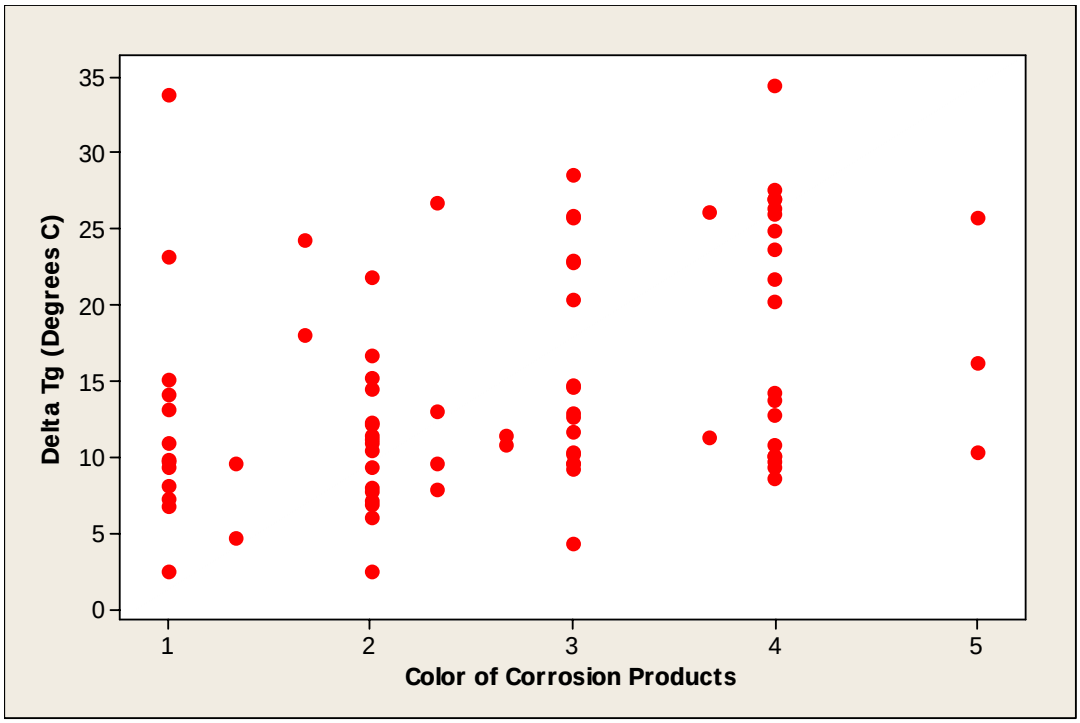

Figure 37. EECR ΔT_g vs. Steel Surface Color

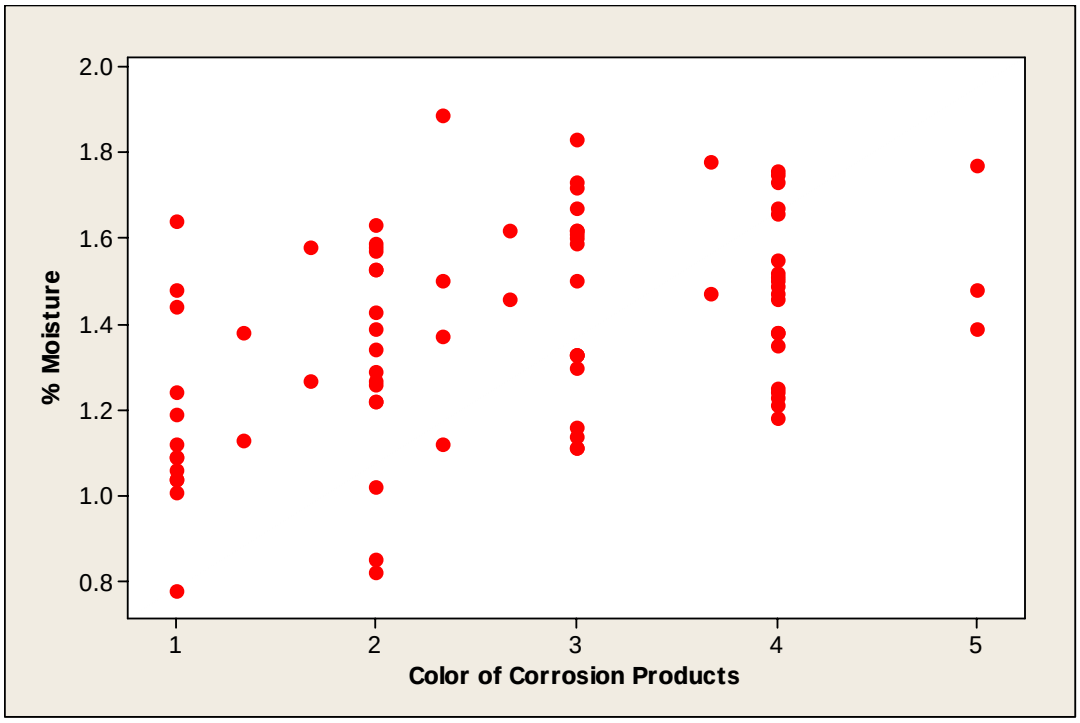

Figure 38. EECR % Moisture vs. Steel Surface Color

Residual Adhesion

The residual adhesion correlated well with three parameters: ΔT_g, the % coating moisture and the steel surface color. The Pearson correlation values were 0.416, 0.522 and 0.764

respectively. Conversely, all the P-values were 0.000. The relationship of ΔT_g with the residual adhesion is presented in Figure 39. The relationship is relevant only insofar as the absorption is concerned. The prevalent thought in the industry was that cross-link density had a significant effect on adhesion based on the availability of hydroxyl pendants. Rouw, however, showed that the effect cross-link density has on adhesion is in fact minimal (Rouw, 1998). This leaves coating permeability as the parameter most affected by the degree of curing.

Pyc, and Sagüés, and Powers have shown that epoxy coatings loose adhesion upon exposure to wet environments (Pyc, 1998; Sagüés and Powers, 1990). This study supports those findings (Figure 40). However, upon removal from concrete, the coating does not regain adhesion as others have observed in laboratory studies; but instead, the adhesion loss is permanent. The ability of the coating to regain adhesion upon drying after short-term exposure to wet environments as well as the permanent adhesion loss exhibited upon long-term exposure would suggest that while mechanical interlocking between the coating and the steel surface may occur on a limited scale, in fact it contributes little to the overall adhesion of the coating to the steel substrate. As illustrated in Figure 41 and supported by EDS spectra in Figures 42, 43 and Table 14. The spectra in Figures 43 and 44 were obtained from locations 2 and 3 in Figure 40. The high carbon content present at location 2 and presented in Table 14 supports the conclusion that the observed material is indeed an epoxy coating fragment. Location 3, however, presents no carbon signal, but the iron signal is exceptionally strong indicating a complete absence of epoxy. In fact there is an approximately 20 µm gap between the coating fragment and the steel surface which may indicate that the coating never adhered to that surface.

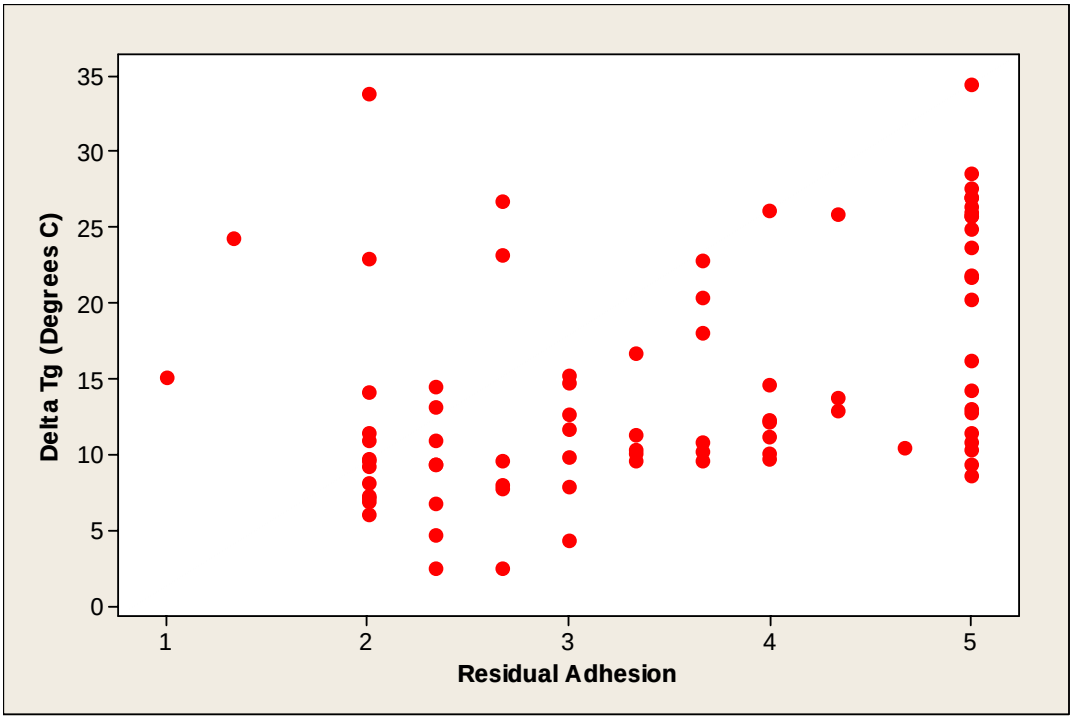

Figure 39. EECR ΔT_g vs. Residual Adhesion

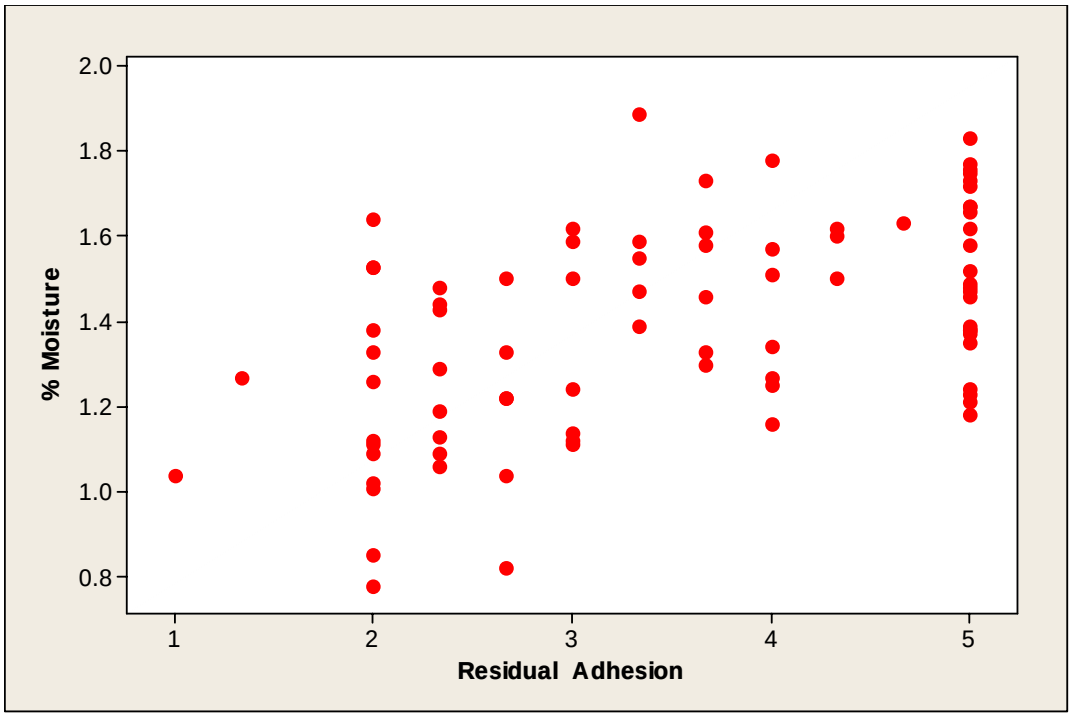

Figure 40. EECR % Moisture vs. Residual Adhesion

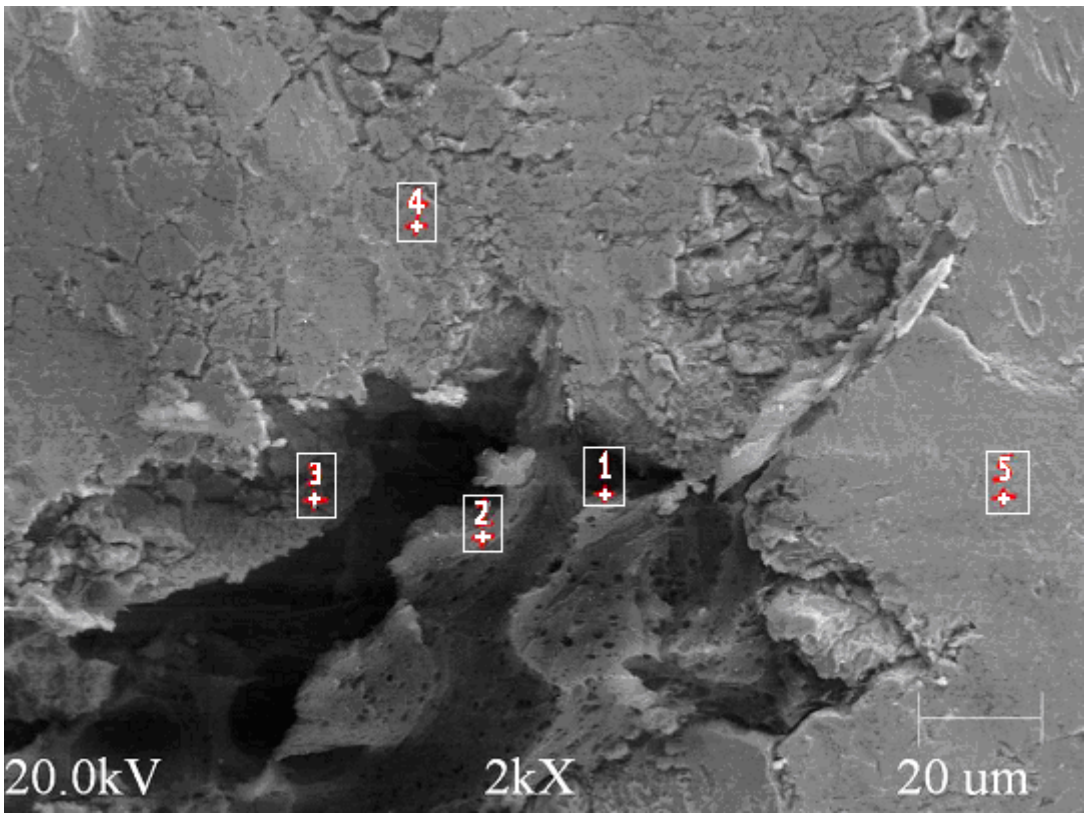

Figure 41. EECR Structure 1133-1 C-6 SEM Micrograph

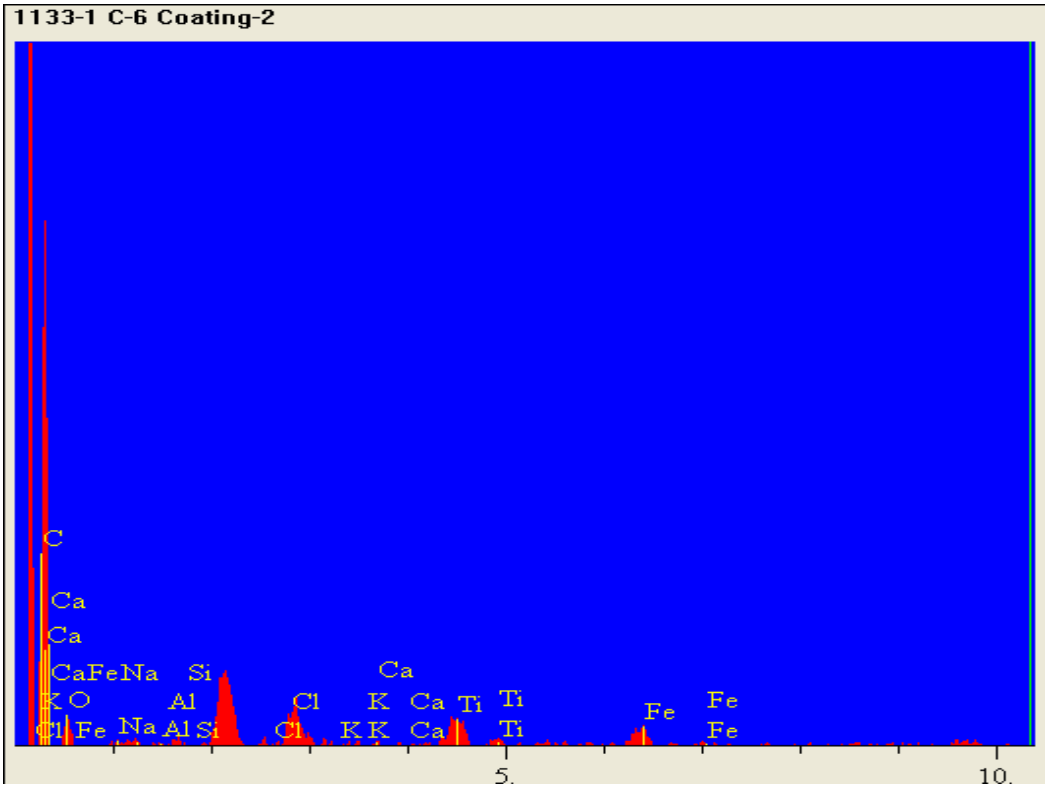

Figure 42. Structure 1133-1 C-6 EDS Coating Spectrum

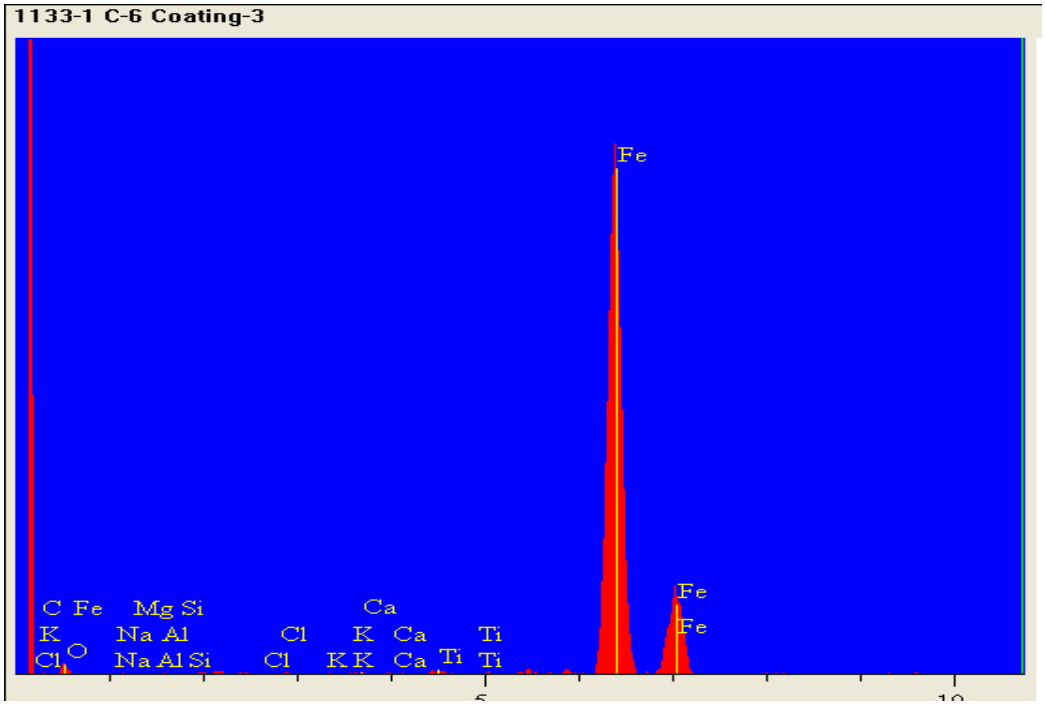

Figure 43. Structure 1133-1 C-6 EDS Metal Spectrum

Table 14. Structure 1133-1 C-6 EDS Chemical Composition

	Test Location 2			Test Location 3		
Element	Intensity (c/s)	Atomic %	Concentration	Intensity (c/s)	Atomic %	Concentration
C	38.61	84.825	76.564	0.000	0.000	0.000
O	3.57	12.844	15.443	1.56	4.621	1.377
Na	0.72	0.212	0.366	0.17	0.409	0.175
Mg	0.74	0.142	0.259	0.10	0.144	0.065
Al	0.39	0.058	0.117	0.03	0.027	0.013
Si	0.33	0.043	0.090	0.30	0.220	0.115
Cl	0.59	0.061	0.163	0.19	0.081	0.054
K	0.00	0.000	0.000	0.20	0.075	0.054
Ca	0.65	0.070	0.212	0.40	0.139	0.104
Ti	7.28	0.895	3.220	1.10	0.314	0.280
Fe	4.57	0.850	3.566	154.73	93.970	97.762
		100	100		100	100

The generalized and permanent nature of the adhesion loss observed occurs through a combination of adhesion loss mechanisms. First, the initial adhesion loss occurs as moisture diffuses through the coating and replaces the hydrogen bonds between the coating and the existing thin oxide layer present on the steel surface. Once sufficient moisture collects at the steel-coating interface, Sagüés theorized that cathodic disbondment may proceed by dissolution of the oxide film by hydroxides rather than by alkaline degradation of the coating itself (Sagüés, 1994). In 1992, Jones noted that cathodic disbondment may also occur at microscopic or smaller flaws in the coating to produce blisters, which do not require a physically obvious defect for initiation (Jones, 1992). Figure 44 clearly illustrates the effect of corrosion activity on the adhesion of the coating to the substrate.

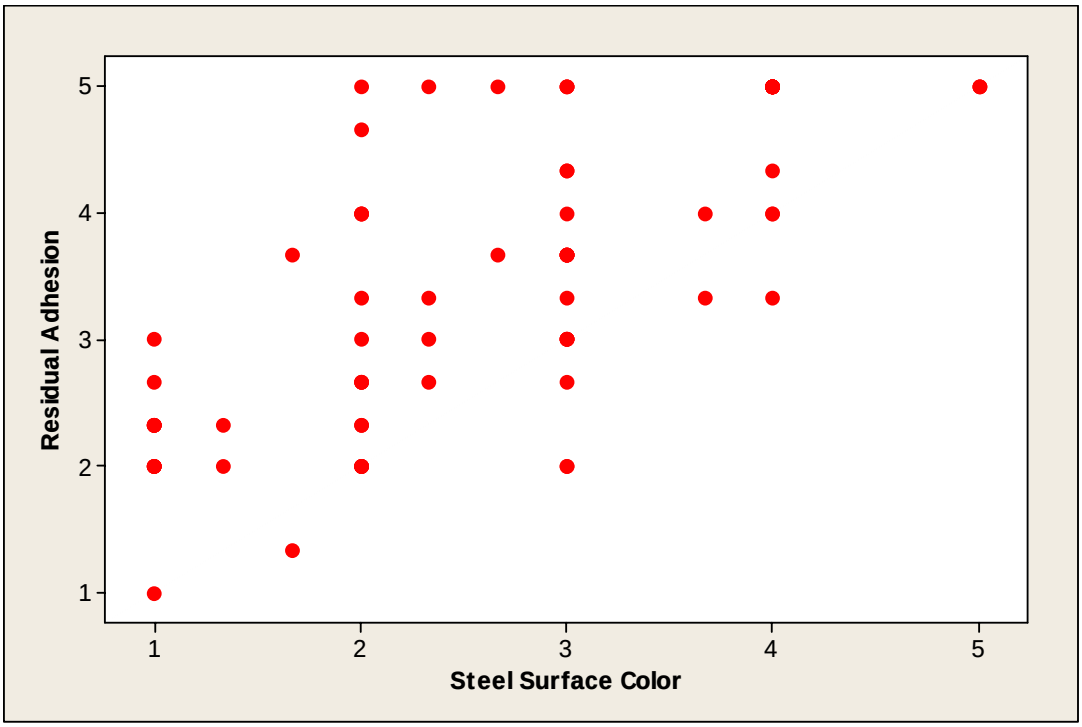

Figure 44. EECR Residual Adhesion vs. Steel Surface Color

In addition, Griffith and Laylor conducted a study of ECR reinforced bridges in Oregon found extensive adhesion loss (Griffith and Laylor, 1999). One of the parameters believed to contribute to adhesion loss in that particular study was the surface profile of the steel bar. ASTM A775, “Standard Specification for Epoxy Coated Reinforcing Bars” (ASTM, 2004), states: "Average blast profile maximum roughness depth readings of 1.5 to 4.0 mils, as determined by replica tape measurements using NACE RP-287-87, shall be considered suitable as an anchor pattern." Based on a total of 150 profile measurements, the mean blast profile for longitudinal bars in the tidal zone was 3.00 mils, with a 95% confidence interval of +/- 0.27 mils yet their samples presented considerable adhesion loss (Griffith and Laylor, 1999). Referencing Figure 40, the spectra obtained from locations 4 and 5 (Figures 45, 46 and Table 15) presented no epoxy residue further supporting the conclusion that the epoxy to rebar adhesion is generally chemical and not mechanical in nature. The carbon signal at both locations is zero.

Corrosion Activity

The extent of corrosion activity in the extracted ECR samples was determined by measuring the total combined size of visibly corroding sites on the coated bar and expressing that value as a percentage of the total surface area. The factors believed to influence the bar corrosion were the concrete chloride concentration at bar level, the age of the sample, the epoxy coating curing level, coating thickness, coating color, residual adhesion, the change in T_g from in-situ to fully cured (ΔT_g), and the coating moisture content as previously discussed, plus the number of holidays and damaged areas per length of bar, the coating cracking number and the % cracking and porosity. Similar to coating cracking analysis, these parameters were regressed with the % corroded area as the response as well as individually correlated to determine parameter inter-dependency.

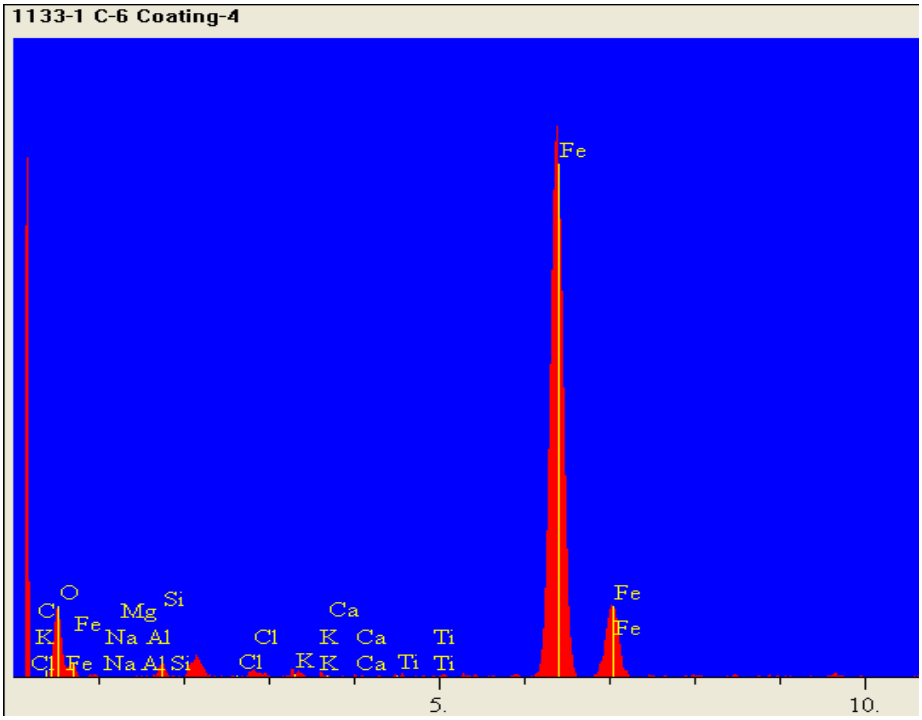

Figure 45. Structure 1133-1 C-6 EDS Coating Spectrum

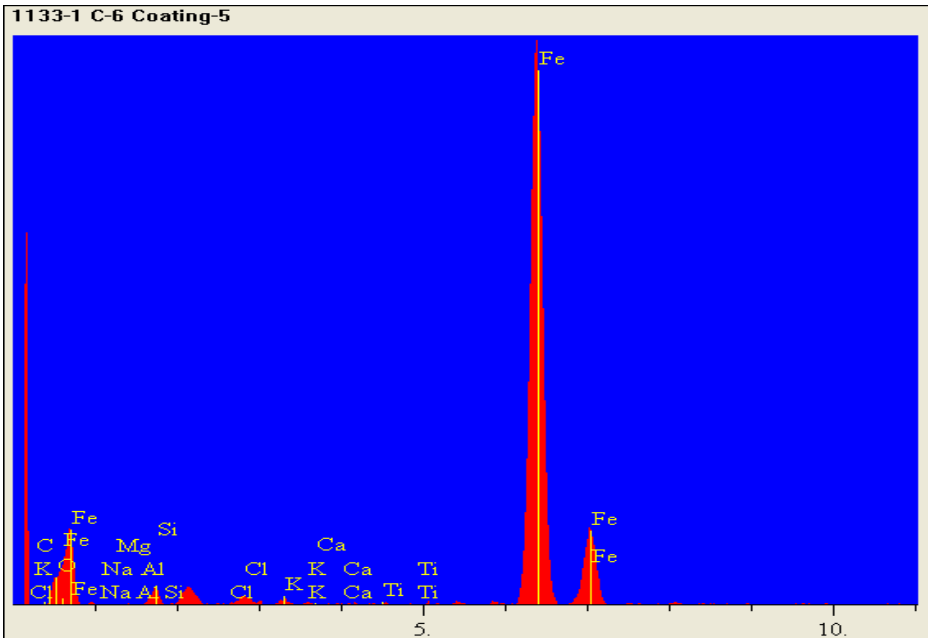

Figure 46. Structure 1133-1 C-6 EDS Coating Spectrum

Table 15. Structure 1133-1 C-6 EDS Chemical Composition

	Test Location 4			Test Location 5		
Element	Intensity (c/s)	Atomic %	Concentration	Intensity (c/s)	Atomic %	Concentration
C	0.00	0.000	0.000	0.000	0.000	0.000
O	33.38	25.634	9.097	20.40	12.810	4.102
Na	0.28	0.170	0.086	0.52	0.258	0.119
Mg	0.04	0.016	0.008	0.22	0.065	0.032
Al	0.35	0.087	0.052	0.19	0.037	0.020
Si	6.54	1.255	0.782	13.00	2.021	1.136
Cl	0.63	0.071	0.056	0.66	0.060	0.043
K	4.11	0.406	0.352	5.39	0.424	0.332
Ca	1.23	0.116	0.103	0.87	0.065	0.052
Ti	1.57	0.129	0.137	1.73	0.111	0.106
Fe	443.33	72.117	89.327	648.68	84.149	94.058
		100	100		100	100

As expected, the % corroded area correlated well with the number of holidays per unit length of bar and the number of damaged areas per unit length of bar. The Pearson correlation values were 0.382 and 0.657. The corresponding P-values were 0.001 and 0.000, respectively. These relationships are presented in Figures 47 and 48.

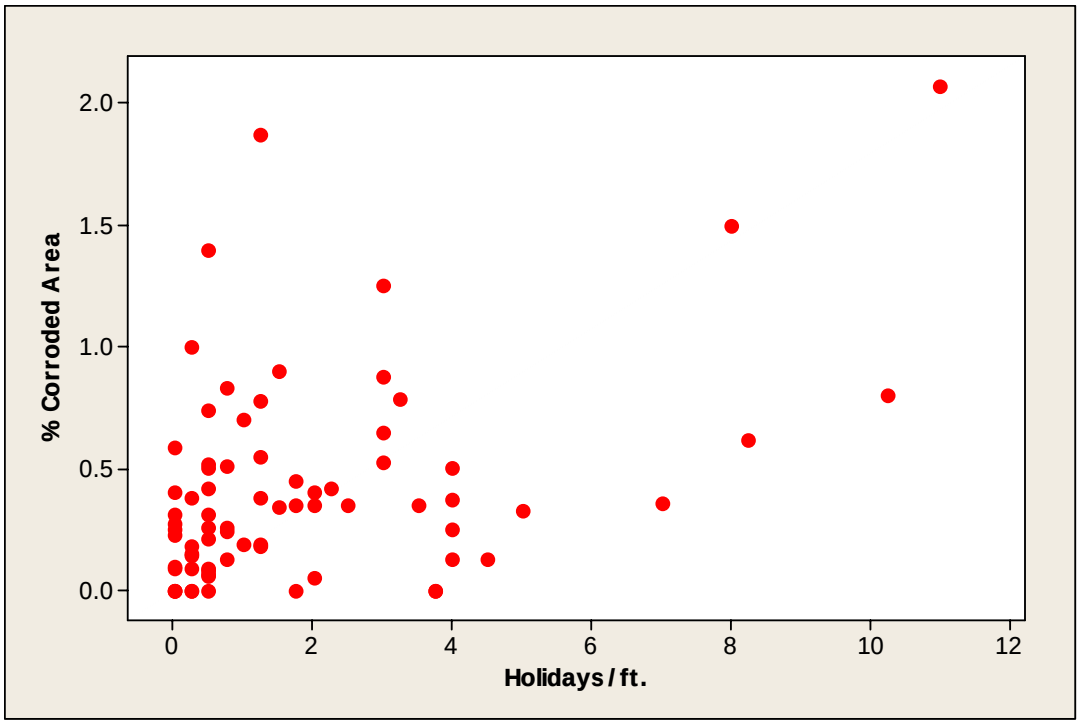

Figure 47. EECR 45% Corroded Area vs. Holidays/0.31 m.

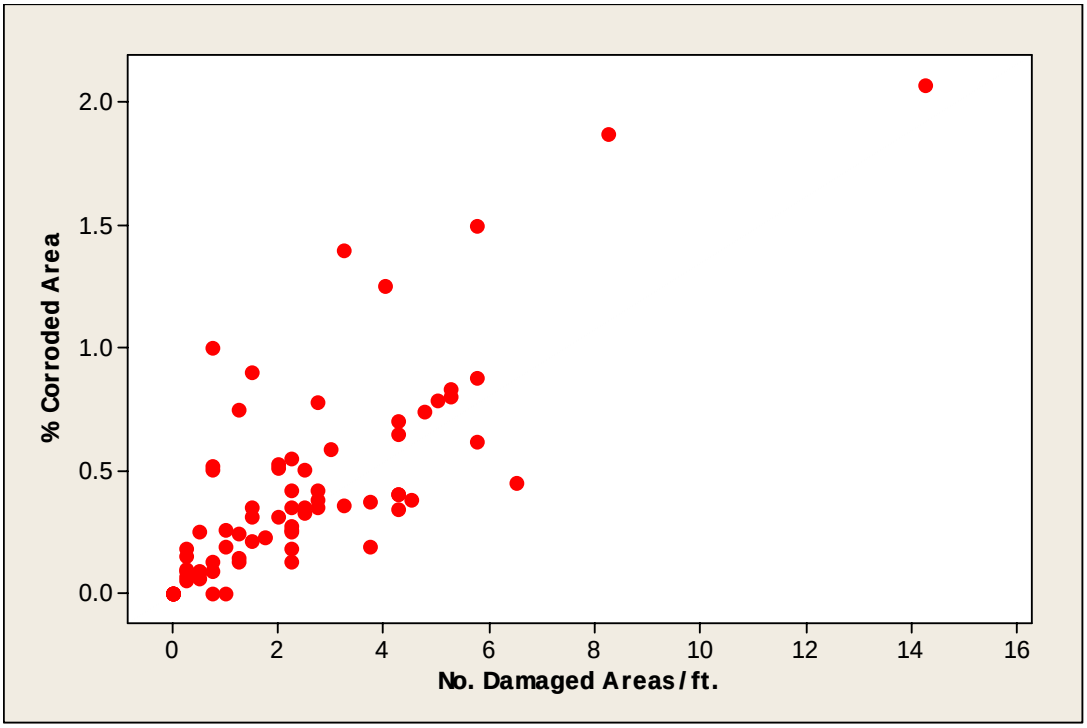

Figure 48. EECR % Corroded Area vs. Number of Damaged Areas/0.31 m.

The analysis confirmed the results of numerous previous reports which state that the corrosion severity is directly related to breaches in the coating barrier. More unusual, however, was the fact that the chloride concentration at bar level did not seem to be a corrosion controlling

parameter as it is in concrete structures reinforced with uncoated steel. The result may be influenced by the low chloride contents. As presented in the results, the chloride concentration in 82% of the tested structure was below a commonly accepted uncoated bar corrosion initiation level.

Additionally, the EDS analysis (Table 16) showed only traces or the complete absence of chlorides on the steel surface, as illustrated by the typical spectra from sample 1007-4 C-3 in Figures 50 and 51. The referenced spectra were obtained from locations 1 and 4 in Figure 49.

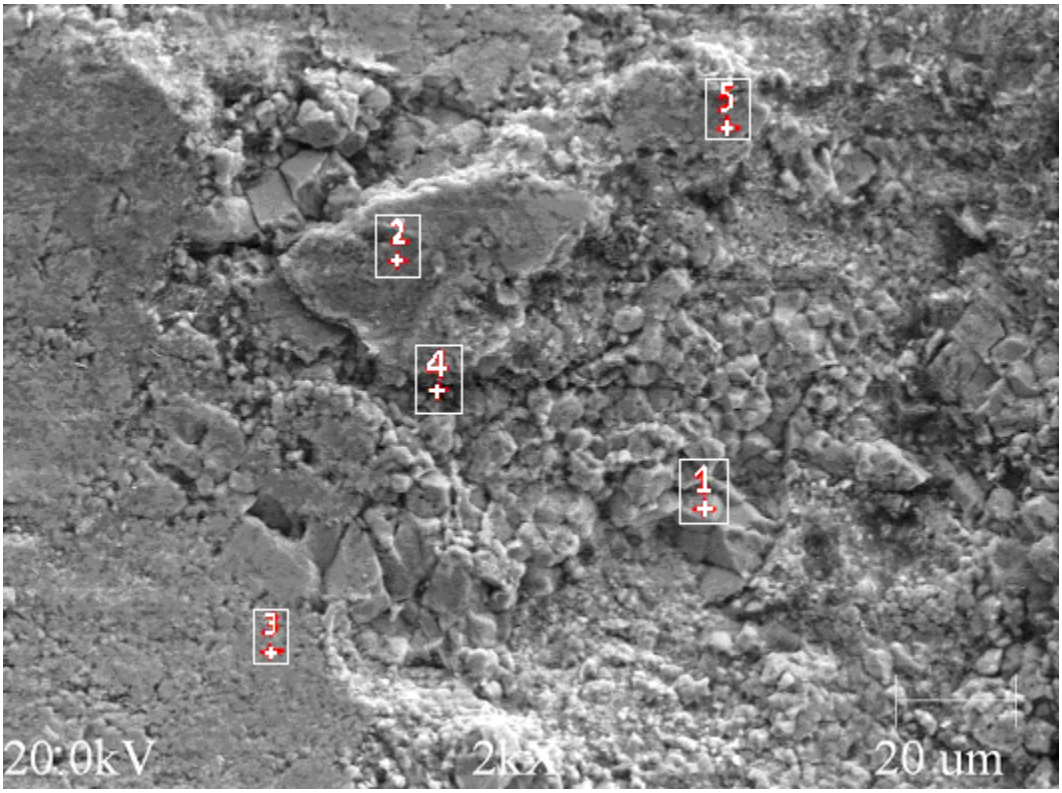

Figure 49. Structure 1007-4 C-3 SEM Micrograph

The absence of chlorides on the steel surface is also supported by the spectra collected from sample 1133-1 C-3 (Figure 52) illustrated in Figures 53 and 54, while Table 17 presents the surface chemical composition at the referenced locations.

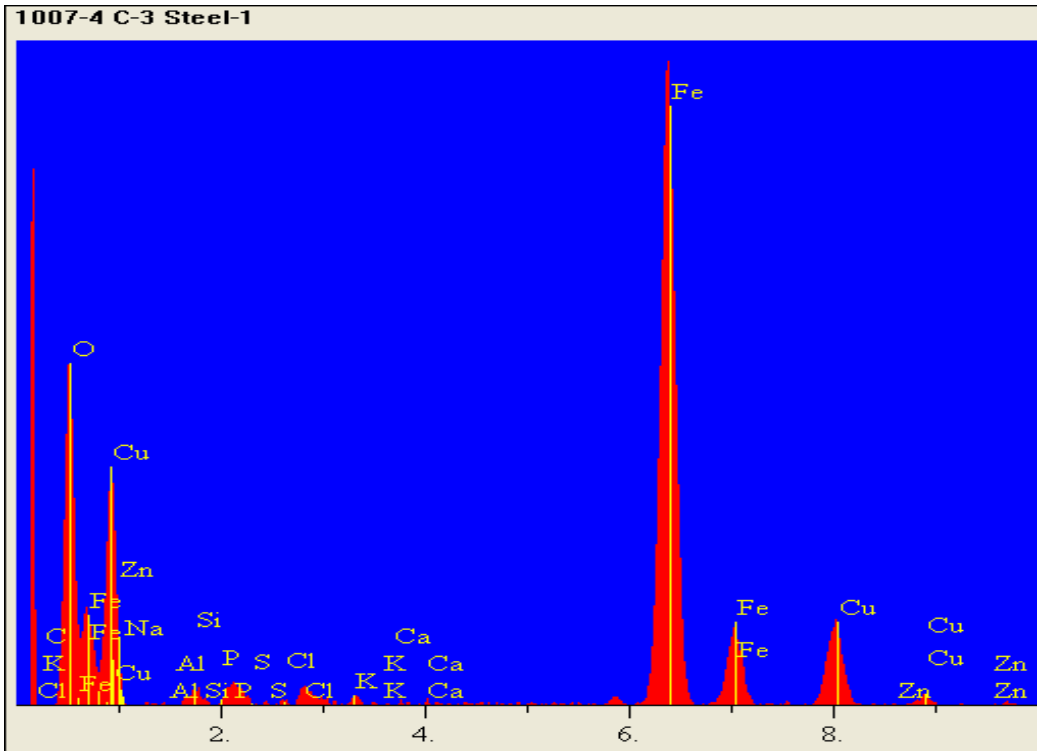

Figure 50. Structure 1007-4 C-3 EDS Coating Spectrum

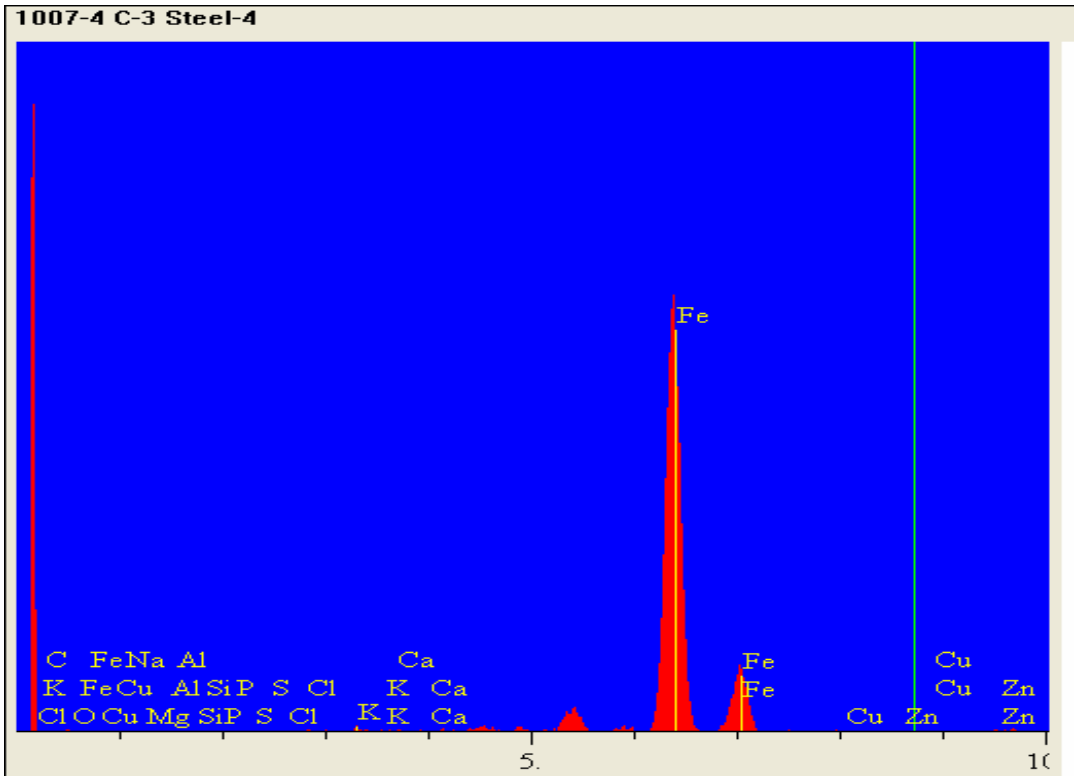

Figure 51. Structure 1007-4 C-3 EDS Coating Spectrum

Table 16. Structure 1007-4 C-3 EDS Chemical Composition

	Test Location 1			Test Location 4		
Element	Intensity (c/s)	Atomic %	Concentration	Intensity (c/s)	Atomic %	Concentration
C	0.00	0.000	0.000	0.000	0.000	0.000
O	137.48	54.728	25.589	0.41	0.838	0.242
Na	0.00	0.000	0.000	0.03	0.048	0.020
Mg	0.58	0.110	0.078	0.03	0.031	0.014
Al	0.27	0.036	0.028	0.38	0.253	0.123
Si	7.61	0.776	0.637	0.26	0.134	0.068
P	3.88	0.322	0.291	0.26	0.108	0.060
S	2.63	0.182	0.170	0.03	0.009	0.005
Cl	2.35	0.145	0.150	0.02	0.006	0.004
K	4.39	0.241	0.276	1.28	0.321	0.227
Ca	0.60	0.032	0.038	0.54	0.127	0.092
Fe	409.69	35.149	57.363	231.22	97.410	98.316
Cu	8.14	8.197	15.223	0.10	0.498	0.572
Zn	0.50	0.083	0.158	0.27	0.217	0.257
		100	100		100	100

Based on the regression analysis, at the 95% confidence level, the number of damages/m was the only predictor of corrosion severity with a P-value of 0.000. Decreasing the confidence level to 80% allows for the inclusion of % moisture, ΔT_g and % cracking and porosity as corrosion severity prediction parameters. The individual P-values were 0.081, 0.093, and 0.171, respectively. Further regression performed using only the parameters with P-values ≤ 0.20 ultimately yielded two parameters as the strongest predictors of corrosion severity: number of damages/m and ΔT_g. The P-values were 0.000 and 0.012, respectively.

While the new ECR showed a moderate degree of improvement compared to the extracted ECR with respect to the degree of curing, comparing the number of damaged areas presents a different observation. Statistically, there is a significant difference between the new and the extracted ECR samples, but not as expected. The new samples presented a disproportionably greater number of damages than the extracted samples as illustrated below.

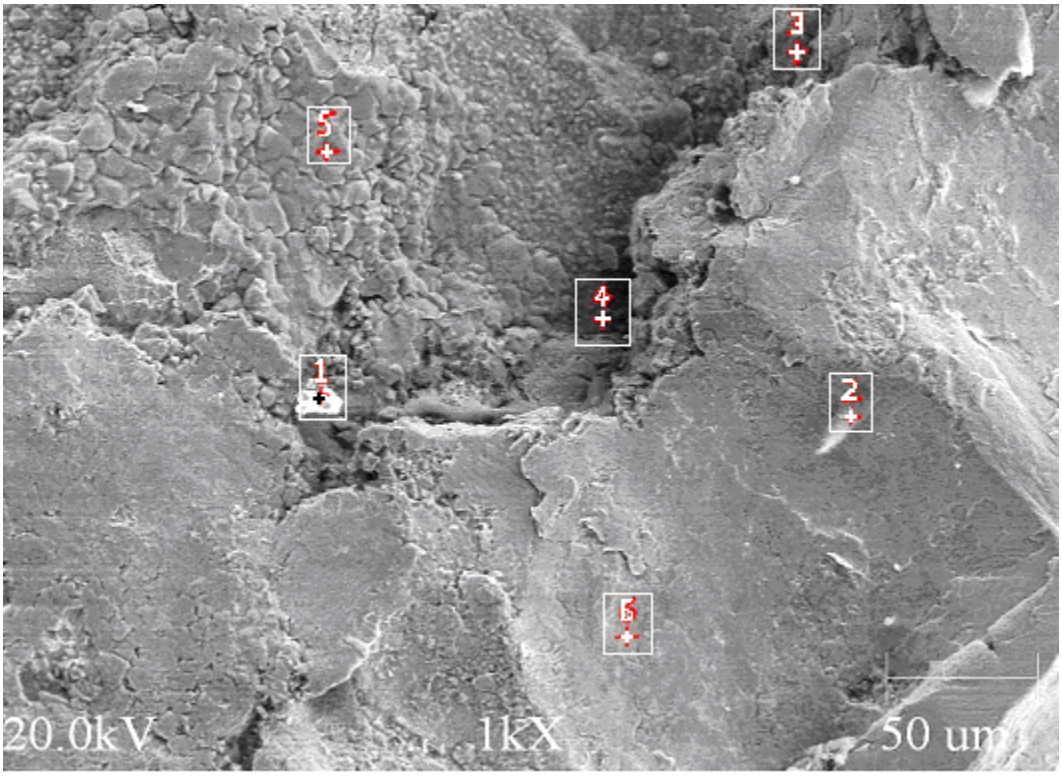

Figure 52. Structure 1133-1 C-3 SEM Micrograph

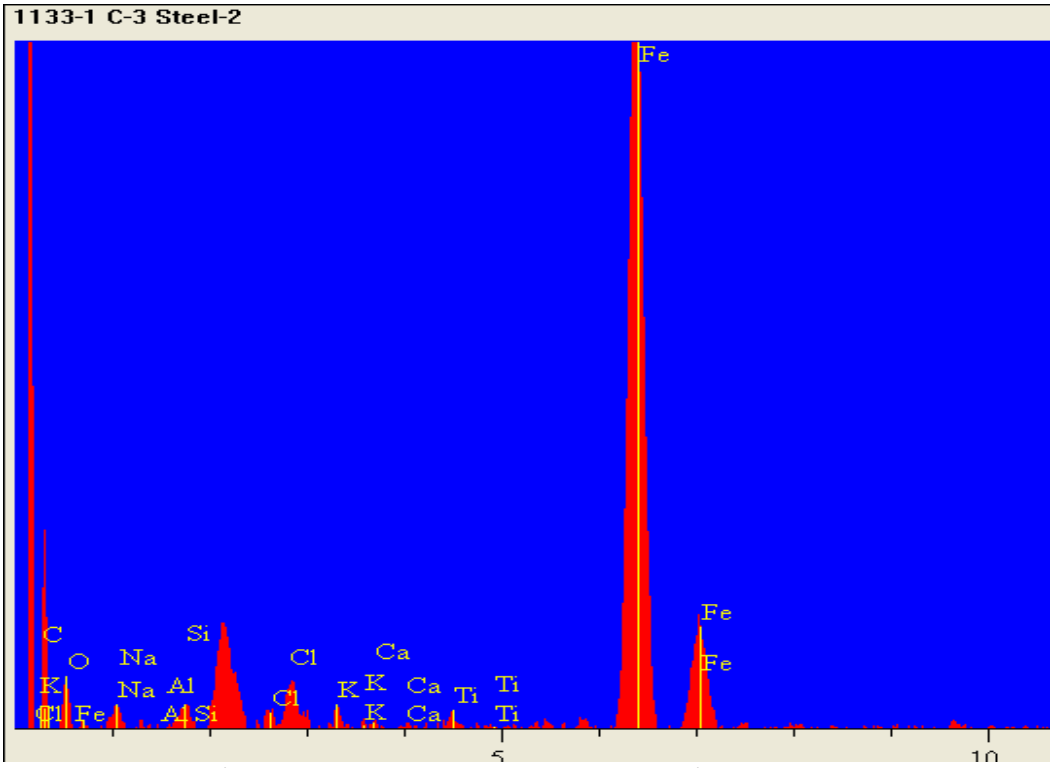

Figure 53. Structure 1133-1 C-3 EDS Coating Spectrum

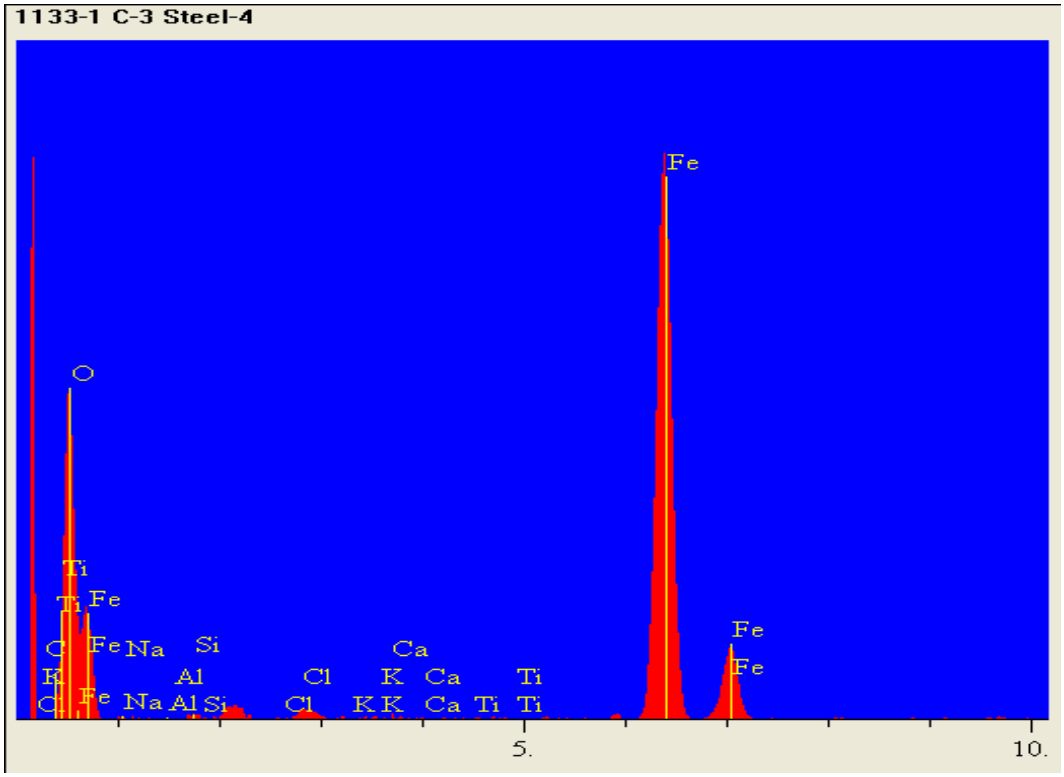

Figure 54. Structure 1133-1 C-3 EDS Coating Spectrum

Table 17. Structure 1133-1 C-3 EDS Chemical Composition

	Test Location 2			Test Location 4		
Element	Intensity (c/s)	Atomic %	Concentration	Intensity (c/s)	Atomic %	Concentration
C	8.94	53.263	22.641	0.000	0.000	0.000
O	6.76	7.822	4.429	165.81	58.381	28.899
Na	4.07	2.037	1.657	1.28	0.376	0.267
Mg	0.44	0.135	0.116	0.43	0.075	0.056
Al	0.07	0.016	0.015	0.28	0.034	0.028
Si	4.72	0.801	0.796	2.98	0.280	0.244
Cl	3.96	0.420	0.528	0.74	0.043	0.047
K	3.65	0.350	0.484	0.61	0.031	0.038
Ca	0.60	0.032	0.038	1.18	0.059	0.073
Ti	3.02	0.262	0.444	0.88	0.040	0.059
Fe	217.48	34.759	68.699	477.46	40.682	70.290
		100	100		100	100

The t-test comparison shows a distinct loss of quality control. Where the extracted samples presented an average of 8.04 damages/m, the new ECR samples had a mean of 34.2 damages/m. Since it is commonly accepted that corrosion generally initiates at breaches in the coating, the performance of the new bar should be severely impacted. This however, will not become evident for decades, with controlling factors being concrete cover depths and chloride diffusivity.

Similarly, the mean number of holidays/m was slightly greater for the new ECR samples at 8.40 holidays/m than for the extracted ECR samples at 6.17 holidays/m. Statistically, however, the t-test showed that there were no differences between the two sample sets.

One of the limitation of measuring the corrosion activity and severity based only on visible corrosion activity is that it underestimates the actual corrosion activity. (Brown, 2002). The high oxygen content present on the metal surface presented in Tables 16 and 17, and the moderate oxygen content presented in Table 15, indicate that active corrosion occurs under the coating even in the absence of chlorides.

Corrosion Measurements

Finally, further analysis of the ability of commonly accepted non-destructive corrosion investigative techniques to assess the level of corrosion in concrete structures reinforced with ECR was performed. The data supported the assertion that although tests such as concrete resistivity, half-cell potentials and linear polarization are highly variable, they can in fact provide valuable information regarding corrosion activity.

Concrete resistivity presented weak correlations with two parameters: the chloride concentration at bar level and coating % moisture content. The Pearson correlation values were -0.206 and -0.234, respectively. The corresponding P-values were 0.064 and 0.036. From a theoretical view point, the results are entirely justifiable; an increase in the chloride concentration and moisture results in a decrease in resistivity. Since during resistivity measurements every reasonable precaution was taken to ensure that the bar effects were minimized, the coating moisture content correlation may be explained by the intimate relationship between concrete moisture content and coating moisture content.

Corrosion half-cell potentials presented a negative correlation with the resistivity values. The Pearson correlation value was -0.207 and the P-value 0.067 (Figure 55), which is also in agreement with theoretical conditions: higher resistivity results in lower corrosion potentials.

Most telling, however, were the linear polarization measurements. At the 95% confidence level, the corrosion current density measurements correlated very well with the chloride concentration at bar level and reasonably well with the coating % moisture content. The Pearson correlation values were 0.408 and 0.268, while the P-values were 0.000 and 0.018, respectively (Figures 56 and 57). At 90% confidence level, the corrosion current density also correlated with residual adhesion and the number of damaged areas. The Pearson correlation values were 0.196 and 0.200 and the P-values were 0.083 and 0.084.

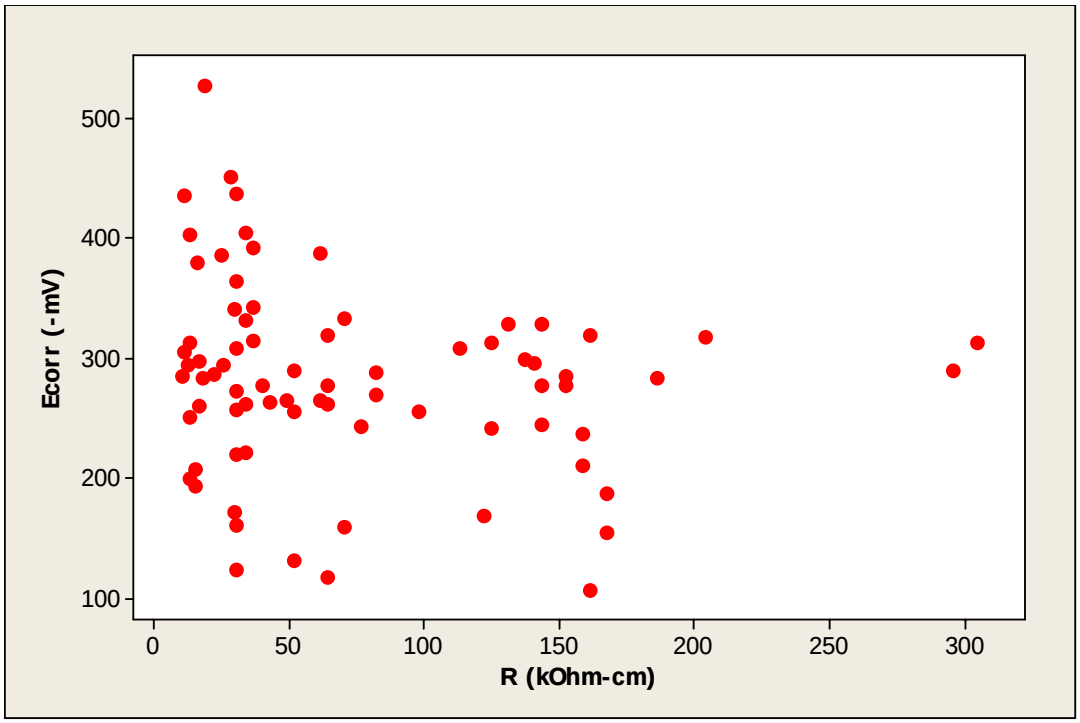

Figure 55. EECR Half-cell Potentials vs. Resistivity

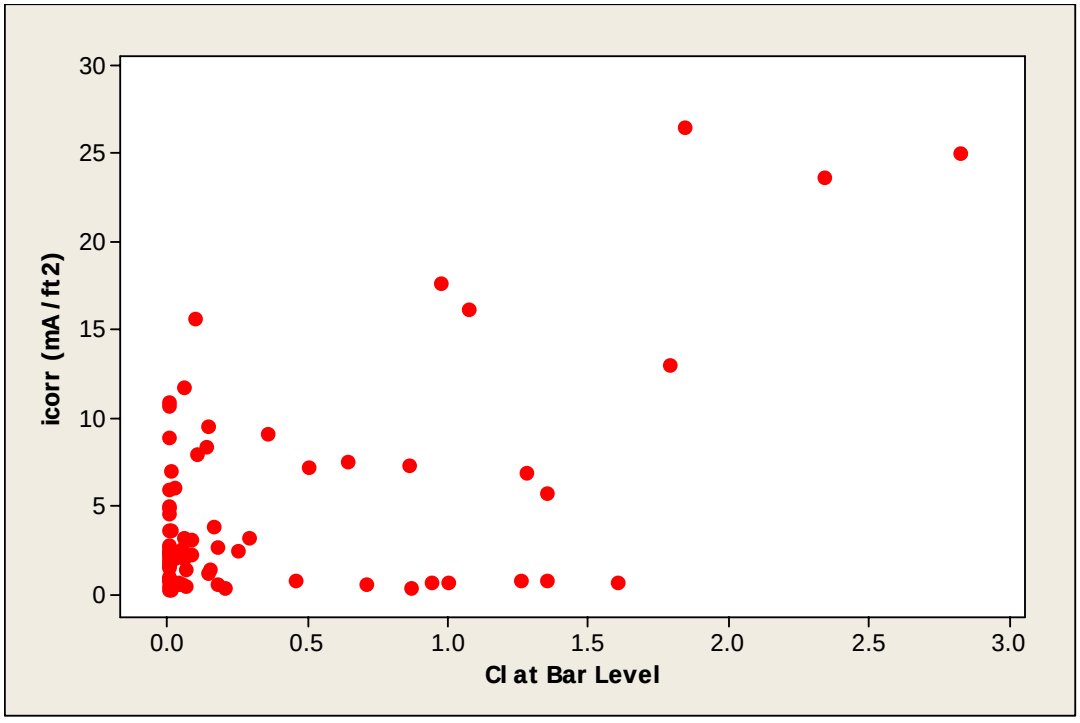

Figure 56. EECR Corrosion Current Density vs. Cl^- at Bar Level

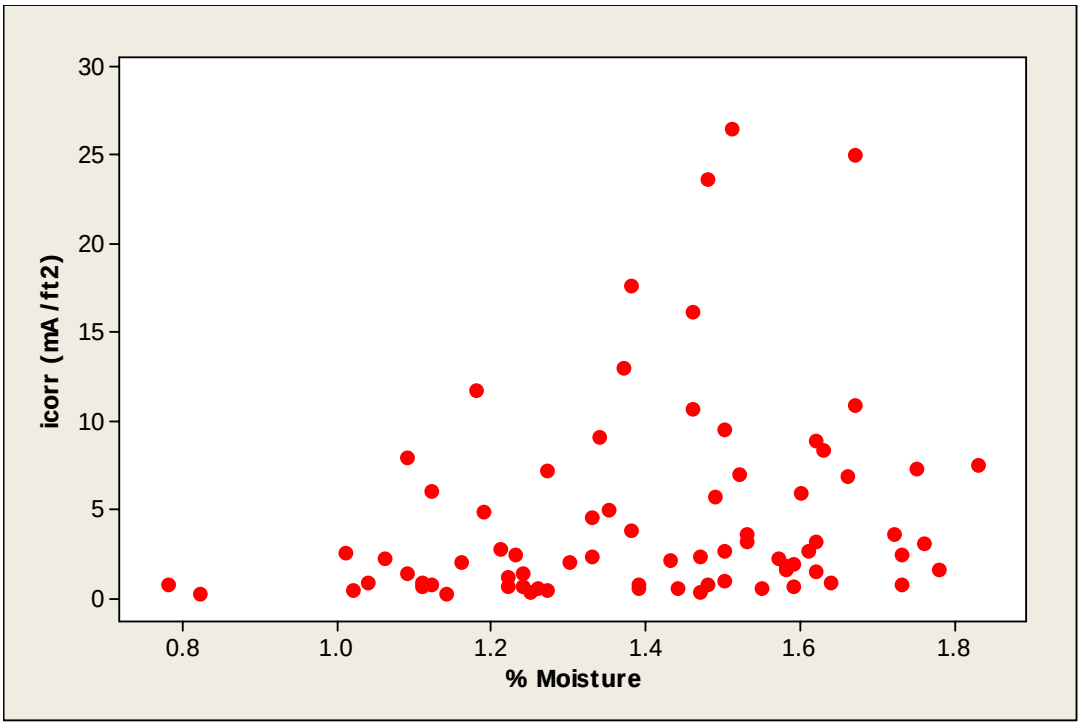

Figure 57. EECR Corrosion Current Density vs. % Moisture

While the level of chlorides was zero or close to zero at locations under the coating, corrosion current density measurements seem to indicate that the contribution of chlorides to corrosion activity, particularly at breaches in the coating is relatively significant. The low correlation numbers reflected by the residual adhesion and the number of damaged areas may be a result of large variability inherent to concrete corrosion measurements coupled with the limited accuracy of residual adhesion and visual assessment of the rebar samples.

Until other corrosion protection methods become more prevalent, improving non-destructive corrosion activity assessment methods in ECR reinforced structures is critical. The analysis shows that while limited, there is value in performing the measurements concomitant with other commonly available corrosion assessment methods.

CONCLUSIONS

The extracted ECR coating samples presented extensive cracking compared to the new ECR samples in which the coating cracking was limited to only one sample. The coating cracking correlated with the level of chlorides at bar level, residual adhesion and percent moisture in the coating. The coating cracking also correlated well with the coating color, indicating that the degradation process affects the coating surface condition. Although the chloride levels, based on bare steel values, may be insufficient to initiate corrosion of the reinforcing steel under the coating, the research has demonstrated that aged epoxy coatings develop cracks in the superficial layers in the presence of chlorides.

The DSC results showed that both the extracted samples as well as new samples were not fully cured during the manufacturing process. While the curing state of the coating may not have

a significant direct influence on residual adhesion, it does however affect the number of holidays and the moisture absorption of the coating. Less cured coatings having a greater number of holidays as well as higher moisture absorption due to their more porous nature.

Additionally, the samples investigated presented significant permanent adhesion loss with little or no epoxy coating residue present on the bar surface. Presently, the absence of coating residue on the bar surface, supported by EDS spectra, indicates that adhesion is primarily chemical in nature and that the contribution of the mechanical dimension of adhesion is minimal at best. Furthermore, the EDS analysis shows that once adhesion is lost, corrosion will proceed unimpeded under the coating even in the absence of chlorides.

The parameters that presented a direct correlation with the observed corrosion activity were the number of holidays and the number of damaged areas per unit length of bar. Thus, indicating that the bare steel exposed to the concrete pore solution at the breaches in the epoxy coating does not passivate as a bare bar under similar exposure conditions allowing it instead to corrode at lower concrete chloride concentration levels than bare bars. Furthermore, the lack of detected chlorides on the surface of the steel bar in the presence of highly elevated oxygen levels demonstrate that the corrosion process continues unimpeded under the coating even in the absence of chlorides.

The results also show a distinct loss of quality control in the handling and possibly storage of new coated bars. The new ECR samples had significantly higher damage density than the samples extracted from concrete, while there was no change in the number of holidays and cure condition.

Finally, the data presented further evidence that while limited, the non-destructive corrosion assessment methods available for bare steel reinforced structures may also be used on ECR reinforced structures. In particular, the corrosion rate measurements correlated reasonably well with the chloride concentrations at bar level; thus indicating that while the chlorides may not influence the corrosion activity under the coating, they do influence the corrosion activity at breaches in the coating.

RECOMMENDATIONS

Handling and exposure limits of freshly coated bars have been addressed through the implementation of ASTM standards and specifications. These standards need to be strictly enforced to limit the amount of damage to the coating prior to being encased in concrete. Other parameters, such as fully cured coating, were assumed to be met during the coating process.

This study, however, has shown that that is not the case. This condition may be corrected in several ways:

- The bars may be preheated prior to blast cleaning to provide a more uniform bar temperature at the time it enters the electromagnetic heating element.
- Increase the distance between the bar exit from powder chamber to the quenching water spray, increasing the cure time without affecting the manufacturing speed.

- After coating, use radiant heat or an IR oven between the coating chamber and the quenching spray to post cure the coating.

However, even though the quality of the coated bar prior to being encased in concrete may be increased, its influence on service life performance over 100 years is highly questionable in a moist/wet-chloride-alkali environment as shown by the degradation of the epoxy coating encased in concrete.

Thus, the final recommendation to be implemented by the Structures and Bridge Division is to use a more reliable corrosion protection for reinforcing steel than is provided by fusion-bonded epoxy coatings.

COSTS AND BENEFITS ASSESSMENT

The resultant of the implementation of the final recommendation to terminate the use of ECR in new construction are initial and maintenance cost savings Previous research has demonstrated that ECR corrosion protection efficiency is poorer at concrete crack locations than in uncracked concrete. Also, bridges built under present cover depth and low permeable concrete using bare bar will provide 100 years of maintenance free service. However, FHWA requires an additional corrosion protection system in all Federal Aid projects. Thus, cost saving would be dependent upon whether a bridge is built with State funds only or includes Federal dollars.

A typical bridge deck contains about 26.63 kg of reinforcing steel per square meter. By terminating the use of ECR, the savings would be about $8.82 per square meter of deck or about $8,820,000 per million square meters of bridge deck built with State funds. For projects using Federal dollars, the additional corrosion protection systems could be MMFX-2, the cost is about equal to ECR. The benefit is maintenance free bridge decks for over 100 years. Thus, absolute minimization of user costs in accidents and delays.

ACKNOWLEDGMENTS

Acknowledgements to VDOT personnel without which this project could not be completed, the Engineering District Bridge Engineers, traffic control personnel, concrete drilling crews, and VTRC technicians. In particular the field survey crew of Andy Mills, Andrei Ramniceanu, Wes Keller, Bill Ordel, Linda DeGrasse, David Mokarem, Michael Brown, and Richard Weyers.

REFERENCES

Apicella, A. Effect of Thermal History on Water Sorption, Elastic Properties and the Glass Transition of Epoxy Resins. *Polymer*. Vol. 20, No. 9, 1979, pp 1143-1148.

ASTM. A 775/A 775M Standard Specification for Epoxy-Coated Steel Reinforcing Bars. *ASTM Annual Book of ASTM Standards*. Vol. 01.04, 2004.

ASTM. C 876-91 Standard Test Method for Half-Cell Potentials of Uncoated Reinforcing Steel in Concrete. *ASTM Annual Book of ASTM Standards*. Vol. 04.02, 1991.

ASTM. G62-87 Standard Test Methods for Holiday Detection in Pipeline Coatings. *ASTM Annual Book of ASTM Standards*. Vol. 01.48, 1998.

Brown, Michael C. *Corrosion Protection Service Life of Epoxy Coated Reinforcing Steel in Virginia Bridge Decks*. Doctoral Dissertation in Civil and Environmental Engineering. Virginia Polytechnic Institute and State University, Blacksburg, VA, 2002.

Clear, Kenneth C. *Measuring Rate of Corrosion of Steel in Field Concrete Structures*. Kenneth C. Clear, Inc. Concrete Materials and Corrosion Specialists, Sterling, VA, 1989.

De′ Néve, B. and Shanahan, M. E. R. Water Absorption by an Epoxy Resin and its Effect on the Mechanical Properties and Infra-red Spectra. *Polymer*, Vol. 34, No. 24, 1993, pp. 5099-5105.

Feliu, S., Gonzalez, J. A., and Andrade, C. Techniques to Assess the Corrosion Activity of Steel Reinforced Concrete Structures. *ASTM STP 1276*, 1996, pp. 107-118.

Griffith, A. and Laylor, M.H. *Epoxy Coating Reinforcement Study*. State Research Project #527, Oregon Department of Transportation Research Group, 1999.

Jones, D.A. *Principles and Prevention of Corrosion*. Macmillan Publishing Company, New York, 1992.

Kotnarowska, D. Influence of Ultraviolet Radiation and Aggressive Media on Epoxy Coating Degradation. *Progress in Organic Coatings*, Vol.37, 1999, pp. 149 – 159.

Liu, Y. *Modeling the Time-to-Corrosion Cracking of the Cover Concrete in Chloride Contaminated Reinforced Concrete Structures*. Doctoral Dissertation in Civil and Environmental Engineering. Virginia Polytechnic Institute and State University, Blacksburg, VA, 1996.

Manning, David G. Corrosion Performance of Epoxy-Coated Reinforcing Steel: North American Experience. *Construction and Building Materials*, Vol. 10, No. 5, 1995, pp. 349-365.

Poon, S.W. and Tasker, I. Extending Building Life with Fusion Bonded Epoxy. *Asia Engineer, The Journal of the Hong Kong Institution of Engineers*, Vol. 26, No. 8, 1998, pp. 17-22.

Pyc, W. A., Weyers, R. E., Weyers, R. M., Mokarem, D. W., Zemajtis, J., Sprinkel, M. M., and Dillard, J. G. *Field Performance of Epoxy-Coated Reinforcing Steel in Virginia Bridge Decks*. VTRC 00-R16, Virginia Transportation Research Council, Charlottesville, VA, 2000.

Pyc, W. A. *Field Performance of Epoxy-Coated Reinforcing Steel in Virginia Bridge Decks*. Doctoral Dissertation in Civil and Environmental Engineering. Virginia Polytechnic Institute and State University, Blacksburg, VA, 1998.

Ramniceanu, A., Weyers, R. E., Anderson-Cook, C., and Brown, M. C. Measuring the Field Corrosion Activity of Bridge Decks Built with Bare and Epoxy Coated Steel. *ASTM International*, Vol. 3, No. 8, 2006, pp. 10-16.

Rouw, A.C. Model Epoxy Powder Coatings and Their Adhesion to Steel. *Progress in Organic Coatings*, Vol.34, 1998, pp. 181–192.

Sagues, A.A., & Powers, R.G. *Effect of Concrete Environment on the Corrosion Performance of Epoxy-Coated Reinforcing Steel.* Paper No. 311, Corrosion 90, Las Vegas, NV, 1990.

Sagüés, A.A. *Corrosion of Epoxy-Coated Rebar in Florida Bridges*. WPI 0510603, Final Report Florida DOT, University of South Florida, College of Engineering, 1994.

Singht, D. D. N. and Ghosh, R. Unexpected Deterioration of Fusion-Bonded Epoxy-Coated Rebars Embedded in Chloride-Contaminated Concrte Environments. *Corrosion*, Vol. 61, No. 8, 2005, pp. 815-829.

Weyers, R.E. *Protocol for In-service Evaluation of Bridges with Epoxy Coated Reinforcing Steel*. NCHRP 10-37B, Final Report. Transportation Research Board, Washington, D.C., 1995.

Wheeler, M.C. *Parameters Influencing the Corrosion Protection Service Life of Epoxy Coated Reinforcing Steel in Virginia Bridge Decks*. Master of Science Thesis. Virginia Polytechnic Institute and State University, Blacksburg, VA, 2003.

Zemajtis, J. *Modeling the Time to Corrosion Initiation of Concretes with Mineral Admixtures and/or Corrosion Inhibtors in Chloride-Laden Environments*. Doctoral Dissertation in Civil and Environmental Engineering. Virginia Polytechnic Institute and State University, Blacksburg, VA, 1998.

APPENDIX

Figure A1. Glossy Green Rebar – 1

Figure A2. Dull Green Rebar – 2

Figure A3. Glossy Light Green – 3

Figure A4. Dull Dark Green – 4

Figure A5. Pale Green – 5